Lawrence Berkeley Laboratory
UNIVERSITY OF CALIFORNIA

Materials & Molecular
Research Division

MOLECULAR BEAM CHEMILUMINESCENCE STUDIES OF THE NO + O_3 REACTION AND MODELING OF GLOBAL NO_2 DISTRIBUTION

Marta Kowalczyk
(Ph.D. thesis)

November 1980

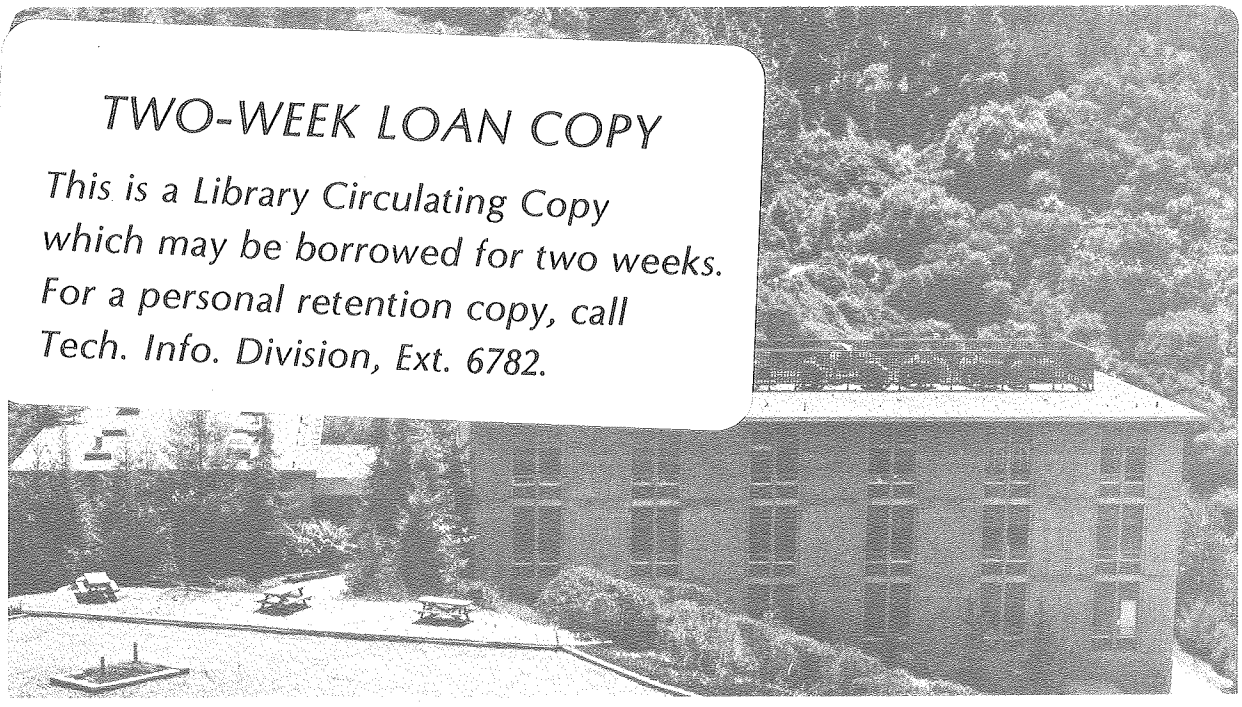

Prepared for the U.S. Department of Energy under Contract W-7405-ENG-48

DISCLAIMER

LBL-12106

MOLECULAR BEAM CHEMILUMINESCENCE STUDIES OF THE NO + O_3 REACTION AND MODELING OF GLOBAL NO_2 DISTRIBUTION

Marta Kowalczyk

Ph.D. thesis

November 1980

Materials and Molecular Research Division
Lawrence Berkeley Laboratory
University of California
Berkeley, CA 94720

This work was supported by the Division of Chemical Sciences, Office of Basic Energy Sciences, U.S. Department of Energy under Contract No. W-7405-ENG-48.

MOLECULAR BEAM CHEMILUMINESCENCE STUDIES OF THE NO + O_3 REACTION AND MODELING OF GLOBAL NO_2 DISTRIBUTION

Marta Kowalczyk

ABSTRACT

The results of a crossed molecular beam study of the chemiluminescent reaction $NO + O_3 \longrightarrow NO_2^* + O_2$ are discussed. The chemiluminescence as a function of collision energy and an excitation function were obtained using a translationally cooled supersonic NO beam. The results have verified a steep translational energy dependence. An investigation into the role of the internal energy states using an effusive NO beam and a supersonic O_3 beam has been presented. The results show that chemiluminescence enhancement occurs when high and low temperature NO experiments are compared. It was shown that this enhancement was inconsistent with the assignment that the upper fine structure state $NO(^2\pi_{3/2})$ was entirely responsible for the enhancement. The role that other energy modes may have is discussed. The observed enhancement is consistent with the concept that the chemiluminescence cross section increases with NO molecular rotation for low J states.

The second part discusses the role of NO_2 in preserving a global ozone balance. NO_2 vertical profiles based on Noxon's (1979) column measurements were derived. The method of instantaneous rates was used to calculate the rate of ozone production and destruction by O_x and NO_x on a grid that covered the entire globe. The results

were presented as a function of altitude and latitude in contour plots. Various latitudinal and altitudinal sums were made and discussed. The global summation between 15 and 45 km shows that the loss of ozone due to O_x is 15 % of the ozone production rate and that the destruction of ozone by NO_x is 45 ± 15 % of the production rate. Noxon's recent recalibration of his experimental method has increased the global estimate of NO_x by 25 % (Noxon 1980), therefore the global values for ozone destruction by NO_x should be increased proportionately.

MOLECULAR BEAM CHEMILUMINESCENCE STUDIES OF THE NO + O_3 REACTION AND MODELING OF GLOBAL NO_2

Contents

Part I : Molecular Beam Chemiluminescence Studies of the NO + O_3 Reaction....1

I. Introduction....1

A. Historical background and justification for this work....1

B. Molecular beam experiments....7

1. Supersonic expansions....7

2. Effusive expansions....9

3. Pumping considerations....10

C. Scope of this work....11

II. Experimental....13

A. Chemiluminescence machine description....13

1. Vacuum system....13

2. The optical system....18

3. Detection and photon counting system....19

B. The chemical reactants....20

C. Time-of-flight....22

1. Experimental....22

2. Time-of-flight to relative flux distributions...25

D. Experimental procedures....28

1. Supersonic NO study....28

2. Supersonic beam flux determination....29

3. Wavelength dependence study....30

4. Effusive NO study....30

III. Results.....32

A. Supersonic NO study.....32

B. Wavelength dependence study results.....39

C. Effusive NO study results.....41

IV. Conclusion.....54

V. Figure captions.....55

VI. References.....58

Part II: Modeling of Global NO_2 Distribution.....63

I. Introduction.....63

II. Experimentally observed quantities.....67

A. Temperature and ozone data.....67

B. Photon flux.....73

C. NO_2 concentrations.....76

III. Calculations with the 1-D model.....83

A. Introduction.....83

B. Calculations.....85

C. Checks of the model results.....92

IV. Instantaneous rates calculations.....97

A. Results.....97

B. Effect of transport on the instantaneous rates.....107

V. Conclusions.....111

VI. Postscript.....117

VII. Figure captions.....118

VIII. References.....121

ACKNOWLEDGEMENTS

I sincerely wish to acknowledge the many people who have helped me during my graduate career. First thanks go to Professor Harold S. Johnston whose guidance during the course of this work has been invaluable and to Professor Yuan T. Lee whose concern for people and love for science infects all who come into contact with him. Next I would like to especially thank Carol Kahler, my co-worker in the NO + O_3 experiments. I thank Susan Solomon, my partner in the global ozone calculation work. I am grateful to Susan for the 1-D model calculations but most of all for her understanding of what it means to be a friend. The help and consideration I received from all the people I have worked with is greatly appreciated: Herb Nelson, Jim Valentini, Rick Buss, Lee Carlson, Kosuke Shobatake, and Randy Sparks, thanks. Finally, I would like to thank most of all Dennis Reuter and the members of my family who have always encouraged me.

I would like to thank all the contributors to this work, particularly Y. T. Lee for instruction and use of various molecular beam apparati, J. S. Chang for generously supplying a copy of the 1974 atmospheric model, H. U. Dütsch for supplying tables of atmospheric temperature and ozone data and J. B. Kerr for tables of data that had previously appeared only as figures.

Both parts of this work were supported by the Division of Chemical Sciences, Office of Basic Energy Sciences, U. S. Department of Energy under contract NO. W-7405-Eng-48.

---------- PART I ----------

MOLECULAR BEAM CHEMILUMINESCENCE STUDIES OF THE NO + O_3 REACTION *

I. INTRODUCTION

A. HISTORICAL BACKGROUND AND JUSTIFICATION FOR THIS WORK

The chemical reaction $NO + O_3 \rightarrow NO_2 + O_2$ has been studied extensively in the last ten years with different approaches and chemical techniques. Thermal studies by Clough and Thrush (1967) laid the foundation by identifying two distinct product channels for the reaction with the following rate constants:

$$NO + O_3(^1A_1) \longrightarrow NO_2^*(^2B_1 \text{ or } ^2B_2) + O_2 \qquad (1)$$

$$k(T) = 1.26 \times 10^{-12} e^{-(4180 \text{kcal/mole/RT})} \text{cm}^3/\text{molec-sec}$$

$$\longrightarrow NO_2^{\neq}(^2A_1) + O_2 \qquad (2)$$

$$k(T) = 7.14 \times 10^{-13} e^{-(2230 \text{kcal/mole/RT})} \text{cm}^3/\text{molec-sec}$$

These authors found that under room temperature conditions the reaction proceeded about 7-10% through the first channel, producing electronically excited NO_2 in an undetermined state which eventually chemiluminesced in the visible and the near infra-red. The second channel resulted in vibrationally excited NO_2 in the ground electronic state. The authors accounted for the different activation energies by postulating that the reaction proceeds along two entirely different potential energy surfaces and that as a result, the two channels observed are the result of a direct collision and not due to an intermediate complex.

The visible chemiluminescence begins at 600 nm and extends to 1400 nm with a peak around 1000 nm. The entire emission spectrum is shifted proportionatly toward the blue when the reactants have more

* Kahler, 1980.

initial energy such as that provided at higher reaction temperatures or with molecular beam methods. Clough and Thrush (1967) also concluded that the visible chemiluminescence from the NO + O reaction involve similar internal states and transitions. The entire emission curve for this reaction is shifted toward the blue by 7000 cm^{-1} which can be accounted for by the increased exoergicity of the reaction. A similar blue shift effect on the NO + O_3 reaction has been observed by studying the wavelength resolved chemiluminescence as a function of added internal energy in a molecular beam study (Braun et al.1974) as well as in this study.

The chemiluminescence intensity from this reaction has generally been studied in a broad band fashion or at best with only a coarse wavelength resolution. Under such conditions it is difficult to assign the chemiluminescence to a particular electronic state. Studies to elucidate this have been done using laser induced fluorescence of NO_2 in a molecular beam (Smalley et al. 1975), however the same internal states may not be operative in the chemical reaction. On the other hand, the threshold behavior and peak emission wavelength of both chemical reactions and the NO_2 flourescence suggest that one is sampling different parts of the NO_2 potential energy surface. Attempts to identify the states in the NO + O_3 reaction explicitly have resulted in the conclusion that a mixture of states is responsible, perhaps complicated by a mutual perturbation or by a perturbation by a near lying electronic state that does not exhibit itself by chemiluminescence, (Brand et al. 1975; Stevens and Zare 1975; Tanaka et al. 1975).

The $NO + O_3$ reaction has been extensively studied by several research teams to determine the effect on the reaction rate of vibrational excitation of the reactants (Gordon and Lin 1973 , 1974; Moy et al. 1977; Bar-Ziv et al. 1978; Kurylo et al. 1974, 1975; Braun et al. 1974; Freund and Stephenson 1976; Stephenson and Freund 1976; Hui and Cool 1978; Hui et al. 1975). Generally a CO_2 laser was used to excite the v_3 mode of O_3. The Stephenson and Freund experiments used a CO laser combined with magnetic state tuning to vibrationally excite the NO molecule. Experimental results showed that the chemiluminescence enhancements observed were proportional to the amount of energy pumped into the reaction; which mode or which molecule introduced this energy seemed to make little difference. Inelastic collisions can result in rapid energy transfer among modes or to the buffer medium and may be obscuring the effects of individual modes on the reaction rate. One way to eliminate this complication would be to repeat these experiments under single collision conditions.

Another type of $NO + O_3$ experiment involved the use of molecular beams to determine whether chemiluminescence enhancement is due to internal or translational energy. Since these experiments are done under single collision conditions, problems due to competing processes are eliminated. The first such study by Redpath et al. (1978), introduced a partially relaxed supersonic NO beam into a gas cell containing O_3. The NO was heated and cooled to change its translational energy as well as its internal energy before collision. The authors observed a chemiluminescence threshold of 3 kilocalories per mole, a rapidly varying cross section with translational energy and an

increase in signal at high temperatures that they assigned to electronic energy contributed by the excited fine structure component in the reactant, NO ($^2\pi_{3/2}$).

This is the first experimental example of a reaction in which the excited spin-orbit state of a molecule seems to affect the reaction cross section. A classical trajectory calculation of the F + H_2 system does show that one would expect the cross section to be greater for the excited spin-orbit state, F($^2P_{3/2}$) (Komornicki et al. 1976). One would not expect this effect on energetic grounds since the separation between the two states is dwarfed by the exoergicity of the chemical reaction in both cases. However, symmetry arguments for the NO + O_3 case indicate that the upper state may be primarily responsible for the chemiluminescence (van den Ende and Stolte 1980; Redpath et al. 1978).

A similar molecular beam and gas cell experiment was carried out by van den Ende and Stolte (1980), at higher translational energies. A velocity selector was placed before the NO beam in order to separate effects due to translation from those due to internal energy. This simplified the analysis as well as eliminated the need for extensive velocity spread deconvolution. At one temperature the velocity selector was scanned to study the translational energy dependence of the chemiluminescent reaction cross section and the temperature was varied to study the internal energy dependence. The results were similar to those reported by Redpath. The threshold extrapolated from higher energies was 2.97 kcal/mole, a similar rise in cross section with translational energy was observed and a similar assignment of additional enhancement due to internal energy which was assigned to the NO

upper spin-orbit state. It was not possible to separate the effects of molecular rotation from the spin-orbit effect in the experiments of both Redpath and van den Ende.

More recent experiments that include state selection and beam orientation studies indicate that rotational rather than electronic energy may be responsible for the observed chemiluminescence enhancements, (Stolte, 1980; Anderson et al, 1980). Anderson used an inhomogeneous magnetic field to focus the NO beam in a beam-gas experiment to separate the two spin-orbit states before reaction. The authors found no effect due to the electronic spin-orbit state, however, the chemiluminescence signal depended strongly on the rotational level for low J.

A different kind of experiment on the same system is presently being carried out by Valentini and Kwei, (1980). Preliminary results of their crossed supersonic molecular beam differential scattering experiments show two peaks in the angular distribution for the NO_2 product. A forward scattered peak with respect to the NO beam has been assigned to NO_2 ($^2B_1$ and $^2B_2$) from the chemiluminescent channel whereas the backward scattered peak is attributed to NO_2 ($^2A_1$), from the vibrationally excited, ground electronic state. When two different nozzle temperatures were used, the ratio of the signal in the two peaks was unchanged. This indicates that the two product channels have either a common precursor or the same activation energy, which is inconsistent with the idea that the reaction proceees on two different potential energy surfaces. Perhaps, after all, nonadiabatic effects are taking place.

The experiment to be described here is a molecular beam chemiluminescence study done in three parts: a supersonic NO stud , a wavelength dependence study and a effusive NO study. First, a dependence of the chemiluminescence on translational energy was observed with a supersonic NO beam and an effusive O_3 beam in order to obtain an excitation function for the reaction. Special care was taken to adequately study the energy region near the reaction threshold. This experiment is a refinement on the approach used by Redpath et al. (1978) since two molecular beams were used rather than a beam-gas arrangement. The result is a much narrower translational energy distribution for the reaction, eliminating the need for an extensive deconvolution.

A major problem still exists with this approach if one wishes to study the effects of the electronic fine structure states since it is possible that they are relaxing along with the rotational, vibrational, and translational states in the supersonic expansion (Miescher et al. 1978; Thuis et al. 1979). It is difficult to determine the extent of this relaxation. Although, in general, relaxation of electronic states does not occur in a supersonic expansion, the small energy separation between the NO states makes them more analogous to rotational states than the typical separation between two electronic states. On the other hand, rotational energy generally couples more easily with translations since both involve nuclear motions.

Redpath et al. solved this problem by assuming that the enhanced chemiluminescence comes entirely from the fine structure states, that the lower state cross section is some fraction of that for the upper state, and that the relaxation falls between the two extremes of no relaxation

and complete relaxation. The only consistent deconvolution of all chemiluminescence data resulted in the conclusion that a partial relaxation was taking place and that the lower to upper chemiluminescence cross section ratio was between 0 and 0.25.

The experiment by van den Ende had a similar relaxation problem which was solved by assuming that complete relaxation with the translational degree of freedom occurs which was supported by the results of Miescher et al. (1978) and Thuis et al. (1979).

We have chosen to approach the relaxation problem by eliminating it entirely. In an effusive beam no relaxation will take place. The second major part of our study was a reverse configuration experiment with an effusive NO beam. The O_3 in He supersonic beam was prepared with a very high velocity to eliminate serious deconvolution problems by narrowing the collision energy distribution. This also has the desirable effect of increasing the chemiluminescence intensity due to its steep translational energy dependence.

B. MOLECULAR BEAM EXPERIMENTS

1. SUPERSONIC EXPANSIONS

A supersonic beam is created when a high pressure gas emerges from a small nozzle hole resulting in mass flow or hydrodynamic flow. The Knudsen number K_n defined by

$$K_n = \frac{\text{mean free path in source}}{\text{smallest dimension of the nozzle orifice}} \qquad (3)$$

is less than unity for such a case. As the gas emerges from the nozzle many collisions among the molecules and with the nozzle surfaces

occur. Energy transfer from the internal energy states to molecular translation as well as internal state temperature cooling occurs. A supersonic expansion can be described as an isentropic process; therefore the increase in translational energy experienced by the gas comes from a reduction in the local enthalpy of the gas. The random translational energy of the gas is converted to forward directed motion so that there is an increase in translational energy on the beam axis accompanied by a decrease in the velocity spread. The narrower velocity spread can be considered to be a decrease in temperature and is given by the following relation;

$$\frac{T_f}{T_i} = \left[1 + \left(\frac{\gamma-1}{2}\right)M^2\right]^{-1} \quad \text{where} \quad \gamma = C_p / C_v \qquad (4)$$

the ratio of heat capacities and M = v/c, the Mach number which is the ratio of the bulk velocity to the local velocity of sound. Mach numbers used in the NO + O_3 experiments varied between 6 and 22 which gives T_f / T_i = 0.12 - 0.01 respectively. The velocity width is given by $\Delta v/v \approx (2/\gamma)^{0.5}/M$. For the two cases given above $\Delta v/v$= 0.2 and 0.05.

As the translational temperature decreases, other internal energy states are cooled as well, depending on how well energy transfer to translation occurs. For example, rotational energy levels are almost completely equilibrated with translation whereas vibration is only slightly relaxed in the expansion. All of the internal and translational relaxation occurs in the early stages of the expansion when many collisions are taking place. Later in the expansion when the molecular density becomes low, this process stops, and one then has a molecular beam of non-interacting molecules that can be translationally charac-

terized experimentally by a time-of-flight analysis.

One can exploit the molecular weight of a species to increase or decrease the velocity of a reactant in the beam. By seeding 10 % NO in He, for example, one causes the heavier NO to be carried along at a much faster velocity as it emerges from the nozzle than it would if NO were used alone, The resulting velocity is a mass weighted velocity; therefore, a 1% NO in He mixture causes NO to travel faster still. It is possible to slow down the emerging velocity by anti-seeding with a heavier species such as Ar or Xe.

Supersonic beams offer a number of advantages in a molecular beam experiment. First, the collapsed velocity spread allows one to work with a more mono-energetic beam. Second, the collapsed internal energy modes causes a significamt simplification in the initial chemical system. Third, much higher beam intensities result because for a given gas load more molecules are travelling on the beam axis. Also since supersonic beams operate best under conditions of high pressure and small nozzle orifices, it is possible to increase the pressure behind the nozzle to a few atmospheres quite easily if necessary. Fourth, the seeding and anti-seeding techniques allow one to vary the translational energy thus controlling the collision energy of the reaction.

2. EFFUSIVE EXPANSIONS

An expansion which occurs by molecular effusion is the most easily characterized, because in the expansion process molecular properties are not changed. The internal energy states can be calculated simply from statistical mechanical and kinetic theory. For this reason such

expansions are also called "thermal" expansions.

An effusive expansion is achieved by using a low pressure gas and a small nozzle orifice . The condition that the mean free path in the source is greater than the smallest dimension of the nozzle orifice means that the Knudsen number is greater than unity. Under these conditions effusion from the orifice presents a negligible perturbation on the gas behind the nozzle and the molecule undergoes no collisions as it emerges.

Kinetic theory predicts that the number of molecules per second leaving such a source is given by

$$N = \frac{1}{4} n \bar{v} A_s \qquad (5)$$

where n is the number density behind the nozzle, $\bar{v}$ is the average molecular velocity of the bulk gas and A_s is the area of the nozzle slit. Molecules emerge in a cosine distribution; therefore, the forward flux intensity is less than the supersonic case where one has flux enhancement on the beam axis. The beam flux is less also because the gas pressures behind the nozzle must be much lower to satisfy the effusive condition. For example, in the NO + O_3 experiments with a 0.0055 inch nozzle diameter at 136K, the maximum pressure that could be used and still maintain an effusive expansion was 0.06 torr NO.

3. PUMPING CONSIDERATIONS

Experiments which must be conducted under single collision conditions must have the pumping capacity to remove the large gas load introduced by molecular beams, especially supersonic ones. For example, the number of He atoms at one atmosphere passing through a 0.003 inch diameter orifice at room temperature is approximately 1.2×10^{20} mole-

cules / second. To achieve a pressure of 10^{-6} torr in the collision center one would need to use unacceptably large and expensive pumping equipment. The pumping requirements are greatly reduced by using differential pumping, that is, using a fore chamber to pump away most of the gas load before the beam passes into the experimental chamber. Certain molecular beam experiments require a second differential pumping chamber to act as a pressure buffer between the source differtial chamber and the experimental chamber to keep the pressure sufficiently low in the collision center. Differential pumping reduces the requirement for exceptionally large vacuum pumps. For example, the NO + O_3 experiment which had one differential pumping stage for the supersonic beam used a 1800 liter/sec source diffusion pump for gas line pressures up to 700 torr and a 3000 liter/sec pump for 1000 torr He behind the supersonic nozzle. Although a machine with differential pumping is more complex, it often can be less expensive than an equivalent single chamber machine and in many cases it is the only way experiments that require ultra high vacuua can be designed.

C. SCOPE OF THIS WORK

This work consisted of two major experimental parts. First the excitation function of the NO + O_3 chemiluminescence was investigated with a supersonic NO beam and an effusive O_3 beam in order to determine how the system responds to an increase in translational energy. Four different translational energies were available using different mixtures of NO in He or Ar. The temperature of NO was varied continuously between 160 and 450K for each of these mixtures in order to have a continuous scan of translational energy. This experiment was intended

to produce a verification of the Redpath et al. (1978) excitation function. The second major part of this work was an investigation of the role of the internal energy states of NO in promoting chemiluminescence. The experiment was repeated with an effusive NO beam and a supersonic beam. The internal states of a molecule are preserved in an effusive expansion. It was possible to separate the effects of translation from internal energy. Internal energy effects were studied by changing the temperature of NO between 136K and 400 K. Translational effects were studied by changing the mole fraction of O_3 in He, thereby changing the collision energy.

II. EXPERIMENTAL

A. CHEMILUMINESCENCE MACHINE DESCRIPTION

1. VACUUM SYSTEM

A crossed molecular beam apparatus designed by C.C. Kahler and Y. T. Lee was used for all the chemiluminescence experiments (Kahler 1980). Figure 1 shows a side view of the machine. The dimensions on the drawing are shown approximately 1:7, i.e., the cover flanges at each end of the machine were 17 inches in diameter. The machine consisted of three chambers; the beam source chamber, the collision chamber, and the beam catcher chamber. Each chamber was pumped by a six inch diffusion pump and each chamber could be isolated from the pump by a gate valve.

The source chamber is the region in which the supersonic beam was formed. The reactant gas mixture was introduced into the gas inlet port at total pressures between 250-1000 torr. At the inner extreme of the gas inlet tube was a small orifice between 0.002-0.006 inches in diameter. As the gas emerged from this nozzle orifice into the vacuum, a supersonic beam was formed. This beam was collimated by a cone shaped skimmer on the front wall of the beam source. The skimmer diameter of 0.024 inches at a distance of 0.28 inches from the nozzle tip, created a beam of 2.5 degrees half angular width. The molecules that did not pass through the skimmer, i.e. 99 % of the total gas load, were pumped away by diffusion pump I. The beam source chamber, a differential pumping chamber for the supersonic beam , is used to reduce the total background pressure in the collision center. The total pressure in the beam source region was monitored by ion gauge I. In general, this pressure was less than 2×10^{-4} torr during the

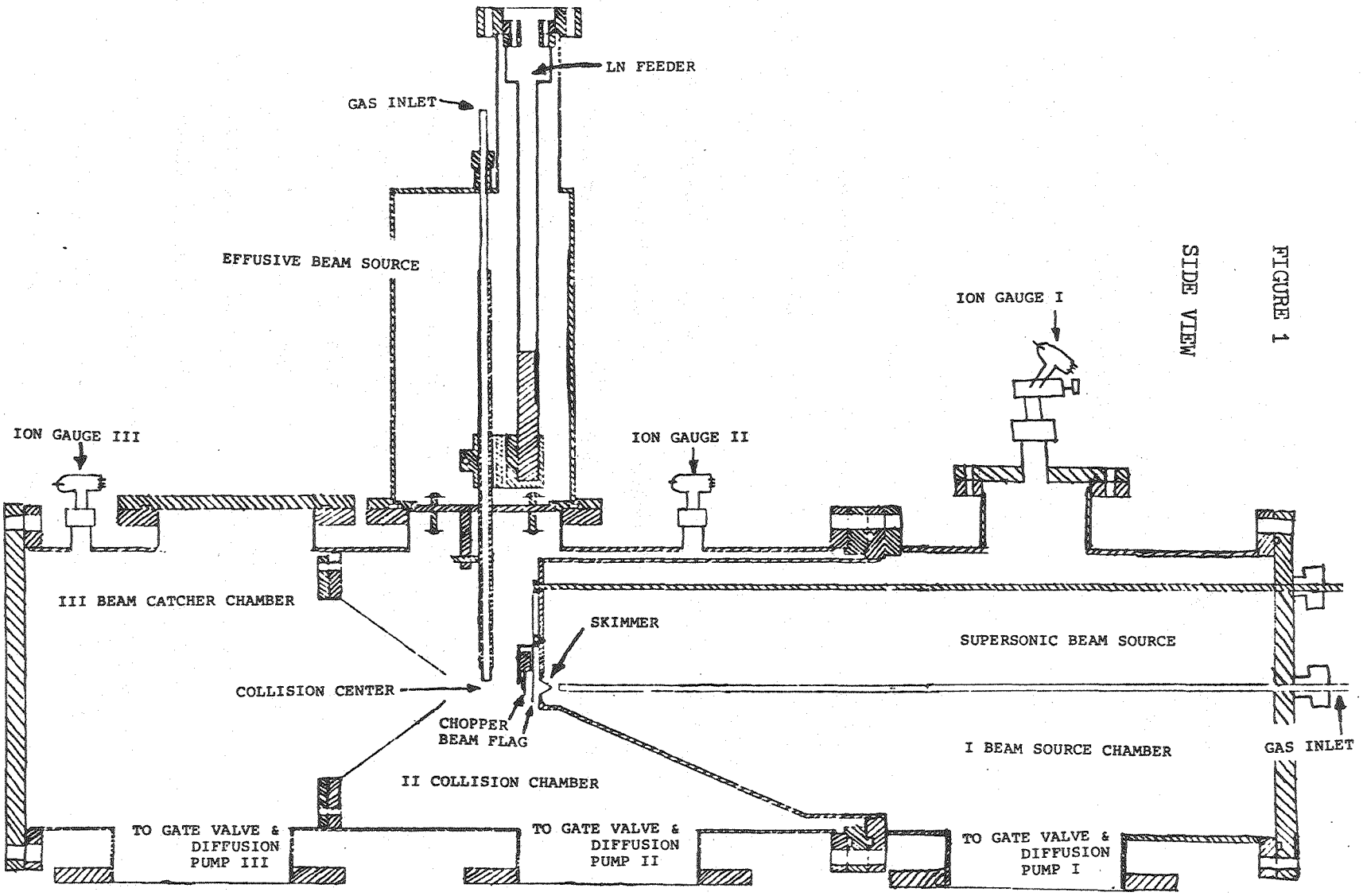

SIDE VIEW

FIGURE 1

experiments. If the pumping system was not efficient enough to keep the pressure below this limit, the supersonic beam would attenuate itself through a cloud of molecules that persist between the nozzle and the skimmer. At the higher gas pressures used in this experiment it was necessary to replace the six inch diffusion pump with a ten inch model backed with a larger mechanical pump to avoid these problems. The reading on the ion gauge I was directly proportional to the gas load introduced into the beam source chamber so that it was used to provide a relative beam number density normalization.

After passing through the skimmer into the reaction chamber, the supersonic beam was modulated with a 150 Hz tuning fork chopper (Bulova L 40). A beam flag, which was controllable from outside the vacuum , could be positioned before the beam to prevent molecules from reaching the collision center. It could also be used as an independent check on the operation of the tuning fork modulator and the two channel data system corresponding to chopper open or closed.

The effusive beam was introduced from above directly into the collision chamber at right angles to the supersonic source. This beam was formed by a low pressure, 0.02-15 torr, reactant gas behind a large nozzle orifice, 0.0055-0.008 inches. The beams produced could be purely effusive or in the transition region between effusive and supersonic, but not supersonic because it was necessary to keep the background pressure in the collision chamber below about 5×10^{-5} torr. At pressures above this value, collisional quenching of the long lived NO_2 will seriously compete with chemiluminescence. The ion gauge II in the collision chamber was used to verify that under operating conditions

the pressure was low enough; however ion gauges II and III were not used continuously, since the red glow of the filament scattered too much light into the light collection system. Gas which scattered from the molecular collisions as well as the entire load from the effusive beam source, was pumped by diffusion pump II. A liquid nitrogen trap before the diffusion pump was used during the experiments to prevent back - streaming which would coat the optical window. When experiments were not being done, the gate valve in this region was kept closed.

For alignment, the nozzle was placed about 0.2 inches above the collision center. A thin wire was placed into the nozzle orifice and was centered as follows. Two cathetometers were aligned through two sets of flanges whose relation to the collision center was known. This defined two axes in the plane of the supersonic beam, and the intersection of these axes defined the collision center. The nozzle was moved manually until the thin wire was exactly centered. The nozzle was then carefully secured outside the vacuum chamber, so that the atmospheric pressure against the vacuum would not disturb its position.

The final beam catcher chamber was separated from the collision chamber with a large cone designed with an aperture large enough to accept the entire width of the supersonic beam. This chamber was used to pump the gas load of the on-axis supersonic beam and to prevent these molecules from scattering back into the collision center. The cone separator was silver plated to act as an O_3 destroying catalyst. When the molecules reached the back flange, they hit a silver surface with a high surface area for more O_3 destruction. The diffusion pumps in regions II and III were fitted with silver foil on the output to

FIGURE 2

TOP VIEW

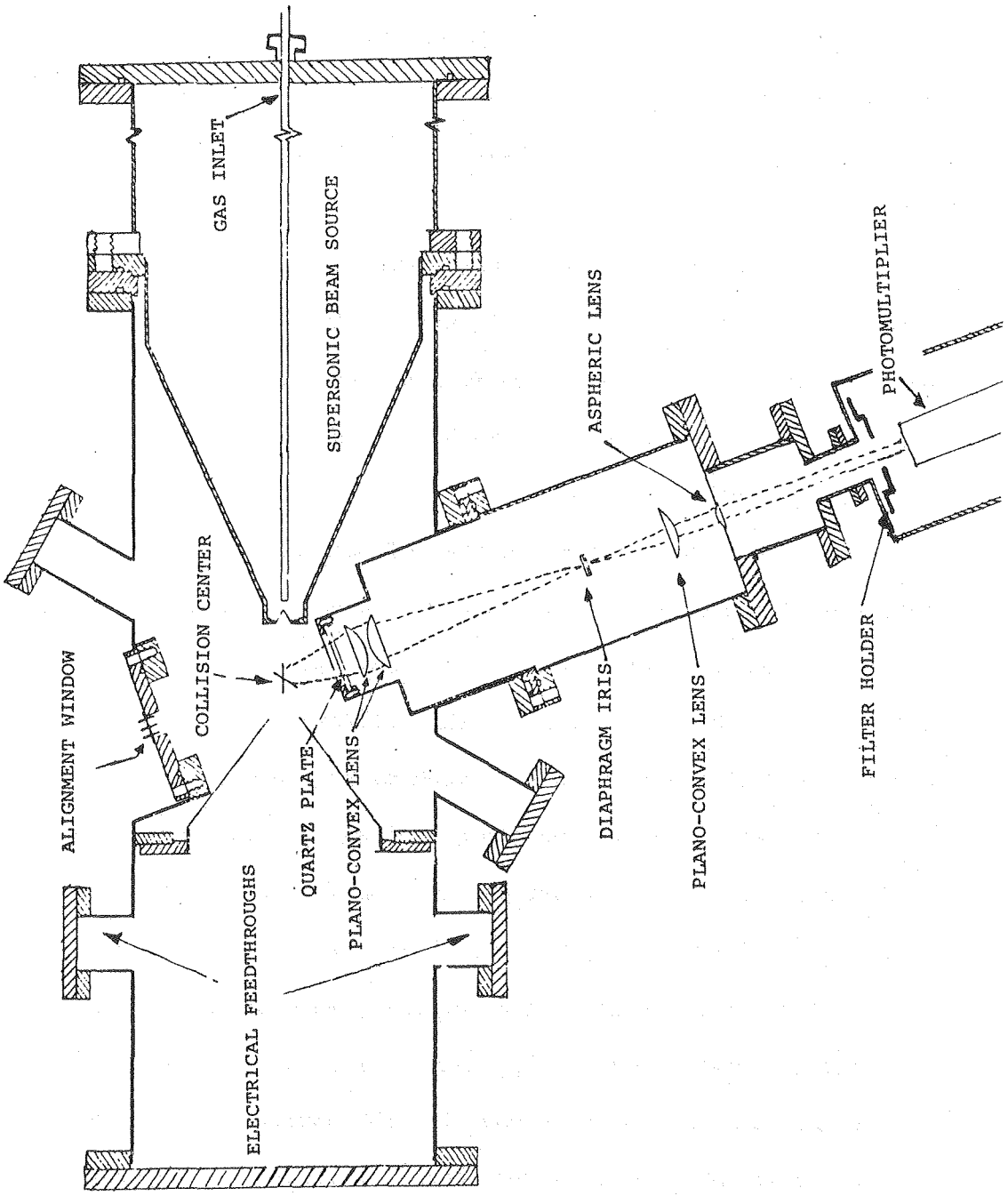

prevent excessive oxidation of the mechanical pump oil.

To minimize light scattering within the machine, the entire inner surface was painted with an oil based paint, 3M-101-C10 Nextel Velvet Black. The painted surfaces were very effective in reducing scattered light. Outgassing from the paint did not present a serious problem while experiments were in progress. It was necessary, however, to pump on the machine for about three days after the inner chamber was exposed to air for a few days, since the paint did slowly absorb atmospheric water vapor. The entire machine was lightproof after the ion gauges II and III were covered with a black cloth.

2.) THE OPTICAL SYSTEM

Figure 2 shows an overhead view of the machine. The beam source chamber and the beam catcher chamber show no additional features. The collision chamber region shows an optical system coupled to a photomultiplier which was focussed on the collision center. The optical system was designed to reduce as much as possible any stray light not originating at the collision center. A quartz plate separated the collision chamber which is under vacuum from the rest of the optical system which is at atmospheric pressure. This assured that the precise alignment of the lenses would not be deformed when the machine was evacuated. Atmospheric water vapor and CO_2 were eliminated by blowing dry nitrogen in the lens region and throughout the photomultiplier housing.

Chemiluminescence from the collision center reached the first plano-convex lens which sent the light out parallel. The second plano-convex lens refocussed the light at the position of the iris diaphragm. The size of the iris determined how large an area was being

sampled. A 1/8 inch diameter aperture sampled about $\frac{1}{4}$ cubic inch. Typically an aperture of about this magnitude was used for the NO + O_3 experiments. The size was varied untilan optimal signal to noise was achieved. The last plano-convex lens took the focused light and sent it out parallel. The final aspheric lens shaped the output light into an oval so that it would match the photomultiplier photocathode more exactly. All of the lenses were made of synthetic fused silica. The diameters of the plano-convex and aspheric lenses were two and one inch respectively. The refocussing scheme used in this optical system causes a significant gain in detection sensitivity since stray light and chemiluminescence not originating at the collision center were blocked by the iris diaphragm.

The light then passed through an adapter region and through narrow band pass filters which were used for the wavelength dependence study. The light then entered the photomultiplier, an RCA C31034A, an extended (to 900 nm) red sensitive tube with a GaAs photocathode.

3. DETECTION AND PHOTON COUNTING SYSTEM

The photomultiplier tube was cooled with dry ice to reduce the tube dark current. At such low temperatures thermal stresses between the glass tube and the metal pins and the Teflon tube socket can easily break the tube, especially during cooldown and warmup periods. To prevent this the Teflon socket pin holes were enlarged and the pins were allowed a 1/8 inch movement latitude within the socket that still adequately functioned as an electrical insulator. To prevent moisture condensation on the pins, the tube and socket assembly were sealed with electrical grade RTV and the voltage divider assembly beneath the

socket was potted. Moisture condensation near the front of the photomultiplier was prevented by inserting an evacuated quartz tube between the cooled housing and the warm air in the lens cavity. The dry ice housing and amplifier-discriminator used were obtained from Pacific Photometric Inc. (PP 3378, PP AD4).

The photomultiplier tube was supplied with -1500 volts from a regulated high voltage power supply. The signal from the photomultiplier was amplified by a high gain amplifier, and then sent to a discriminator which was set so that signals not originating as photons were rejected. The count rate was low enough so that digital photon counting was possible. The signal was then sent to a dual channel digital scaler (Ortec 9315). The dual digital scaler was gated by a timer gate module, which received pulses from the chopper and put out a gate signal to the scaler. The gate width was arranged so that 40 % of the chopper cycle corresponded to the chopper open, and the rest to partially or fully closed. The net chemiluminescence signal was the difference between the two scaler channels. Data averaging was done by accumulating counts for ten minutes and repeating this ten times. Each data point, therefore, is reported with a standard deviation based on ten separate determinations.

B. THE CHEMICAL REACTANTS

Four different NO reactant gas mixtures were used in these experiments, 1 % NO in He, 10 % NO in He, 100 % NO, and 24 % NO in Ar. The first two gas mixtures were supplied by the Matheson Company as was the pure NO. Care was taken by Matheson to insure that the mixture had the concentration specified and was free from decomposition product

impurities. The tanks used were passivated with the appropriate mixture for one month and the gas replaced with a fresh supply before being used. A verification by mass spectrometer indicated that the mixtures were correct and were not changing as a function of time. The 24 % NO in Ar mixture was prepared in our laboratory in a similar fashion and was also tested in the mass spectrometer.

The ozone reagent was prepared by a home made ozonizer. First, technical grade oxygen was passed through a low pressure regulator, a Rotometer flowmeter and into a 500° C simple quartz tube oven that contained copper turnings which oxidize the hydrocarbons present in the gas. The gas passed through an ascarite column to remove the CO_2 produced and through a silica gel tube cooled to dry ice temperatures to remove water and NO_2. The purified oxygen then entered the ozonizer.

The ozonizer consisted of two concentric tubes which created an annulus one centimeter wide through which the gas flowed. A sheet of Al foil was pressed to the outside of the outer tube and to the inside of the inner tube to create the two electrodes. 10-13 thousand volts AC were supplied by a neon sign transformer until some breakdown discharge began occuring. The best ozone yield ocurred at a discharge current of 24 milliamperes.

The ozone-oxygen mixture was passed through a four armed silica gel trap at dry ice temperature where the ozone was preferentially bound to the silica gel. Before the trap was used the silica gel was heated and pumped to remove adsorbed water and after saturation by ozone it was pumped again to remove the remaining oxygen within the

the trap.

For the effusive ozone experiments the ozone was connected directly to the nozzle tube. The supersonic ozone experiments used helium as a carrier gas which was introduced at one end of the cooled trap. As the carrier gas flowed through the trap, mixtures between 0.6 % O_3 and 1.2 % O_3 in He at a total pressure of 1000 torr were made. In both experiments the O_3 passed through a single beam ultraviolet spectrophotometer set at 300 nm in order to measure the O_3 concentration in the beam. All transfer lines were made of pyrex or quartz and the connections between the tubes were made of stainless steel Cajon fittings to prevent as much O_3 decomposition as possible. Special care was taken to insure that the glass tubes and vessels used were not cleaned with organic solvents or dichromate solutions which can leave an ozone destroying residue on the glass surface. Even with all these precautions it took four hours of gas flow through the lines before O_3 was detected flowing through the nozzle the first time.

C. TIME-OF-FLIGHT

1. EXPERIMENTAL

Each of the supersonic beams used needed to be velocity analyzed to determine how much energy was present in the molecular reaction. This was done in a separate vacuum chamber that had a quadrupole mass spectrometer (Extranuclear Corp.). The time-of-flight apparatus consisted of a differential pumping chamber and the flight chamber which contained a 17.8 inch diameter time of flight wheel with a 0.84 mm wide slot on one end and the mass spectrometer detector 19 cm away. The wheel was driven at 200 Hz when slowly moving species were

FIGURE 3

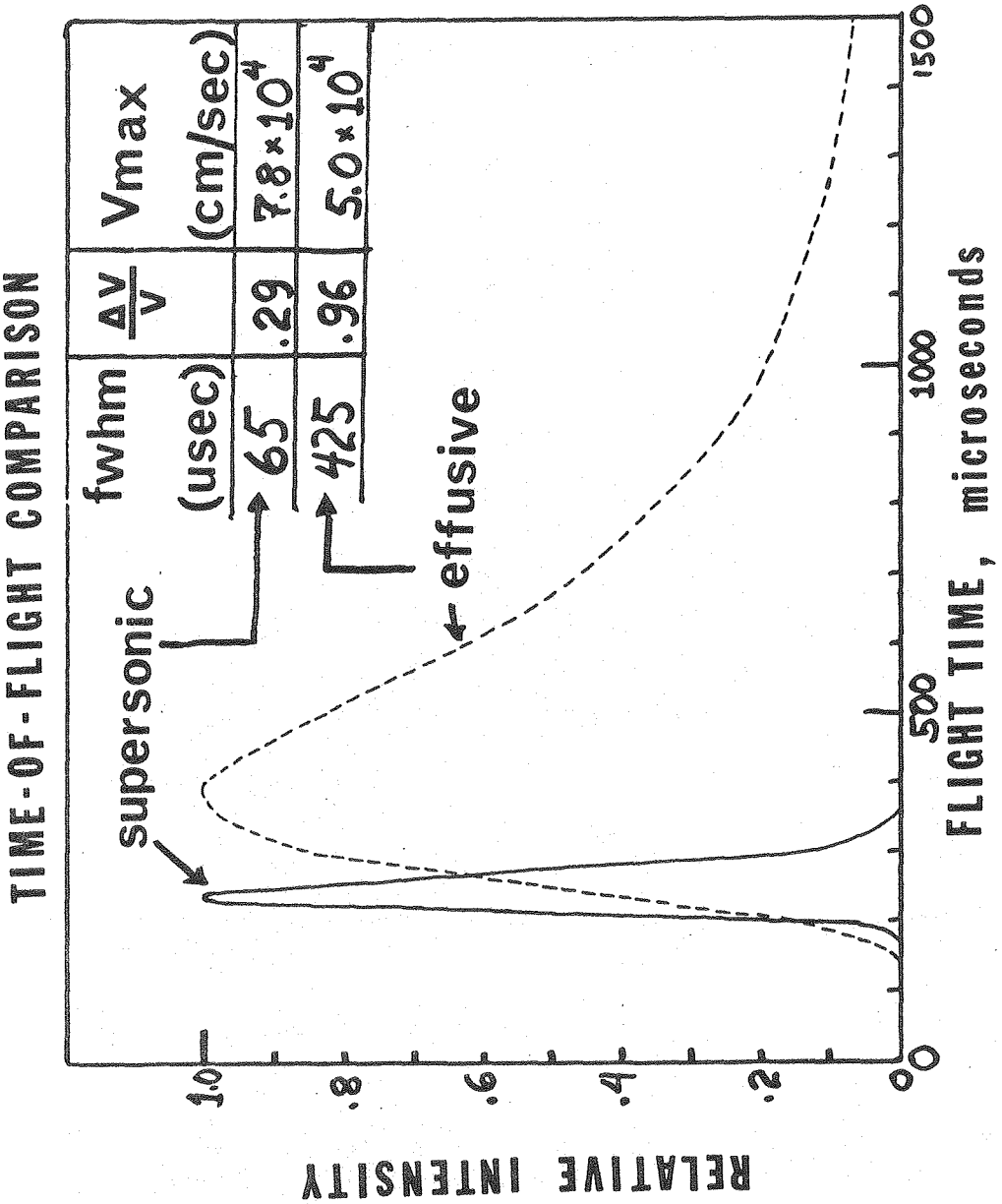
TIME-OF-FLIGHT COMPARISON
fwhm (usec)
ΔV/V
Vmax (cm/sec)
65
.29
7.8×10⁴
425
.96
5.0×10⁴
supersonic
effusive
RELATIVE INTENSITY
1.0
.8
.6
.4
.2
0
0
500
1000
1500
FLIGHT TIME, microseconds

FIGURE 4

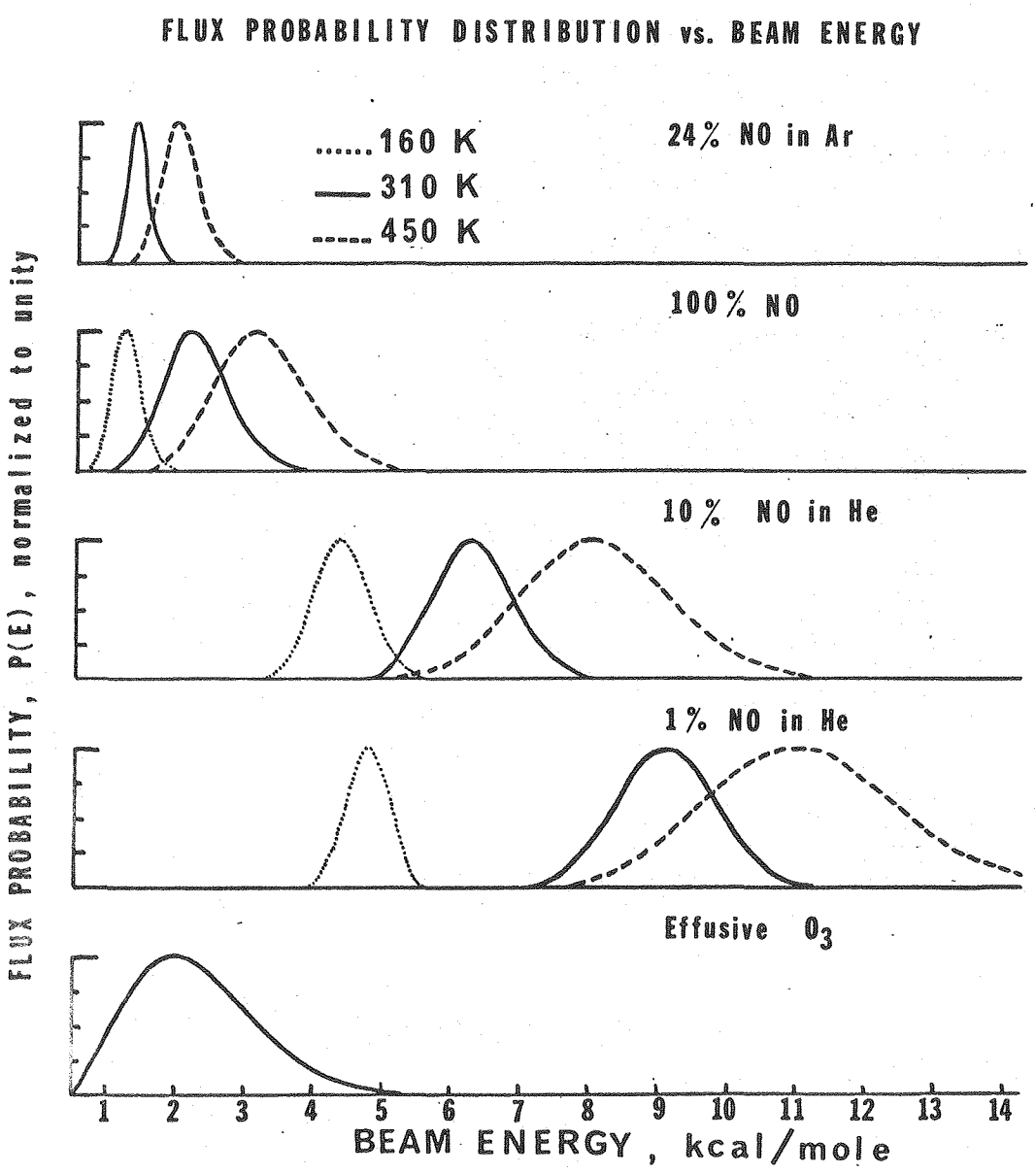
FLUX PROBABILITY DISTRIBUTION vs. BEAM ENERGY
.....160 K
——310 K
-----450 K
24% NO in Ar
100% NO
10% NO in He
1% NO in He
Effusive O_3
FLUX PROBABILITY, P(E), normalized to unity
1 2 3 4 5 6 7 8 9 10 11 12 13 14
BEAM ENERGY, kcal/mole

studied or at 300 Hz for faster moving ones. A separate gating signal was obtained from a small aperture on the time-of-flight wheel that passed in the path of a small light-emitting diode and detector. The arrival of the gate pulse signalled the beginning of a timing sequence on a multichannel scaler. Signal counts were accumulated for four microsecond intervals then stored in sequential channels of the multichannel scaler. The total spectra were accumulated until visual examination of the data on a storage oscilloscope showed negligible scatter, which generally took one minute. For the supersonic NO experiment TOF spectra were taken for each mixture at room temperature and at the extreme high and low temperatures used. For the effusive NO experiment TOF spectra were taken at six different O_3 in He gas mixtures. An example of the TOF spectrum obtained for 100 % NO at room temperature is shown in figure 3. The effusive distribution is calculated from kinetic theory and is shown for comparison.

2. TIME-OF-FLIGHT TO RELATIVE FLUX DISTRIBUTION

Computer program KELVIN was used for an initial deconvoltion of the data to eliminate experimental bias and program FLUX was used to convert the number density distribution vs. channel number to a flux probability distribution vs. velocity (Valentini 1976). Figure 4 shows the flux distributions normalized to unity for the gas mixtures used in the supersonic NO study. The velocity scale was converted to energy. One can see that the energy range spanned by the gas mixtures and temperatures is comprehensive.

In order to transform the TOF data which at this stage describe the individual beams to data which will describe the entire collision system,

it is necessary to use the center of mass coordinate system. The individual beam velocities are partitioned between the center-of-mass velocity which remains unchanged during the collision and the relative velocity between the particles which is available to the two reactants. This conversion was done by program RELAT. The total flux probability is given by

$$P(v) = F_1(v_1)\, F_2(v_2)\, V_{rel} \tag{6}$$

$$\text{where } V_{rel} = (v_1^2 + v_2^2 - 2v_1 v_2 \cos\theta)^{\frac{1}{2}} \tag{7}$$

$$E_{coll} = \tfrac{1}{2}\, \mu\, V_{rel}^2 \tag{8}$$

and where $F_1(v_1)$ and $F_2(v_2)$ are the flux distributions for beam 1 and 2 respectively, V_{rel} is the vector sum of the two beam velocities and θ corresponds to the angle between the two velocity vectors.
It was not necessary to consider collisions at angles other than 90 degrees because, although the molecular beams were quite wide, the photomultiplier detecting the chemiluminescence was focused on a small collision volume of about one cubic centimeter.

All possible combinations of the two beam velocities were made, and a relative velocity and a total flux probability were calculated for each combination. In a predetermined relative velocity interval, the flux values are summed then normalized to the highest value. A collision energy was also calculated and the histogram type summing and normalization were repeated so that the flux data were available for both equal velocity and equal energy spacings.

The output of the program RELAT is shown in figure 5 for the supersonic NO study. Again the same trends are seen in the total collision

FIGURE 5

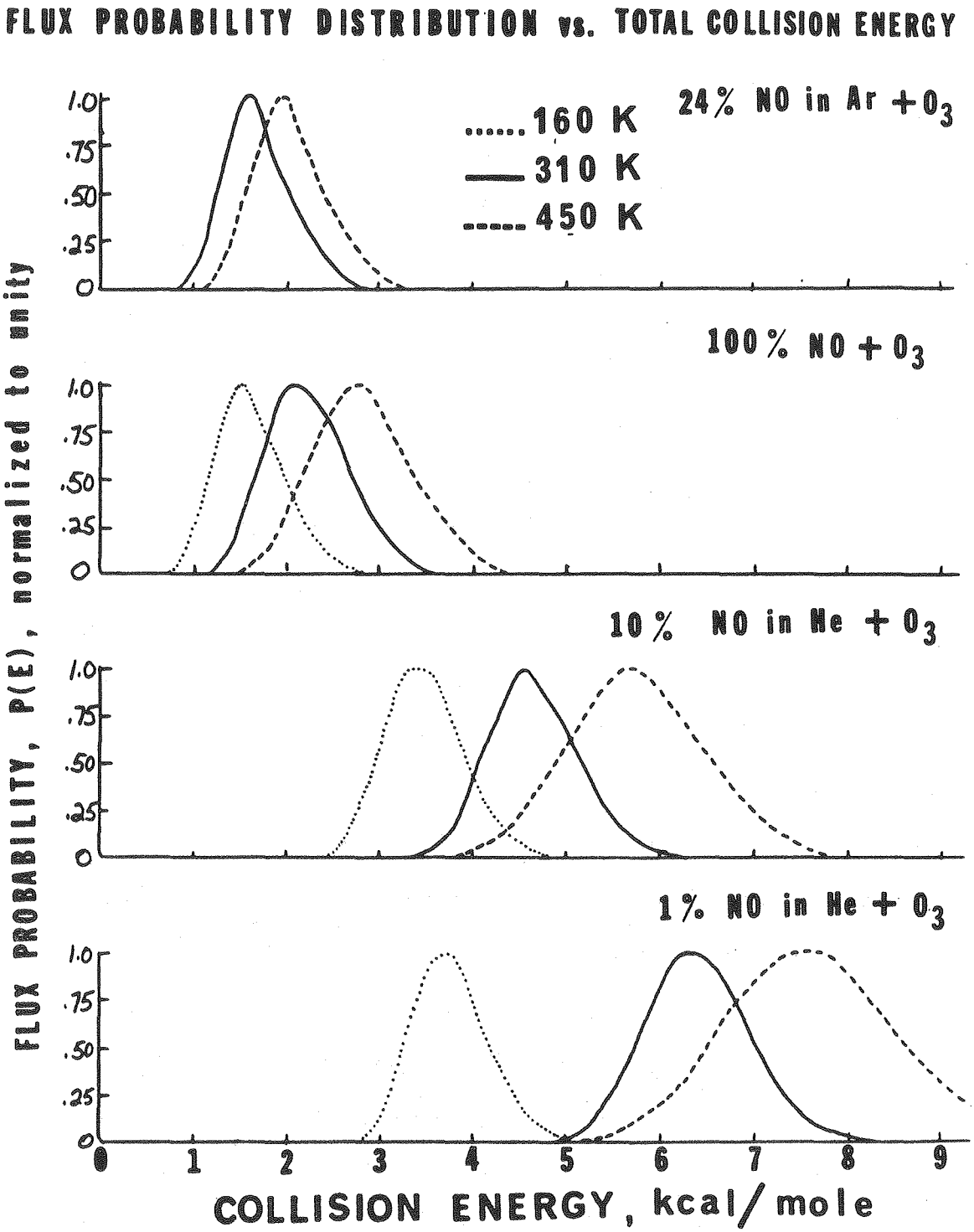
FLUX PROBABILITY DISTRIBUTION vs. TOTAL COLLISION ENERGY
24% NO in Ar + O3
160 K
310 K
450 K
100% NO + O3
10% NO in He + O3
1% NO in He + O3
FLUX PROBABILITY, P(E), normalized to unity
1.0
.75
.50
.25
0
0
1
2
3
4
5
6
7
8
9
COLLISION ENERGY, kcal/mole

flux probability as are seen in the individual beam flux probability The distributions are widened due to the large width of the effusive O_3 beam. In the effusive NO study the NO beam contributed even more velocity spread; however, since the supersonic O_3 beams are much narrower, the resulting collision energy spread was almost the same. As one expects, the distribution is shifted to higher energies and is widened with increasing gas temperatures.

D. EXPERIMENTAL PROCEDURES

1. SUPERSONIC NO STUDY

A 1 % NO in He mixture was prepared as stated previously . The pressure was continuously monitored during the experiment with a Wallace- Tiernan pressure gauge. The gas passed through a stainless steel tube that was held in place by a copper block which could be heated or cooled. Liquid nitrogen was supplied into the vacuum chamber through a large diameter tube that was in contact with the copper block. The bottom of the copper block was threaded eight times with high resistance heater wire in a ceramic insulator, which was connected to a vacuum feedthrough so that the heater current could be continuously controlled. The combination of liquid nitrogen, liquid nitrogen plus heat, and heat alone made it possible to have a continuously variable temperature-controlled nozzle source. The temperature of the nozzle was monitored with an iron-constantan thermocouple connected through a vacuum feedthrough that was later calibrated with the identical feedthrough configuration.

The ozone beam was fed into the chemiluminescence machine directly

above the collision center through a quartz tube at room temperature . The NO beam was slowly heated and stabilized at various intervals from room temperature to 400 K. The chemiluminescence at each temperature step was accumulated for 10 minutes and repeated 10 times for a total count time of 100 minutes. The temperature was then lowered by adding liquid nitrogen to the copper block, was stabilized at various temperature intervals and the chemiluminescence accumulated as before. The lowest practical temperature was 160 K, since below this the NO condensed. The temperature was then increased by adding more heat to the copper block until room temperature was reached. This gave two separate chemiluminescence determinations; one with an increasing temperature gradient and one with a decreasing gradient. These agreed with each other excellently. (See figures 7 and 8.) This entire procedure was repeated for each of the four seeding mixtures used.

2. SUPERSONIC BEAM FLUX DETERMINATION

In order to obtain the concentration normalized intensity, the O_3 concentration in the beam was measured by UV absorption as stated previously. The NO concentration needed to be normalized for the different number of molecules emerging as the temperature of the supersonic beam was changed. This was done by observing the pressure reading in the ion gauge above the source chamber, which gave a response directly proportional to the beam flux. This was verified by a beam flux determination. An ion gauge with a small entrance orifice was placed directly in the path of the supersonic beam. A steady state concentration develops within the gauge, signifying a condition where the flux into the gauge equals the flux out. The pressure reading of the gauge

gives the number density of the gas and the velocity distribution is known to be thermal therfore, one can easily calculate the flux of molecules leaving the ion gauge. The velocity of the supersonic beam is known from time-of-flight; therefore it is possible to also calculate the number density in the supersonic beam. The temperature dependence study of the 100 % NO supersonic beam flux showed that a direct correlation exists with the reading on the ion gauge I, which sits on top of the source chamber.

3.) WAVELENGTH DEPENDENCE STUDY

Both 400K and 300K with the 1 % NO in He and 10 % NO in He were used for the wavelength dependence study since these exhibited the most chemiluminescence. Narrow band pass interference filters from Bausch and Lomb were used for 450, 500, 550, 600, and 650 nm. These filters had a full width at half max band pass of 2 nm. In order to eliminate undesired windows present in the interference filters, a Corning 3-70 long pass cut off filter was used at 550, 600, and 650 nm. A Corning 3-73 cut off filter was used for 500 nm. Corning interference filters 2-78 and 7-85 were used for 700 nm and 800 nm respectively. These filters did not contain any undesirable windows. The use of a monochrometer was not attempted, since the chemiluminescence intensity was quite low, and dispersion losses through a monochrometer would have made the experiment impossible. The chemiluminescence was collected in the same way as outlined in the supersonic NO study.

4.) EFFUSIVE NO STUDY

The molecular beam configuration was reversed. The NO was intro-

duced from above and was now the effusive molecular beam. NO pressures low enough to ensure an effusive expansion were used, i.e. 0.01- 0.12 torr with a 0.055 inch nozzle diameter. The pressure was monitored before passing into the nozzle tube by a Pace Industries Transducer Model CD25 with a 5 torr maximum pressure head. The nozzle tube was stainless steel with a thick coating of electroplated copper on the outside. The copper coated tube was held in a solid copper clamp which had ceramic coated resistance wire threaded through it. The upper portion of the clamp was attached to a liquid nitrogen dewar through a large diameter closed feed tube. The chemiluminescence was collected as before at 400 K. The temperature was rapidly lowered to 136 K with liquid nitrogen, and again the chemiluminescence was accumulated. The time to change the temperature from 400K to 136 K was minimized so that the concentration in the supersonic beam would not change much. Since the process by which O_3 was mixed with the helium was a physical desorption of the O_3 from silica gel, its concentration steadily decreased with time. It became necessary to investigate the effect of these different concentrations on the chemiluminescence since they resulted in a change of the collision energy.

III RESULTS

A. SUPERSONIC NO STUDY

A calibration curve was set up for each gas mixture showing the relationship between the NO beam temperature and the mean collision energy which was determined from the maximum in the flux probability distributions shown in figure 5. This calibration is shown in figure 6. The linear appearance of the three lowest energy mixtures shows that good supersonic beams were created and that the seeded gas was carried along well by the carrier gas. The decrease one sees at the highest temperature of the 1 % NO in He shows that some slippage between the reactant and carrier gas occured. This could have been prevented by using a higher pressure behind the nozzle. In any case this is just a point of interest and does not affect the experimental results in any way.

A mean collision energy was identified for each temperature where chemiluminescence data were obtained. The results of the experiment for 1 % NO in He and 10 % NO in He are shown in figure 7. The count rate was sufficiently high that one standard deviation error bars would be contained within the data points as drawn. The experimental results for the 100 % NO and the 24 % NO in Ar are shown in figure 8. Here the error bars are one standard deviation of ten separate count accumulations. The ordinate is presented as a concentration normalized chemiluminescence. One can see that all the chemiluminescence data lie quite close to each other. Under identical expansion conditions these curves would trace each other perfectly. In reality one sees effects such as different energy distribution widths and different

FIGURE 6

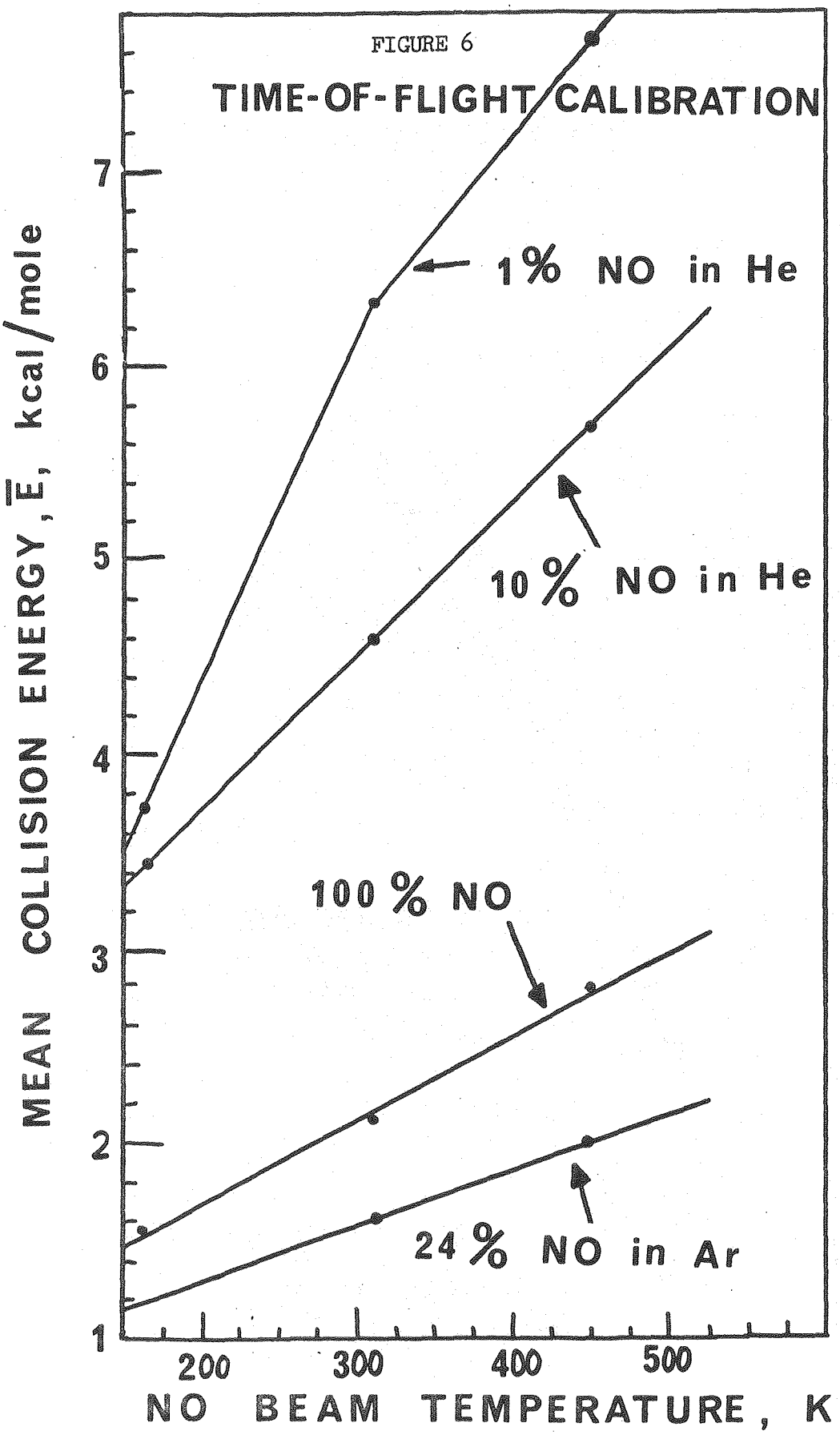
TIME-OF-FLIGHT CALIBRATION
1% NO in He
10% NO in He
100% NO
24% NO in Ar
MEAN COLLISION ENERGY, $\bar{E}$, kcal/mole
1
2
3
4
5
6
7
200
300
400
500
NO BEAM TEMPERATURE, K

FIGURE 7

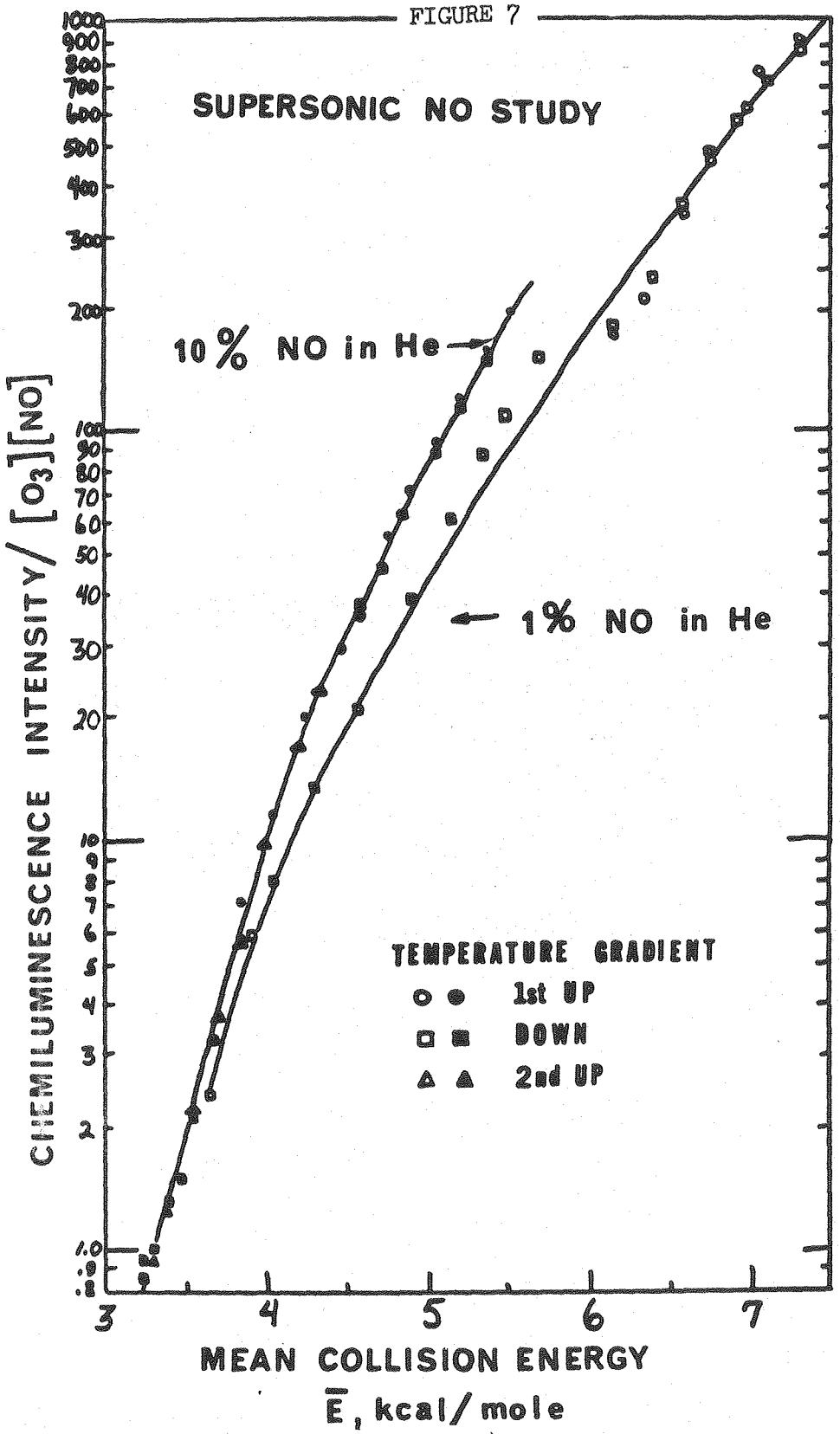
SUPERSONIC NO STUDY
10% NO in He
1% NO in He
TEMPERATURE GRADIENT
1st UP
DOWN
2nd UP
CHEMILUMINESCENCE INTENSITY/ [O3][NO]
MEAN COLLISION ENERGY
Ē, kcal/ mole

FIGURE 8

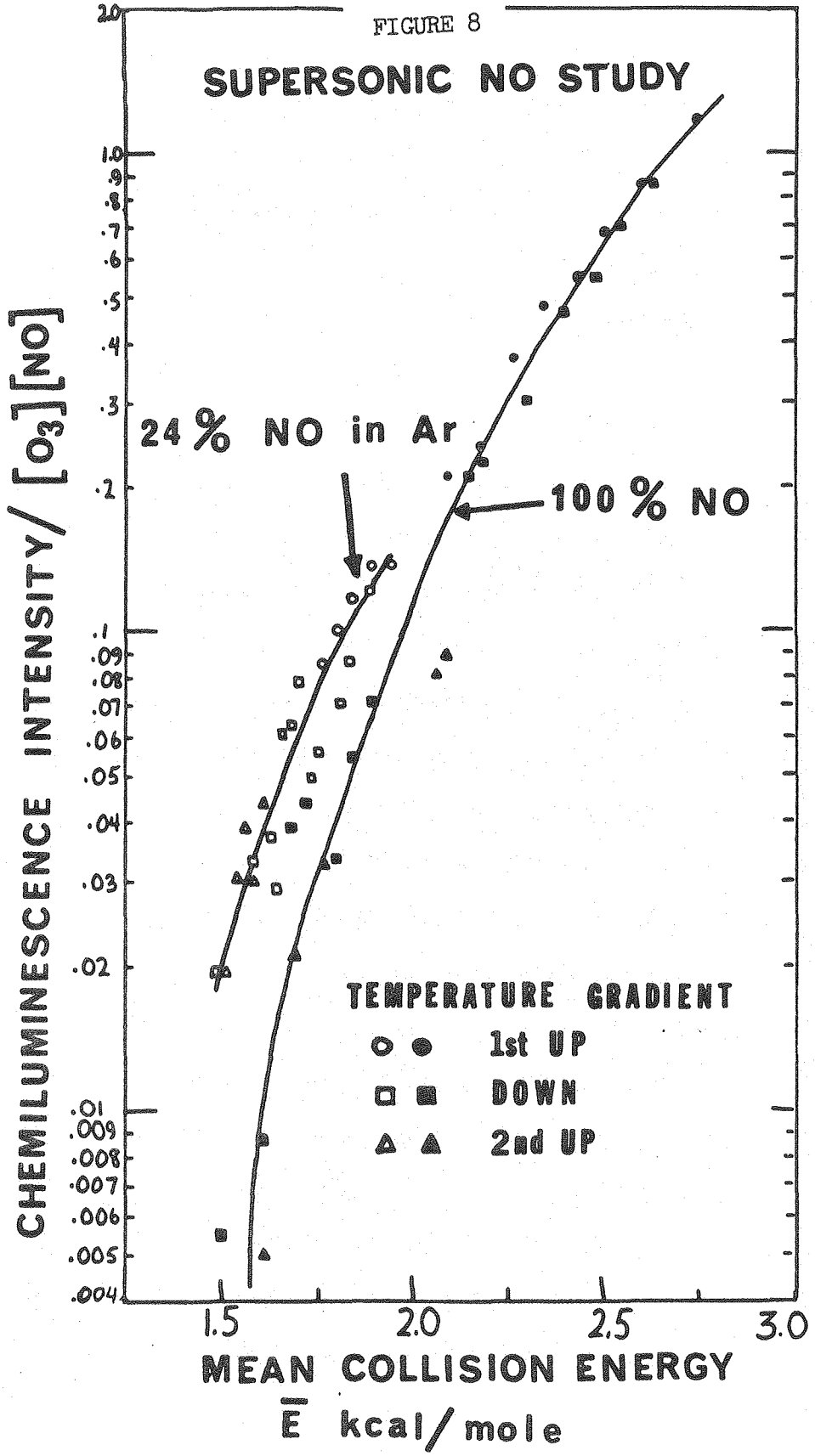
SUPERSONIC NO STUDY
24 % NO in Ar
100 % NO
TEMPERATURE GRADIENT
1st UP
DOWN
2nd UP
CHEMILUMINESCENCE INTENSITY / [O3][NO]
MEAN COLLISION ENERGY
Ē kcal/mole
1.5
2.0
2.5
3.0

flux intensity on the beam axis which can cause the data to diverge from each other. This clearly shows that it is not meaningful to discuss the results in terms of an absolute chemiluminescence yield.

The data were fit to

$$\sigma(E) = \sigma_o \left[\frac{E}{E_o} - 1 \right]^n \qquad E > E_o \qquad (9)$$

$$= 0 \qquad E \leqq E_o \ .$$

Values for E_o and n were chosen, and the theoretical cross section equation was convoluted with the total collision flux probability distribution to generate a calculated chemiluminescence signal. An experimental chemiluminescence intensity was available for each of the mixtures and temperatures for which a time-of-flight study was done. Both the calculated and experimental signals were normalized to unity with the highest temperature of each gas mixture. It was not possible to obtain a consistent fit by normalizing all the gas mixtures together. This is really not surprising due to expansion caused factors such as different reactant intensities on the beam axis. It had been considered that a suitable fit had been found when the calculated and experimental signal agreed reasonably well for the 10 % NO in He, 100 % NO and 24 % NO in Ar. The 1 % NO in He was not fit because the time-of-flight analysis showed that at the highest temperature significant beam slippage was occuring. This slippage disturbed the linear trend in collision energy and most certainly in the velocity width as well. Good fits were obtained by a wide variety of parameters; the best fit is given by

$$\sigma(E) = \sigma_o\left[\frac{E}{3.5} - 1\right]^{3.4} \qquad (10)$$

It is shown in figure 9. A comparison with the data for 10 % NO in He in figure 7 shows that the deconvoluted cross section over the energy range 4-5.5 kcal was steeper by a factor of two. This is an expected result due to the extreme energy dependence.

It is more justifiable to discuss a threshhold energy by using a line of centers model where the reaction occurs in all collisions whenever the potential energy at the distance of closest approach reaches a critical value E_o. It is generally given as

$$\sigma(E) = \sigma_o\left[1 - \frac{E_o}{E}\right] \qquad E > E_o \qquad (11)$$

$$= 0 \qquad E \leq E_o$$

The true chemiluminescence signal is an integral over all wavelengths, but the photomultiplier only senses about $\frac{1}{4}$ of the entire emission curve. When more energy is added to the system the entire emission curve is shifted toward the blue, hence the astronomical increases in signal. An excitation function for the reaction cross section as obtained from a molecular beam scattering experiment will differ from an excitation function for the chemiluminescence cross section. For this same reason it was necessary to raise the line-of-centers cross section to some large exponential factor before an adequate fit could be done. The best fit obtained was

$$\sigma(E) = \sigma_o\left[1 - \frac{3.5}{E}\right]^{5.1} \qquad (12)$$

FIGURE 9

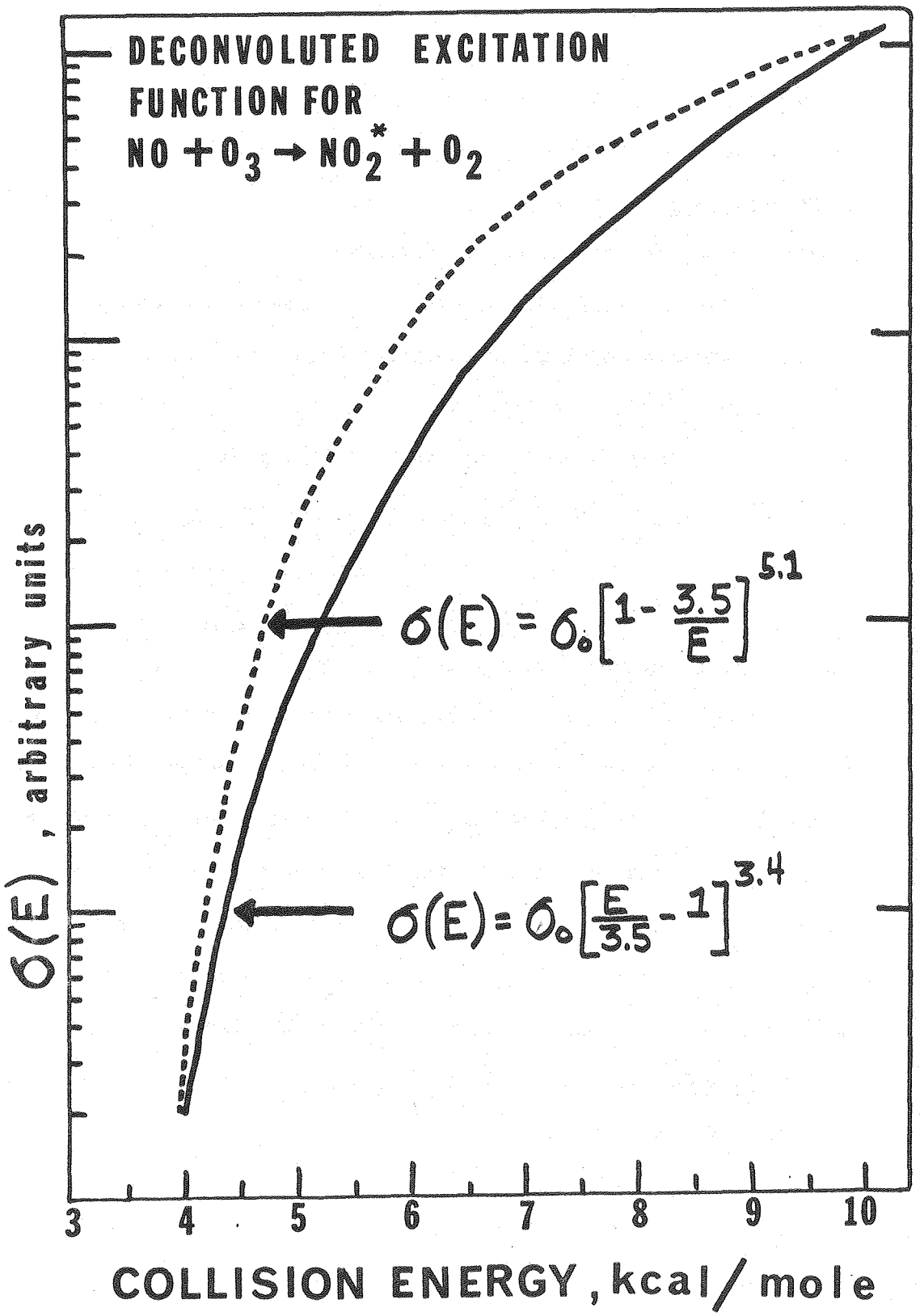
DECONVOLUTED EXCITATION FUNCTION FOR
NO + O3 → NO2* + O2
σ(E) = σ0 [1 - 3.5/E]^5.1
σ(E) = σ0 [E/3.5 - 1]^3.4
σ(E), arbitrary units
3
4
5
6
7
8
9
10
COLLISION ENERGY, kcal/mole

The deconvoluted line-of-centers excitation function is shown in figure 9. This equation did fit the lower energy data somewhat better than the previous fit.

B.) WAVELENGTH DEPENDENCE STUDY RESULTS

The wavelength dependence study was done with 1 % NO in He and 10 % NO in He at both 300 K and 400 K. The chemiluminescence intensity was normalized for the NO in the beam then plotted in figure 10 . All four experiments show a similar trend and turn downward near 800 nm. The room temperature emission of the NO + O_3 reaction has a threshold at 600 nm and peaks at 1200 nm (Clough and Thrush 1967). The emission curve for NO + O has a threshold at 400 nm and peaks at 600 nm (Ibaraki et al. 1972). The difference in these two curves can be explained exactly by the available energies from the exothermicities; 47.7 kcal/mole for NO + O_3 and 72 kcal/mole for NO + O. The added available energy resulted in a blue shift for the emission. In the experiment presented here the added 7 kcal/mole collision energy should move the emission peak to about 950 nm. The peak acually occurs between 700 and 800 nm and does appear to move toward lower wavelengths for increased collision energies. Perhaps this indicates that a mechanism other than a simple energy blue shift is ocurring, possibly introduced by the supersonic beam. The result of the effusive NO experiment that rotational states, especially the low J states of NO, have a strong effect on the total cross section point in this direction (Anderson et al. 1980). In a supersonic beam these low J states would be preferentially populated. Figure 10b with the data plotted as a function of mean collision energy shows that each wavelength parallels the other,

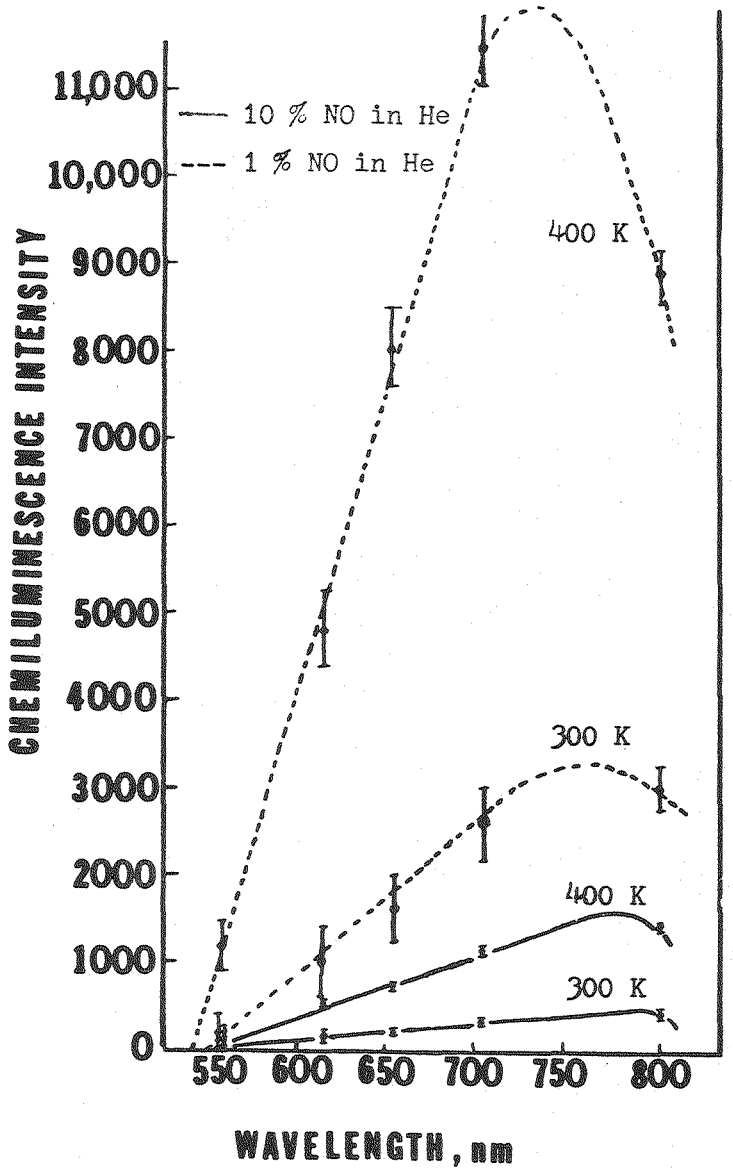
11,000
10,000
9000
8000
7000
6000
5000
4000
3000
2000
1000
0
CHEMILUMINESCENCE INTENSITY
10 % NO in He
1 % NO in He
400 K
300 K
400 K
300 K
550 600 650 700 750 800
WAVELENGTH, nm

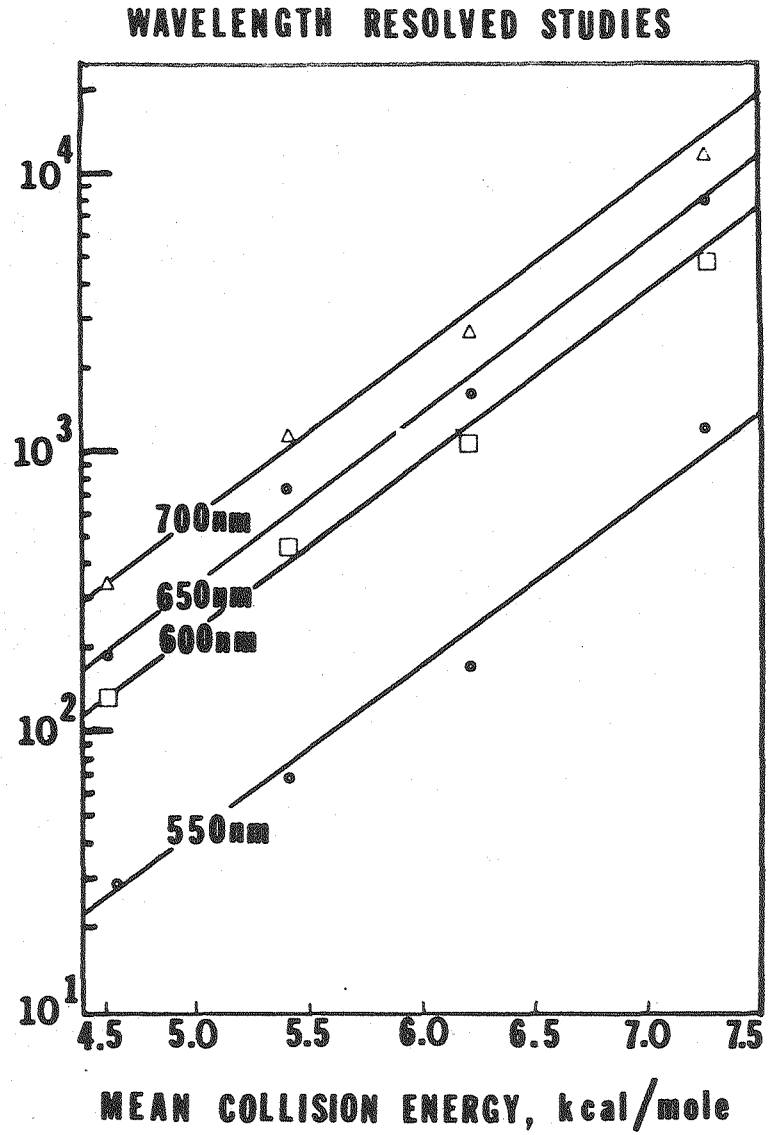
WAVELENGTH RESOLVED STUDIES
10^4
10^3
10^2
10^1
700nm
650nm
600nm
550nm
4.5 5.0 5.5 6.0 6.5 7.0 7.5
MEAN COLLISION ENERGY, kcal/mole

FIGURE 10

and upon comparison with figure 7 it is clear that they also parallel the unresolved (wavelength) chemiluminescence intensity as well.

C. EFFUSIVE NO STUDY RESULTS

A crucial aspect to this study was the verification that the NO beam was truly effusive. From kinetic theory it is possible to calculate the pressure regime under which effusive conditions should exist for a specific nozzle size and gas temperature. Experimentally this was checked by doing a pressure dependence study of the chemiluminescence intensity. If effusive conditions prevail then the result will be a straight line, since the beam flux is directly proportional to the pressure behind the nozzle as stated in equation 5. Both figures 11a and 11b show a marked curvature indicating that a flux enhancement on the beam axis is occuring. In order to eliminate this supersonic effect it was necessary to use pressures about a factor of ten more conservative than the calculated limit.

Figure 12 show the final result where effusive conditions occur. The chemiluminescence data are shown for 400 K and 136 K. Since the lower temperature beam has a higher beam flux from the increased gas density, it was necessary to normalize the curves to each other. The gas pressure in the line was measured at room temperature. The delivery tube was wide enough to permit assuming that this pressure persists throughout the heated and cooled region of the tube up to the nozzle tip. One desires the same NO beam flux at both temperatures; therefore, using equation 5 one gets the following ratio;

$$\frac{N_c}{N_h} = \frac{\sqrt{T_h}}{\sqrt{T_c}} \frac{P_c}{P_h} = 1 \qquad (13)$$

FIGURE 11

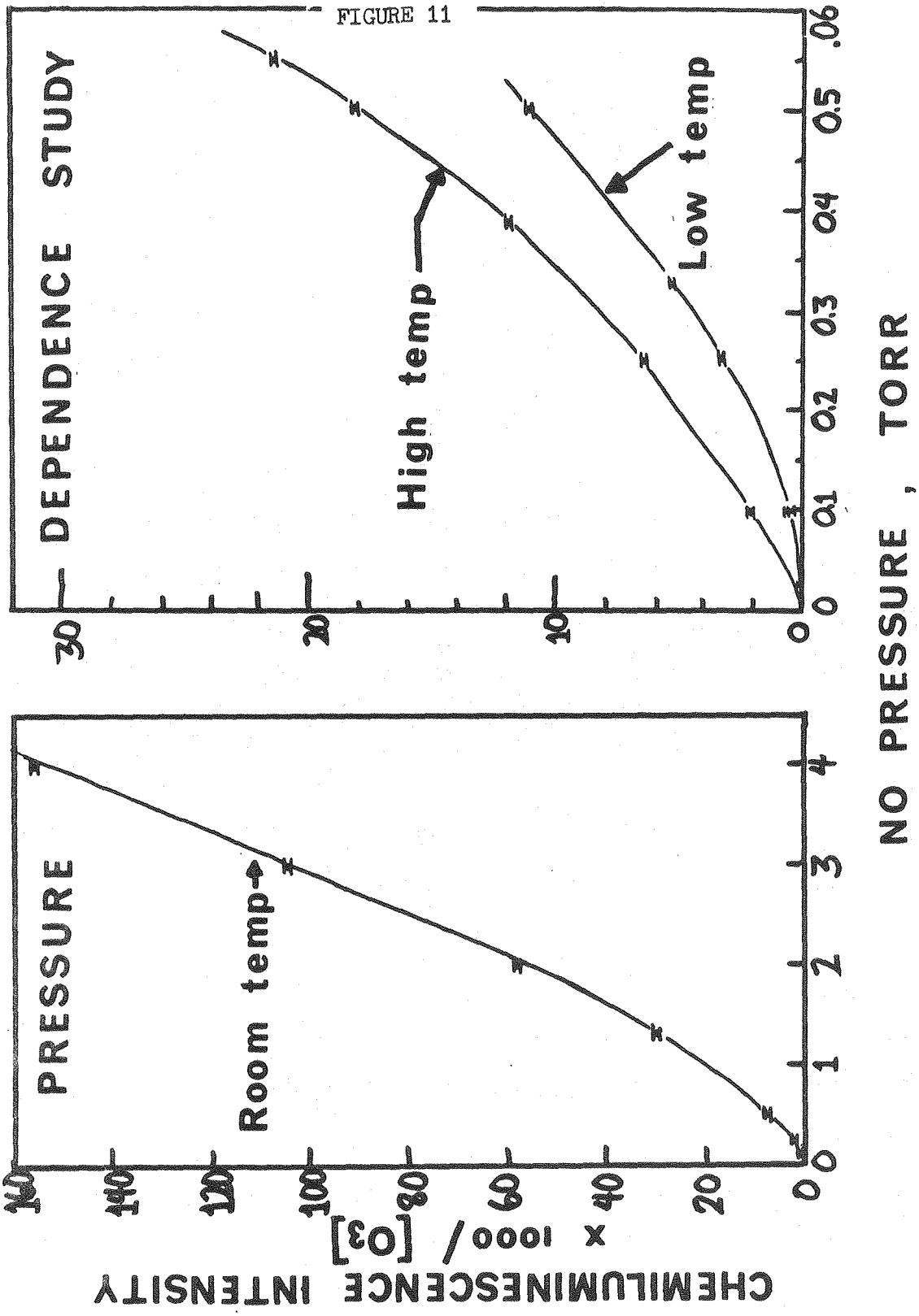
DEPENDENCE STUDY
High temp
Low temp
PRESSURE
Room temp
CHEMILUMINESCENCE INTENSITY
x 1000 / [O3]
NO PRESSURE , TORR

FIGURE 12

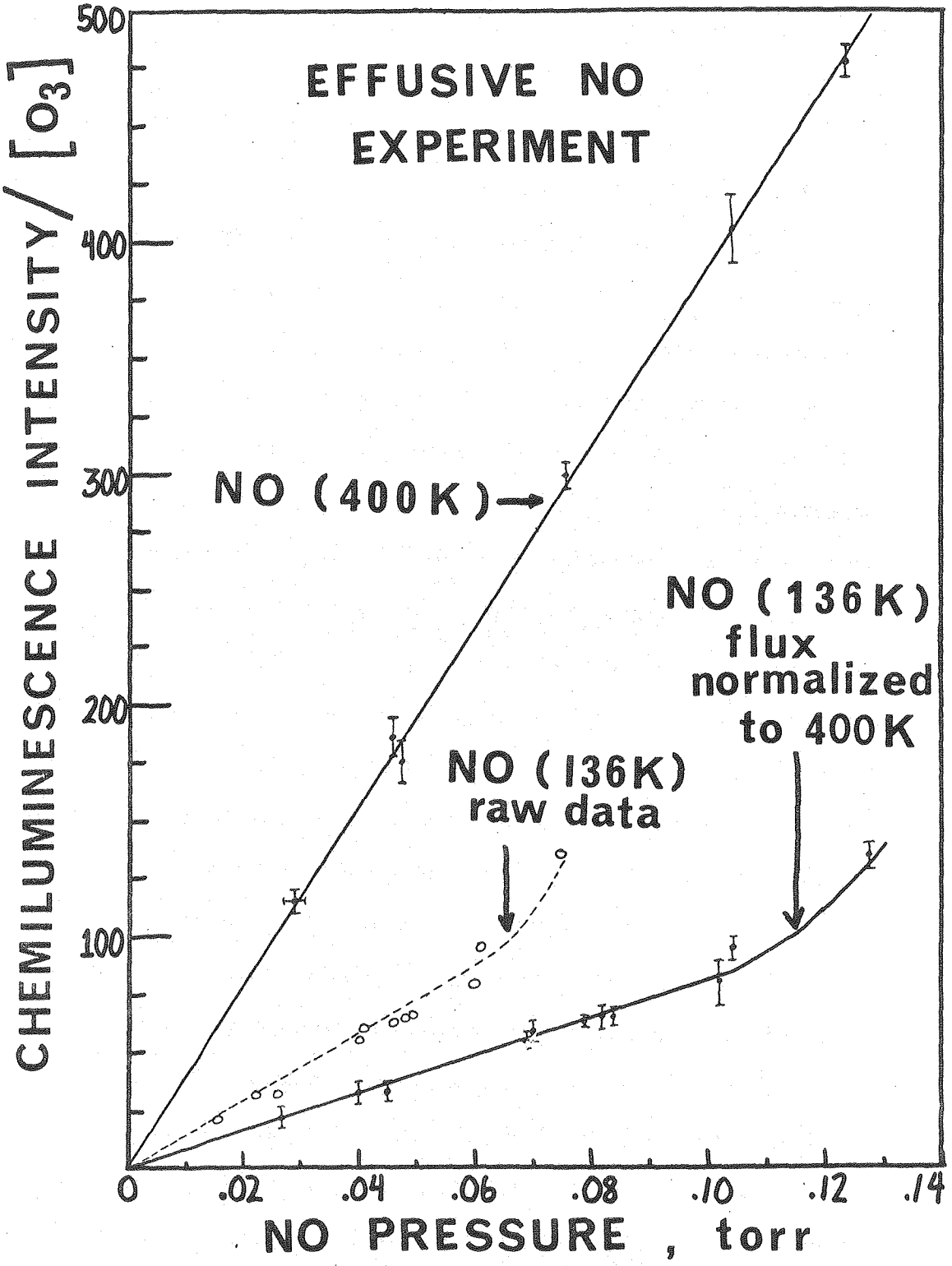
EFFUSIVE NO
EXPERIMENT
NO (400K)
NO (136K)
flux
normalized
to 400K
NO (136K)
raw data
CHEMILUMINESCENCE INTENSITY/ [O3]
NO PRESSURE , torr
500
400
300
200
100
0
.02
.04
.06
.08
.10
.12
.14

which becomes P(400 K) = 1.71 P(136 K) . This was used to lower the NO pressure at 136 K so that it would correspond to the same beam flux as the 400 K curve.

Ideally the O_3 concentration in the supersonic beam should not change while the experiment is in progress. In practice the O_3 was physically desorbing from the silica gel trap, so that its concentration was slowly decreasing with time. This was easy to account for in the supersonic NO experiment where the O_3 was an effusive beam by just correcting for the concentration change. In this study the changing O_3 concentration is changing the seeding ratio of the O_3 in He, thereby also changing the energy of the O_3 beam. This is especially true since the O_3 is seeded in a very light gas. The desorption rate off the silica gel is also much faster for the seeded beam because of the greater flux due to the helium gas. The NO + O_3 reaction is strongly dependent on collision energy; therefore, this must be considered rather carefully. Figure 13 shows a separate experiment where the NO beam was kept at either 400K or 136K and the seeding ratio of the O_3 was varied. As one can see over the range of gas mixtures used in this experiment, the chemiluminescence varied by as much as 40 %. The dashed lines as drawn were used to energy normalize the data in figure 12. The data for the effusive NO experiment are summarized in table I.

An energy normalization of this sort could have been done using the chemiluminescence vs collision energy results of figures 7 and 8; however, it is not clear that the same chemical behavior operates for both studies (supersonic and effusive NO). In order to verify that the same mechanism was indeed operative, one needs to compare the results

FIGURE 13

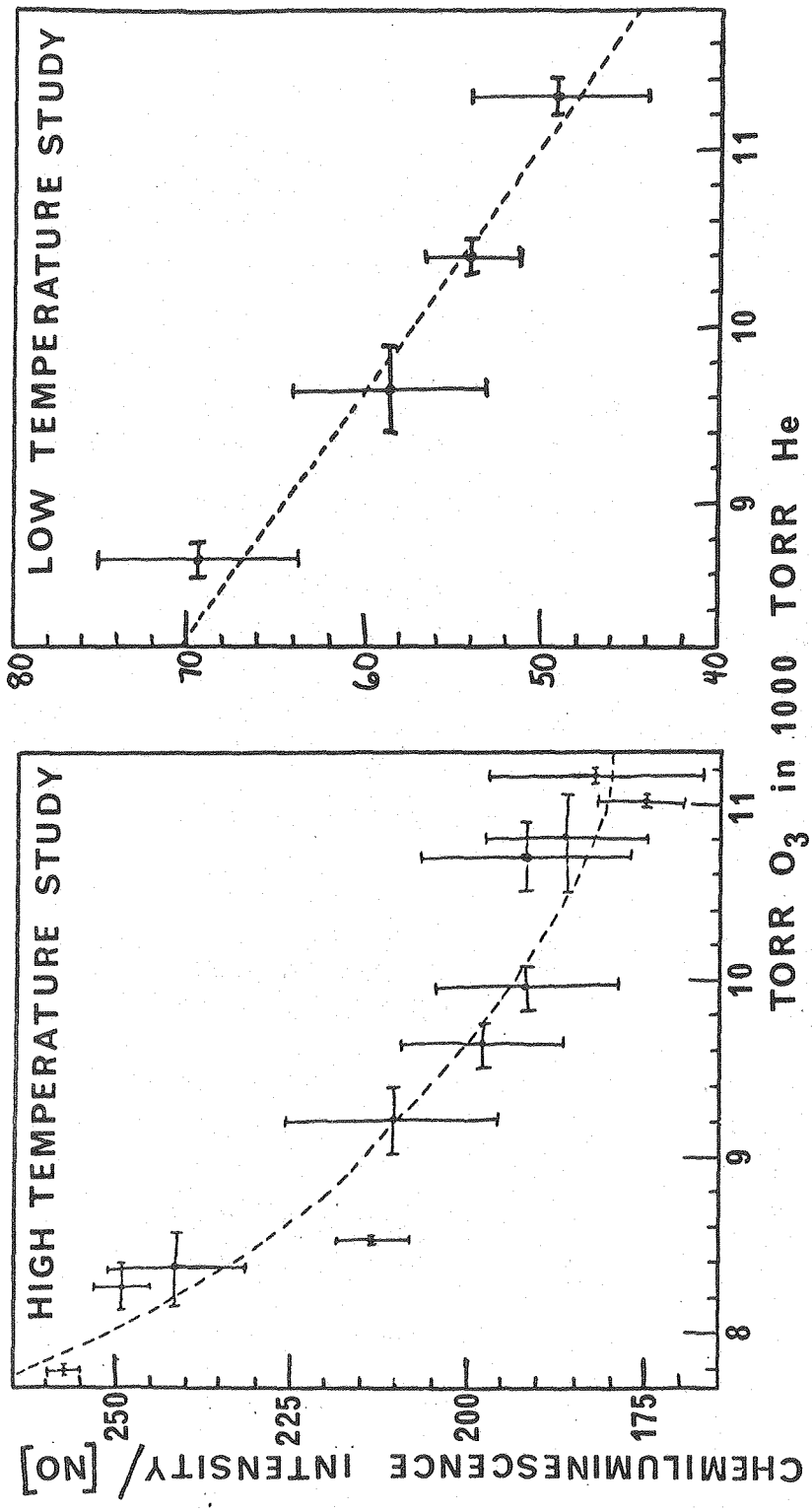
LOW TEMPERATURE STUDY
HIGH TEMPERATURE STUDY
CHEMILUMINESCENCE INTENSITY/ [NO]
TORR O_3 in 1000 TORR He
80
70
60
50
40
250
225
200
175
8
9
10
11

TABLE I

DATA AND ANALYSIS SUMMARY: EFFUSIVE NO STUDY

TEMP, K	PRESSURE TORR		CHEMILUMINESCENCE/[O_3]		
	NO (136K IS FLUX NORMALIZED TO 400K)	O_3 IN 1000 TORR He	DATA arbitrary units	ENERGY NORMALIZED	[NO] NORMALIZED
400	.030	8.8-9.4	123.2±7.2	116.0±6.7	3867
136	.016(.027)	8.8-9.0	25.5±5.6	22.5±4.9	833
400	.047	8.0-8.4	190.9±10.8	178.0±10.1	3787
136	.023(.039)	8.7-9.2	37.4±4.5	33.1±4.0	846
400	.046	10.3-10.4	185.4±8.5	187.3±8.5	4065
136	.026(.045)	9.3-10.7	33.0±3.9	33.0±3.9	733
400	.076	7.3-7.6	348.3±7.2	297.4±6.1	3908
136	.041(.071)	7.7-8.0	76.2±6.2	60.0±4.9	857
400	.104	9.9-10.9	397.8±13.9	404.2±14.1	3885
136	.061(.104)	8.9-9.2	105.9±6.2	94.7±5.5	910
404	.123	7.6-8.0	550.4±8.9	478.5±7.7	3886
135	.075(.128)	7.6-8.1	172.9±6.7	136.2±5.3	*
400	.055	8.1-8.5	252.1±9.8	224.1±8.7	4072
400	.058	7.0	285.3±4.2	234.0±0.4	4034
400	.061	7.4-7.7	305.6±13.1	259.8±11.1	4263
136	.060(.102)	10.4-10.7	74.5±8.7	80.5±9.4	789
136	.049(.084)	8.7-9.2	73.6±8.3	65.1±7.3	774
136	.048(.082)	7.5-7.6	86.0±8.9	65.9±6.8	805
136	.046(.079)	9.6-9.8	65.8±3.1	63.8±3.0	810
136	.040(.069)	10.5-10.6	52.8±5.1	56,4±5.5	817

* Supersonic effects, point was neglected.

of both studies in the center-of-mass coordinate system. A time-of-flight study of the supersonic beam was done, a beam velocity and energy flux distribution for O_3 was calculated with program FLUX, and a relative collision energy for the NO + O_3 system was determined from program RELAT. Once collision energies were identified for the effusive O_3 system, it was possible to compare energy dependence results with the supersonic NO study. The chemiluminescence at 136 K for the two O_3 pressure extremes shown in figure 13b was identical with that determined from the 1 % NO in He and 10 % NO in He shown in figure 7. This seems to indicate that the same chemiluminescence mechanism is operative for both the supersonic and low temperature effusive NO studies. The results from the high temperature experiment do not agree as well. This is an expected result which will be discussed near the end of this chapter.

The time of flight analysis shows that the mean collision energy for the NO(400K) + O_3 is 5.7 kcal/mole, and for the NO(136K) + O_3 it is 5.2 kcal/mole. Since this is a purely translational energy effect caused by the hot and cold NO, it is valid to use the supersonic NO data to determine its contribution to the difference observed in the two systems. From the 1 % NO in He experiment it is clear that the higher temperature chemiluminescence data in the effusive NO study must be divided by two to remove the higher collision energy effect introduced by the 400K NO.

From figure 12 it is possible to determine a chemiluminescence enhancement from the ratio of the signal at 400K to 136K. It is easier to use an NO concentration normalized value to discuss these ratios.

The final column in table I gives these for all the data. Note that the data are arranged in 400K - 136K pairs for experiments done sequentially and are listed separately for some individual determinations. All the data regardless of how they were collected show similar concentration normalized values. The average of the 400 K data is 3974 ± 146 and the average of the 136 K data is 817 ± 49. The last data point for 136 K was disregarded because supersonic effects were beginning to appear. The ratio of the chemiluminescence intensity at 400 K to 136 K is 4.86. When one accounts for the enhanced 400 K signal due to NO translation, the ratio becomes 2.43 ± 0.17.

So far this ratio has been corrected for differences in NO beam flux, NO and O_3 concentrations, collision energy due to O_3 seeding difficulties, and for collision energy due to the two NO temperatures. The two NO temperatures also affect the internal energy levels of the NO molecule. It is well established that an enhancement in chemiluminescence is observed when the v = 1 vibrational level of NO is pumped by a CO laser, i.e. $\sigma(v=1)=5.7\,\sigma(v=0)$, (Stephenson and Freund 1976). The fractional increase in v=1 one would obtain by the temperature change is calculated by using $N_1/N_0=\exp-\omega/kT$, where $\omega=1904\ cm^{-1}$. The ratio $N_1/N_0=1.06 \times 10^{-3}$ for 400 K NO and 1.54×10^{-9} for NO at 136 K. There is insufficient population in v=1 to change the chemiluminsescence enhancement ratio.

One can next consider that the chemiluminescence enhancement ratio may be caused by the electronic spin-orbit state which will be enhanced at 400 K. A large change in the relative populations of the $^2\pi_{3/2}$ and $^2\pi_{3/2}$ states is accessible with the 400 K and 136 K NO beams, since the

splitting between the two states is only 121 cm^{-1}. The fraction of NO in the $^2\pi_{3/2}$ state can be calculated from

$f = \exp(-h\nu/kT) / (1+ \exp(-h\nu/kT)$ and is shown in figure 14.

The expected chemiluminescence enhancement ratio can be calculated from

$$R = \frac{\left[X_{3/2}\sigma_{3/2} + X_{1/2}\sigma_{1/2}\right]_{T=400\,K}}{\left[X_{3/2}\sigma_{3/2} + X_{1/2}\sigma_{1/2}\right]_{T=136\,K}} \qquad (14)$$

where X is the mole fraction obtained from figure 14. If one assumes the chemiluminescence cross section reported by Redpath et al. (1978), i.e. $\sigma_{1/2} = n\sigma_{3/2}$ where $0<n<0.25$, one obtains a range $1.86>R>1.32$ for the chemiluminescence enhancement ratio. If one is more drastic and assumes that $\sigma_{1/2} = \sigma_{3/2}$, the ratio equals one. Clearly the ratio of 2.43 ± 0.17 obtained in the effusive NO study cannot be accounted for by the electronic state enhancement alone. Rotational effects remain by exclusion.

A closer examination of figure 6 reported by Redpath et al. (1978), shows that for the NO in He mixture the signal intensity ratio for 573 K / 281 K at 5 kcal/mole is 2.5, for the NO in H_2 at 5 kcal/mole is 5 and at 8 kcal/mole it is 4.3. Applying equation 14 using the change in the electronic population states at 573K(f_2= 0.35) and 281K(f_2=0.41) one calculates that the ratio should be 1.17 if only the upper state contributes to the chemiluminescence and 1.09 if the lower state is 0.25 times as effective as the upper one. It seems that the data presented by Redpath are inconsistent with the conclusion that primarily electronic excitation is responsible for the observed

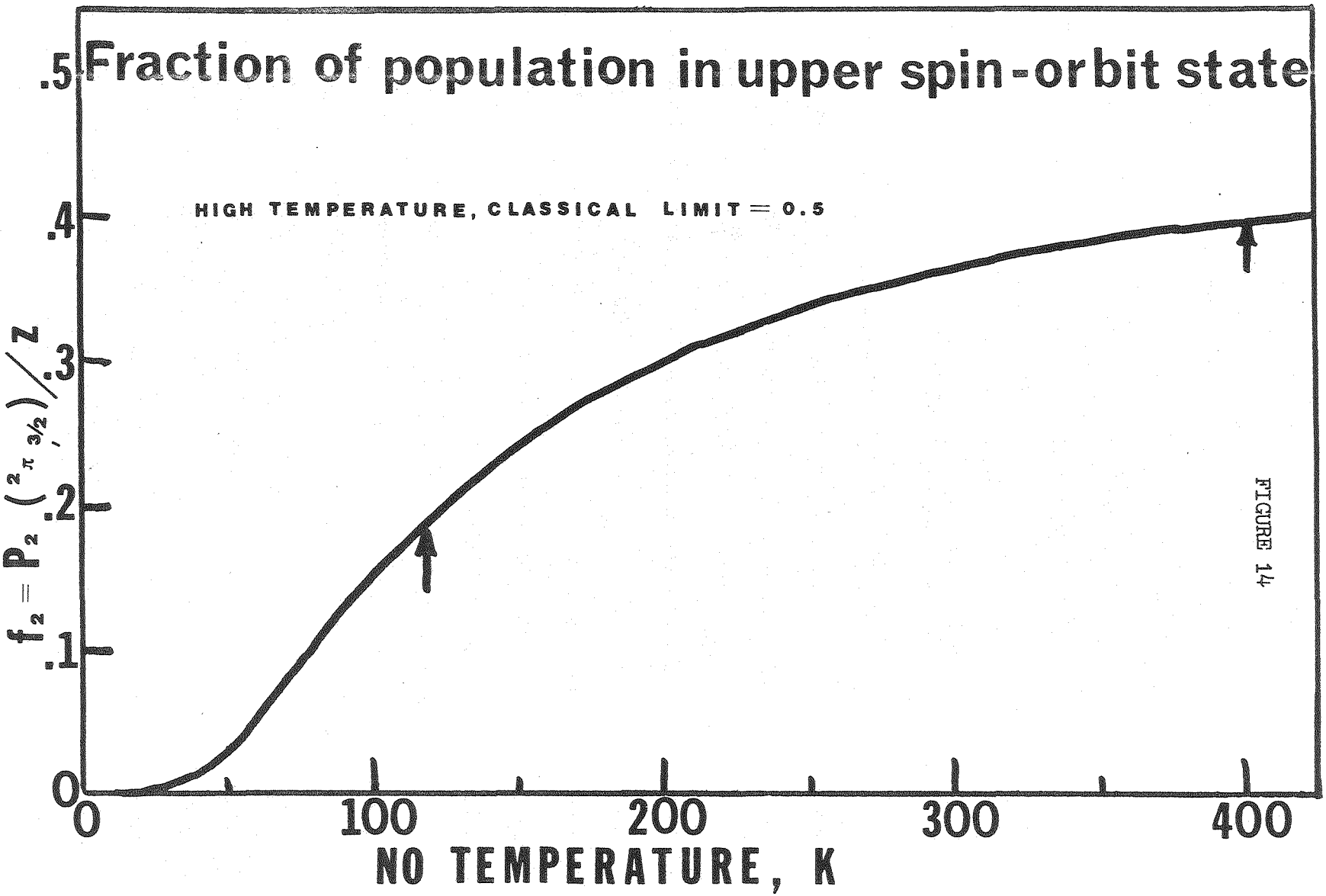
Fraction of population in upper spin-orbit state
HIGH TEMPERATURE, CLASSICAL LIMIT = 0.5
$f_2 = P_2 \left({}^2\pi_{3/2} \right) / Z$
.5
.4
.3
.2
.1
0
0
100
200
300
400
NO TEMPERATURE, K

FIGURE 14

enhancement and that $\sigma(^2\pi_{1/2}) =$ n $\sigma(^2\pi_{3/2})$. Deconvolution of the data will change the experimental ratios somewhat, but even with quite wide energy distributions shown in their figure 4, it seems unlikely that the experimental ratio could be brought into agreement with the calculated one. The experimental data agrees with those presented in this study and in both cases rotational effects must be contributing to the observed enhancements.

It is interesting to compare the experimental ratios of NO in He vs NO in H_2 shown by Redpath et al. The beams seeded in H_2 are more effective in promoting the enhancement. One would expect more relaxation to be taking place in the NO in H_2 case, since v-v energy transfer could occur. This does not help to resolve the electronic vs low J rotational contribution to the enhancement because more relaxation would diminish the effect of both similtaneously.

A similar examination of the results in figure 4 presented by van den Ende and Stolte (1980) can be done for 100 K and 300 K. The enhancement ratios calculated by equation 14 are 2.4 for $\sigma_{1/2} = 0$ and 1.4 for $\sigma_{1/2} = 0.27\ \sigma_{3/2}$. The experimental ratios are 1.36, 1.48 and 1.66 for the 14.3, 17.5 and 19.3 kcal/mole translational energy curves. These fall within the limits set by $\sigma_{1/2} = 0.27 \pm 0.03\ \sigma_{3/2}$, but the trend of decreasing slopes with translational energy indicates that at translational energies below 14 kcal/mole this would no longer be true. It is likely that the NO + O_3 reaction becomes less energy specific with high collision energies, so that it is difficult to extrapolate high energy data to predict behavior near the reaction threshold.

The experiments of Anderson et al. (1980), done with magnetic state selection of the spin orbit state, is not consistent with the result that the $^2\pi_{3/2}$ state is more reactive than the $^2\pi_{1/2}$ state. The results indicate that the $^2\pi_{1/2}$ state is five times as reactive as the $^2\pi_{3/2}$ state, the exact reverse. Another consistent explanation is that rotational states are responsible for the enhanced chemiluminescence. Their data were fit to $\sigma = E_{rot}^{\ n}$ where $1.8<n<2.5$.

The role of the rotational states cam be examined by calculating the rotational energy distribution from the statistical mechanical relation $N_1/N_0=(2J+1)\exp(-1.7cm^{-1}J(J+1)/kT)$ and the rotational energy as a function of J state from $E(J)=4.9x10^{-3}J(J+1)$kcal/mole. It is easy for us to characterize the NO beam, since the expansion used is an effusive one as opposed to the supersonic ones used by both Redpath et al. and van den Ende and Stolte. The mean rotational energies calculated for 400 K and 136 K are 0.8 and 0.27 kcal/mole. If one assumes the simple model where the reactive cross section increases with J, it is useful to set up a ratio and estimate a value for n.

$$R = \frac{E_{rot}^{\ n} \text{ at } 400 \text{ K}}{E_{rot}^{\ n} \text{ at } 136 \text{ K}} \qquad (15)$$

The observed chemiluminescence ratio of 2.43 yields n=0.84. A similar analysis done by Anderson et al. on the data of Redpath et al. indicates a value of $1.5<n<2.5$.

Other indications in our experiment point in favor of the rotational energy explanation. The low temperature energy dependence study shown in figure 13 for the effusive NO study agreed quite well with the energy dependencies shown in figure 7 for the supersonic NO

study. The high temperature data of figure 13 showed a much greater increase in chemiluminescence than would be indicated by just a translational energy effect. A difference in these two cases could be expected because the low temperature NO beam would be expected to resemble the supersonic NO beam in its internal state distribution more than would the hot NO beam. It is also possible that a rotational effect is responsible for the blue shift of the emission peak with respect to its threshhold which can be seen in figure 10 (discussed in the wavelength dependence study results).

It must be mentioned that implicit in this whole discussion has been the assumption that the different modes of energy are separable. Although in general this is not the case, it is a reasonable approximation for a first estimate.

IV CONCLUSION

The chemiluminescent NO + O_3 reaction was studied to determine the effect of the various forms of energy on the chemiluminescence cross section. The first experiment, done with a supersonic NO beam and an effusive O_3 beam, showed a steeply varying excitation function in th energy range between 3 and 9 kcal/mole. A wavelength dependence study showed a blue shift with collision energy. The final experiment, done with a supersonic O_3 and effusive NO beam was designed to preserve the internal energy states of the NO. It showed a similar energy dependence for 136 K NO but not for 400 K NO. An enhancement of the chemiluminescence intensity was observed when normalized data for NO(400K)+O_3 and NO(136K)+O_3 were compared. It was shown that this enhancement was not consistent with the premise that it was due entirely to the upper state, NO $^2\pi_{3/2}$, enhancement at higher temperatures. It was shown that the results were consistent with the idea that rotational states contribute to the enhancement. The results of Redpath et al. (1978) were examined and the data were found to agree with those presented here, even though the conclusions reached by the authors was different. If only rotation was the source of the enhancement, the chemiluminescence reaction cross section increased with increasing J for low J. It is still possible that the electronic state $^2\pi_{3/2}$ is responsible for some of the enhancement observed.

V. FIGURE CAPTIONS

Figure 1. Side view of the chemiluminescence machine.

Figure 2. Overhead view of the chemiluminescence machine.

Figure 3. Flight times from time-of-flight determination for the supersonic 100 % NO beam. A calculation of the effusive flight time is given for comparison. The flight path length is 19 cm.

Figure 4. Flux probability distributions obtained at three temperatures for each gas mixture used in the supersonic NO study. The effusive O_3 is actually "quasi-effusive" since time-of-flight analysis showed it to have Mach number =3.

Figure 5. Flux probability distributions obtained for the entire collision system, calculated from program RELAT.

Figure 6. Mean collision energy has been determined for each mixture at which a time-of-flight study has been done. This was identified with a NO beam temperature to permit the calibration of the chemiluminescence data to follow.

Figure 7. Results for the higher energy regime chemiluminescence for the supersonic NO study. The chemiluminescence intensity has been normalized for the NO and O_3 concentrations,

however the absolute value of the ordinate is in arbitrary units i.e. counts/100 minutes.

Figure 8. Results for the lower energy regime. The intensity of chemiluminescence is on the same scale as figure 7.

Figure 9. Deconvoluted excitation function determined from the supersonic NO study.

Figure 10. Wavelength dependence studies. These show a consistent energy behavior and a peak in the wavelength region 750 - 800 nm.

Figure 11. Pressure dependence study for the effusive NO study. The curvature seen here indicates that supersonic effects are present at these pressures.

Figure 12. Final results of the effusive NO study. No curvature is evident at 400 K. The 136 K data shows some curvature at the highest pressure point. This point was eliminated from the subsequent analysis. The raw data line for 136 K has been obtained at the pressure values listed. A flux normalized line has been included to allow direct comparison with the 400 K data.

Figure 13. An energy dependence study for the effusive NO study, done

at both NO= 136 K and 400 K.

Figure 14. Fraction of the population that is in the upper spin orbit state, NO($^2\pi_{3/2}$). The arrows show the two temperature extremes used in the effusive NO study.

VI . REFERENCES

ANDERSON, S. L., BROOKS, P. R., FITE, J. D., VAN NGUYEN, O. (1980), Reaction of Magnetically-State Selected NO with O_3: Effect of fs States and Rotational States on Reactivity, manuscript in preparation.

BAR-ZIV, E., MOY, J., GORDON, R. J. (1978), Temperature Dependence of the Laser Enhanced Reaction Nitric Oxide + Ozone (001) II. Contribution from Reactive and Nonreactive Channels, J. Chem. Phys. 68, 1013-1021.

BRAND, J. C. D., CHAN, W. H., and HARDWICK, J. L. (1975), Rotational Analysis of the 8000-9000 Å Bands of Nitrogen Dioxide, J. Molec. Spectry. 56, 309-328.

BRAUN, W., KURYLO, M. J., KALDOR, A., and WAYNE, R. P. (1974), Infrared Laser Enhanced Reactions: Spectral Distribution of the NO_2 Chemiluminescence Produced in the Reaction of Vibrationally Excited O_3 with NO, J. Chem. Phys. 61, 461-464.

CLOUGH, P. N. and THRUSH, B. A. (1967), Mechanism of the Chemiluminescent Reaction Between Nitric Oxide and Ozone, Trans. Faraday Soc. 63, 915-925.

FREUND, S. M. and STEPHENSON, J. C. (1976), Laser Enhanced Chemical Reaction Between Ozone (001) and Nitric Oxide, Chem. Phys. Lett. 41, 157-159.

GAUTHIER, M. and SNELLING, D. R. (1973), Possible Production of $O_2(^1\Delta g)$ and $O_2(^1\Sigma g^+)$ in the Reaction of NO with O_3, Chem. Phys. Lett. 20, 178-181.

GORDON, R. J. and LIN, M. C. (1973), Reaction of Nitric Oxide with Vibrationally Excited Ozone, Chem. Phys. Lett. 22, 262-268.

GORDON, R. J. and LIN, M. C. (1976), The Reaction of Nitric Oxide with Vibrationally Excited Ozone II, J. Chem. Phys. 64, 1058-1064.

HUI, K. K., ROSEN, D. I. and COOL, T. A. (1975), Intermode Energy Transfer in Vibrationally Excited Ozone, Chem. Phys. Lett. 32, 141-143.

HUI, K. K. and COOL, T. A. (1978), Experiments Concerning the Laser Enhanced Reaction Between Vibrationally Excited Ozone and Nitric Oxide, J. Chem. Phys. 68, 1022-1037.

IBARAKE, T., KUSONOKE, I. and KODERA, K. (1972), Study of the Chemiluminescence by Means of Crossed Molecular Beams: Nitric Oxide- Oxygen Atom System, Chemistry Lett.,Chem. Soc. of Japan, 309-312.

KAHLER, C. C. (1980), Crossed Molecular Beam Studies of Chemiluminescent Reactions, Ph.D. Thesis, UC Berkeley.

KOMORNICKI, A., GEORGE, T. and MORAKUMA, K. (1976), How Much do Multiple Electronic Surfaces Influence Chemical Reactivity? $F + H_2$: A Case Study, J. Chem. Phys. 65, 4312-4314.

KURYLO, M. J., BRAUN, W., KALDOR, A., FREUND, S. M. and WAYNE, R. P. (1974), Infra-red Laser Enhanced Reactions: Chemistry of Vibrationally Excited O_3 with NO and $O_2(^1\Delta)$. J. Photochem. 3, 71-87.

KURYLO, M. J., BRAUN, W., XUAN, C. N. and KALDOR, A. (1975), Infra-red Laser Enhanced Reactions: Temperature Resolution of the Chemical Dynamics of the NO + O_3 Reaction System, J. Chem. Phys. 62, 2065-2071.

KURYLO, M. J., BRAUN, W., XUAN, C. N. and KALDOR, A. (1975), Eratum: Infra-red Laser Enhanced Reactions: Temperature Resolution of the Chemical Dynamics of the NO + O_3 Reaction System, J. Chem.Phys. 63, 1042.

MIESCHER, E., LEE, Y.T. and GÜRTLER, P. (1978), Autoionization of Nitric Oxide (NO) at the First Ionization Limit, J. Chem. Phys. 68, 2753-2756.

MOY, J., BAR-ZIV, E. and GORDON, R. J. (1977), Temperature Dependence of the Laser Enhanced Reaction Nitric Oxide + Ozone (001) $\longrightarrow$ Nitrogen Dioxide ($^2B_{1,2}$), J. Chem. Phys. 66, 5439-5446.

REDPATH, A. E. and MENZINGER, M. (1971), Molecular Beam Chemiluminescence: I. Kinetic Energy Dependence of the NO + O_3 $\longrightarrow$ NO_2 + O_2 Reaction, Can. J, Chem. 49, 3063-3066.

REDPATH, A. E. and MENZINGER, M. (1975), Molecular Beam Chemiluminescence. V. Reactivities of Nitrogen Monoxide ($^2\pi_{1/2}$) and ($^2\pi_{3/2}$)

Fine Structure Components in the Nitrogen Monoxide + Ozone → Excited Nitrogen Dioxide + Molecular Oxygen Reaction, J. Chem. Phys. 62, 1 1987-1988.

REDPATH, A. E., MENZINGER, M. and CARRINGTON, T. (1978), Molecular Beam Chemiluminescence. XI: Kinetic and Internal Energy Dependence of the $NO + O_3 \rightarrow NO_2^* \rightarrow NO_2^f$ Reaction, Chem. Phys. 27, 409-431.

SMALLEY, R. E., WHARTON, L. and LEVY, D. H. (1977), The Fluorescence Excitation Spectrum of Rotationally Cooled NO_2, J. Chem. Phys. 63, 4977-4989.

STEPHENSON, J. C. and FREUND, S. M. (1976), Infra-red Laser Enhanced Reactions: Chemistry of NO(v=1) with O_3^*, J. Chem. Phys. 65, 4303-4310.

STEVENS, C. G. and ZARE, R. N. (1975), Rotational Analysis of the 5933 Å band of Nitrogen Dioxide, J. Molec. Spectry. 56, 167-187.

STOLTE, S. (1980), private communication.

TANADA, T., FIELD, R. W. and HARVIS, D. O. (1975), Microwave Optical Double Resonance and Continuous Dye Laser Excitation Spectroscopy of Nitrogen Dioxide. Rotational Assignment of the K=0-4 Subbands of the 593 nm Band, J. Molec. Spectry. 56, 188-199.

THUIS, H., STOLTE, S. and REUSS, J. (1979), Invesigation of the Angle Dependent Part of the Internal Potential of NO-inert Gas Systems Using Crossed Molecular Beams, Chem. Phys. 43, 351-364.

VALENTINI, J. (1976), Reactive Scattering of Halogen Molecules, Ph.D. Thesis, UC Berkeley.

VALENTINI, J. and KWEI, to be published.

VAN DEN ENDE, D. and STOLTE, S. (1980), Influence of Translational and Internal Energy Upon the Chemiluminescent Part of the Exothermic Reaction $NO + O_3 \longrightarrow NO_2^* + O_2 \longrightarrow NO_2 + h\nu + O_2$, Chem. Phys, 45, 55-64.

PART II

MODELING OF GLOBAL NO_2 DISTRIBUTION

I. INTRODUCTION

The role of the nitrogen oxides in maintaining a global ozone balance in the stratosphere has been studied with increasing understanding in recent years. Ozone is continually being produced by photolysis of molecular oxygen which produces the oxygen atoms at high altitudes. These atoms recombine with molecular oxygen at altitudes where three body collisions can occur to produce ozone. The balance of ozone concentration is maintained by simultaneous ozone destruction mechanisms catalyzed by the nitrogen oxides, hydrogen oxides, chlorine oxides and oxygen atoms. These mechanisms are written out in detail in Table 1.

The highly reactive ozone destroying species shown in Table 1 are generally produced in-situ in the atmosphere by photolysis or by chemical reaction involving stable precursors such as N_2O, H_2O, CCl_4, CCl_3F, and CCl_2F_2, which are carried upwards in trace quantities from the earth's surface. Once formed, these trace radical species partition themselves through a series of complicated chemical reactions into families such as the nitrogen oxides or NO_x (NO, NO_2, NO_3, N_2O_5), the hydrogen oxides of HO_x (HO, HOO, H_2O_2), and the chlorine oxides or Cl_x (Cl, ClO, OClO, ClOO). Reactive species which can be thought to represent combinations of the above families are also formed, i.e. $ClONO_2$, $HOONO_2$,etc., as well as species which terminate the reactive chain mechanisms such as HCl, HF, and H_2O. These chain terminators generally dissolve in water or

or stick to the surface of particles and after stratospheric-tropospheric mixing are eventually returned to the earth's surface with rain.In a natural atmosphere all these chemical species have a role in preserving a steady state ozone balance. The purpose of the calculation described here is to determine this role for the nitrogen oxides on a global scale.

The most direct method for doing this is to examine the ozone production and loss pathways. The rate of ozone production represented by mechanism 1 in Table 1 is equal to $2j[O_2]$ where j is the photolysis rate constant for the rate determining step. This rate will be referred to as $P(O_3)$. The rate of ozone destruction by pure oxygen species , which will be referred to a $L(O_x)$, is given by the rate determining step of mechanism 2 in Table 1 which is $2k[O][O_3]$. In the same fashion the rate of ozone destruction by the nitrogen oxides is given by $2k[O][NO_2]$ from the rate determining step of mechanism 4 in Table 1. This rate will be denoted by $L(NO_x)$. The actual value of the rate constants used are listed in the list of reactions used in the model calculation. See table 4 on page 87.

From the above considerations it is clear that if one wants to calculate the global distribution of of ozone destruction due to the nitrogen oxides, $L(NO_x)$, one needs values for the concentrations of NO_2 and O at each volume element as well as the temperature, since k_6 has an activation energy and is therefore a temperature dependent quantity. Rather than being a completely theoretical study, this calculation is based very heavily on <u>observed</u> global distributions

TABLE I

MECHANISMS OF OZONE PRODUCTION AND CATALYTIC DESTRUCTION

OZONE PRODUCTION MECHANISMS: Net reaction $3\ O_2 \longrightarrow 2\ O_3$

$P(O_3)$	$O_2 + h\nu\ (\lambda = 242\ nm) \longrightarrow 2\ O$	RDS	(1)
	$2 \times (O + O_2 + M \longrightarrow O_3 + M)$		

OZONE DESTRUCTION MECHANISMS: Net reaction $O_3 + O \longrightarrow 2\ O_2$

$L(O_x)$	$O_3 + h\nu\ (uv, vis) \longrightarrow O_2 + O$		(2)
	$O_3 + O \longrightarrow 2\ O_2$	RDS	
$L(HO_x)$	$HO + O_3 \longrightarrow HO_2 + O_2$	RDS	(3)
	$HO_2 + O \longrightarrow HO + O_2$		
$L(NO_x)$	$NO + O_3 \longrightarrow NO_2 + O_2$		(4)
	$NO_2 + O \longrightarrow NO + O_2$	RDS	
$L(Cl_x)$	$Cl + O_3 \longrightarrow ClO + O_2$		(5)
	$ClO + O \longrightarrow Cl + O_2$	RDS	

RDS = rate determining step of the reaction mechanism.

of stratospheric NO_2 (Noxon et al.1979; Noxon 1979), ozone concentrations and temperature (Dütsch 1978). By using observed values one avoids the complication of calculating concentration flux due to horizontal and vertical transport, since such behavior is implicit in a direct measurement.

The method of instantaneous rates which was used here has been previously described in detail (Johnston and Whitten 1973, 1975; and Johnston 1975). Instantaneous rates calculations use concentrations of chemical species and photon flux in one atmospheric volume element frozen at one instant in time. One then calculates the rate of the various chemical reactions that must be taking place. This procedure would give the most accurate answers for such rates if the concentrations of all chemical species were known or measured very accu - rately. If such measurements are nor available, one can calculate them provided that a photochemical steady state exists in each volume element, that is ,the chemistry being calculated must take place quickly when compared with vertical and horizontal transport rates. The approach used here exploits the fact that all chemical species needed to consider the problem of ozone destruction by NO_x are directly measured, or as in the case of oxygen atoms, are calculatable from a directly measured species. Here the photochemical lifetime of O atoms is so short that its concentration is determined entirely by the local ozone concentration. More will be said about the implications of instantaneous rates in the results and discussion section.

II. EXPERIMENTALLY OBSERVED QUANTITIES

This calculation relied rather heavily on experimentally observed concentrations of atmospheric species so some effort was made to see that these included the newest available data. This section will describe the input data and will discuss the data transformations that were done.

A. TEMPERATURE AND OZONE DATA

In order to adequately represent all the available data in this calculation, Dütsch's ozone and temperature profiles were updated with his recent analysis of available measurements (Dütsch 1978). The temperature and ozone partial pressure profiles as a function of total atmospheric pressure reported by Dutsch were the result of careful analysis of many previous independent measurements. The most consistent and complete coverage was given by measurements from the Nimbus IV satellite using backscateered ultraviolet radiation and from the ground using the Umkehr method. These data combined with all other consistent data from chemical sondes provided the basis for the interpolation Dütsch used to cover the globe. The data grid consisted of every ten degrees latitude, twelve longitudes or months of the yaar, and nineteen equal vertical levels defined by the barometric equation i.e. the logarithm of the total atmospheric pressure. The data for ozone partial pressure and temperature were averaged over every three months to reduce the longitudinal grid from twelve to four. This gave average values for each season of the year, for example, March, April and May were combined for the spring value etc.

It was necessary to convert the vertical grid form the barometric to a scale with one kilometer steps between one and fifty kilometers. This was easily done at each of the nineteen vertical levels starting at the 250 millibar level, by using the barometric equation which related the logarithm of the pressure change to an altitude change as stated,

$$-\ln \frac{P_2}{P_1} = \frac{Mg}{RT} (Z_2 - Z_1) \qquad (6)$$

where P_1 and P_2 are the atmospheric pressures at the altitudes Z_1 and Z_2, M is the atmospheric molecular weight, T is the atmospheric temperature and R and g are the gas constant and gravitational acceleration. In order to represent the atmospheric temperature gradient Dutsch's temperature data at each of the nineteen levels was used. In between the levels a linear interpolation was done. The barometric equation implies an isothermal atmosphere over the region it is used. This condition does not hold for the atmosphere as a whole, however since the temperature change between each of the nineteen levels used was relatively small, the isothermal approximation and linear interpolations are valid. Atmospheric regions below 250 millibars were covered by Dütsch's earlier data compilation (Dütsch 1969; Johnston and Whitten 1973). Once the altitude grid was established it was a simple matter to convert the ozone partial pressures to concentrations.

An example of the result of the data transformations is shown in the contour plots of temperature and ozone concentration versus

FIGURE 1

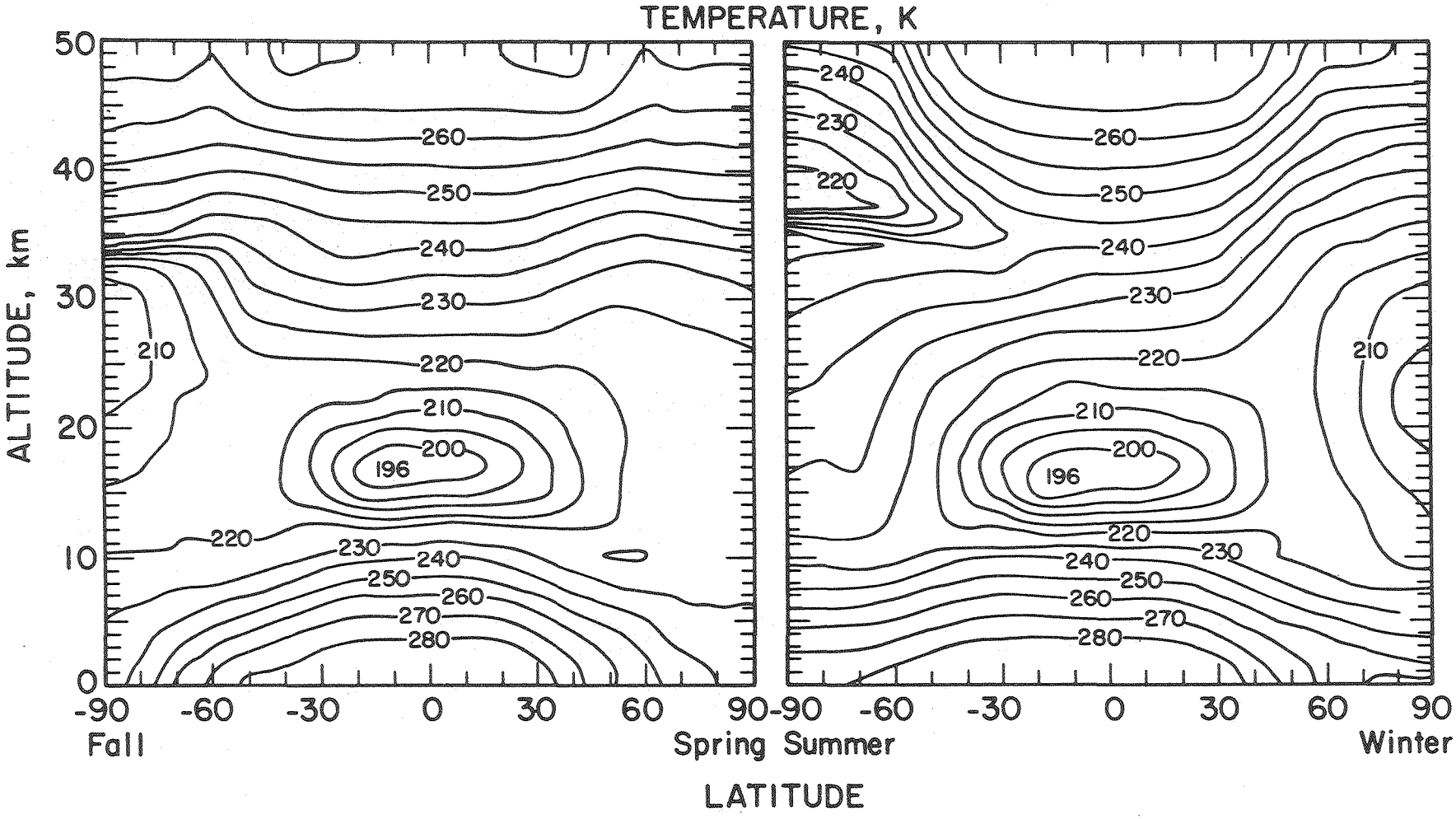
TEMPERATURE, K
ALTITUDE, km
50
40
30
20
10
0
240
230
220
260
250
240
230
210
220
210
200
196
220
230
240
250
260
270
280
-90
-60
-30
0
30
60
90
Fall
Spring
Summer
Winter
LATITUDE

FIGURE 2

OZONE CONCENTRATION, 10^{12} MOLECULES CM^{-3}

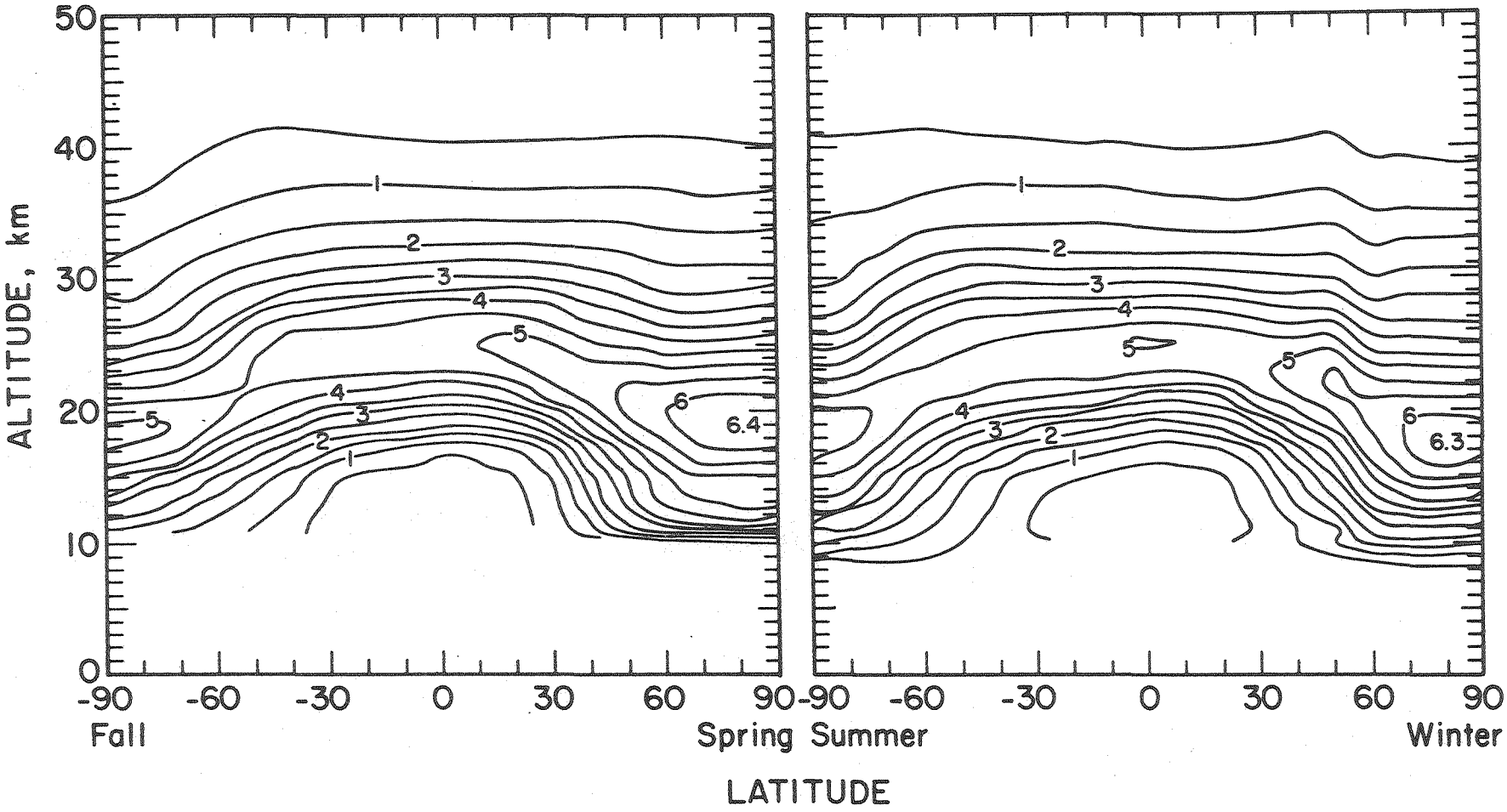

FIGURE 3

OXYGEN ATOM CONCENTRATION, MOLECULES CM^{-3}

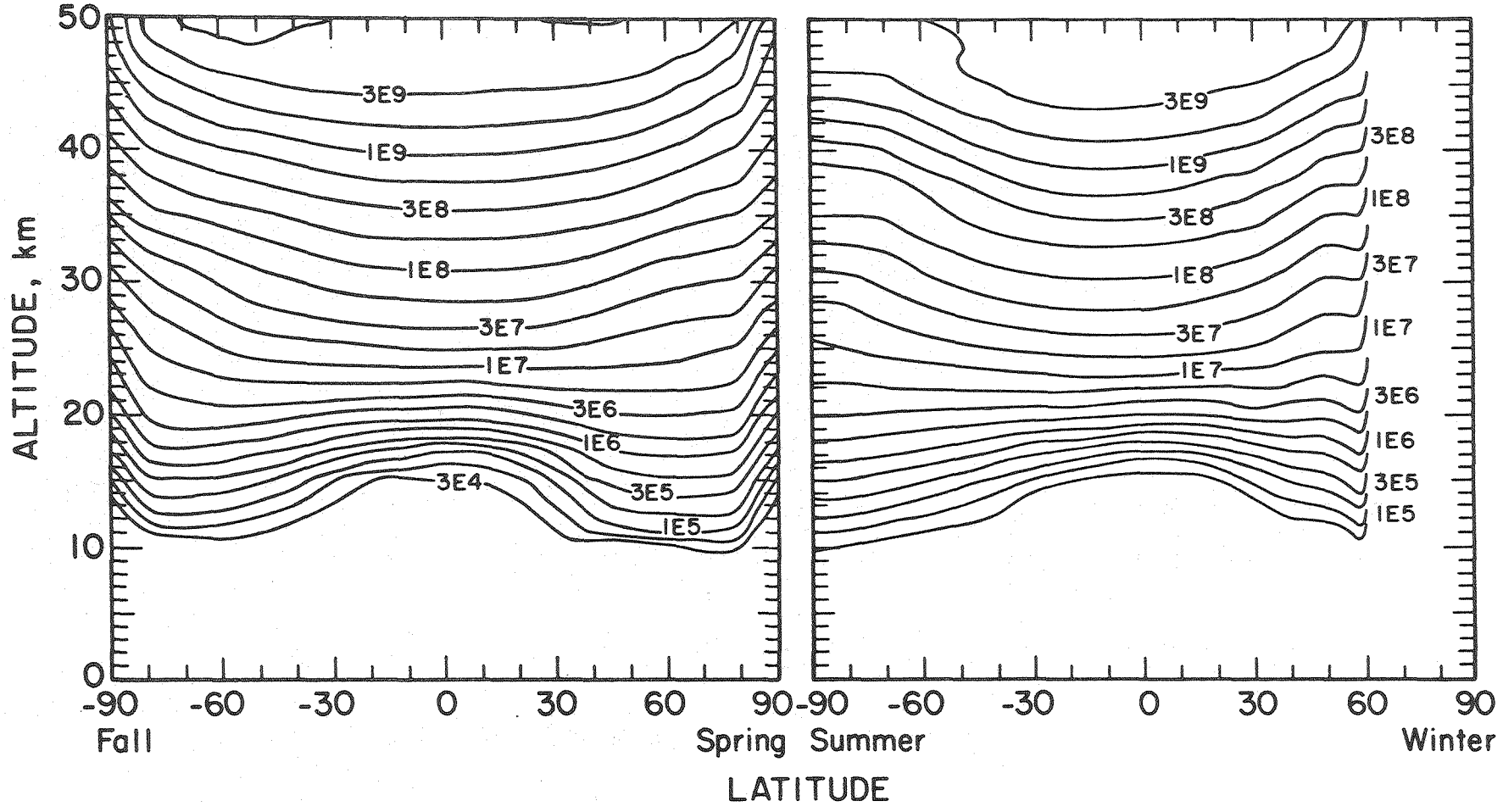

FIGURE 4

NITROGEN DIOXIDE CONCENTRATION, 10^9 MOLECULES CM^{-3}

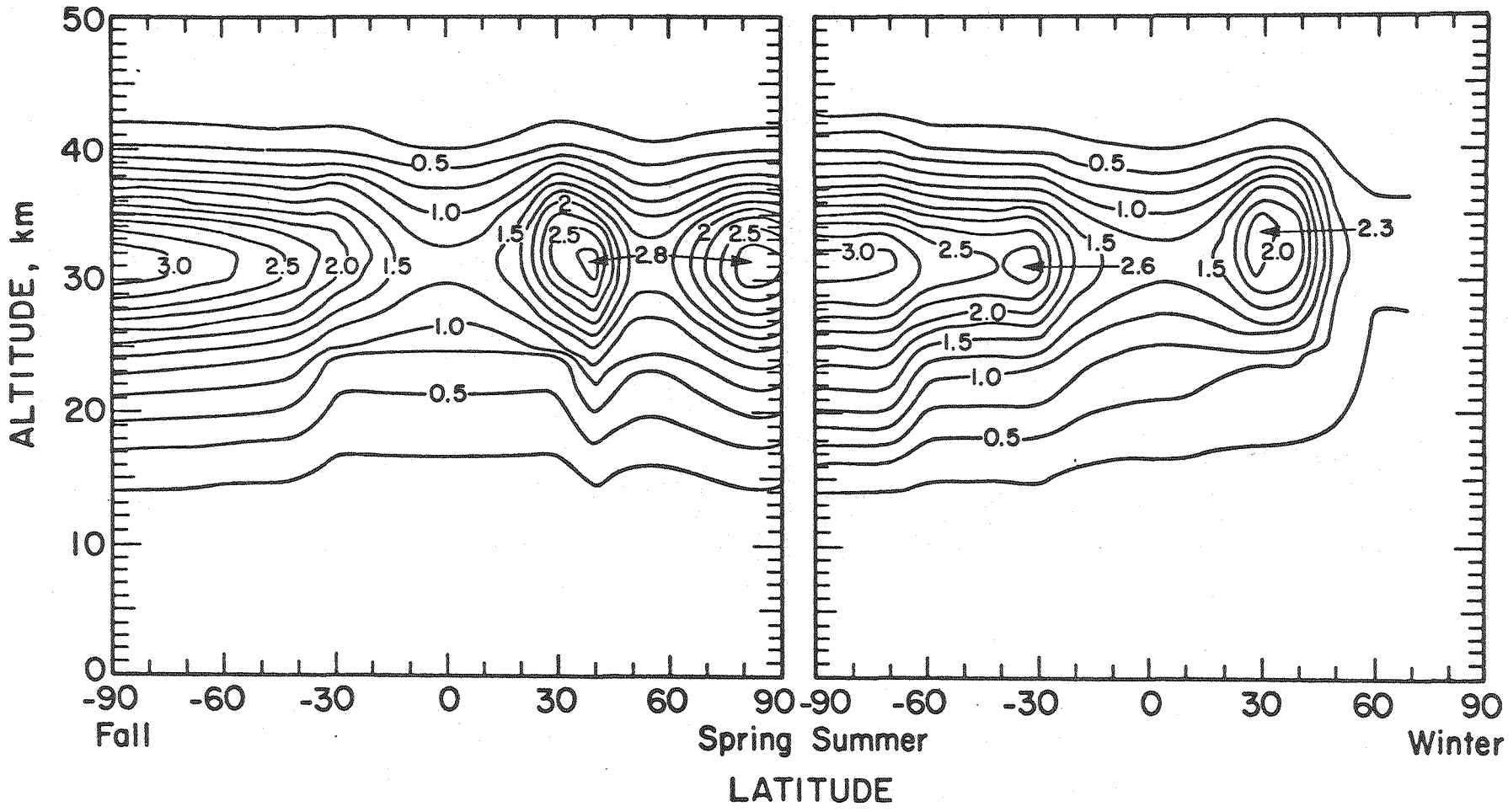

altitude and latitude in figures 1 and 2. The ozone contour plot differs slightly from a similar one used previouly (Johnston and Whitten 1973), primarily because the new ozone concentrations are higher in the poles at mid elevation and lower in the equator at high elevations. The new temperature contours however, remain almost identical to the previously used ones. Thus the transformed and interpolated data are consistent and the transformation approach used is verified.

B.) PHOTON FLUX

The ozone concentrations obtained as discussed in the previous section were used to calculate in each volume element an oxygen atom concentration which results primarily from ozone photolysis at lower altitudes and from both ozone and oxygen photolysis higher in the stratosphere. The result of the calculation is shown in figure 3.

In order to calculate such photolysis reactions it is necessary to calculate the photon flux at each wavelength in each atmospheric volume element. The incident sunlight at the top of the atmosphere was taken to be a plane wave which impinges on a sphere. The radiation density as it propagated through the atmosphere was calculated by including the absorption of O_2 and O_3 above each volume element as well as single and multiple scattering. When all these effects are considered, Beer's law in the atmosphere becomes,

$$I(\lambda,T,z,\theta)=I_\infty(\lambda)\exp\left\{-\left(\sigma_1(\lambda,T)C_1(z)+\sigma_2(\lambda,T)C_2(z)+\sigma_R(\lambda,T)M(z)\right)F(\theta)\right\} \tag{7}$$

where

$I_\alpha(\lambda)$=sunlight intensity at outer limits of the atmosphere, (Ackerman 1971).

σ_1, σ_2, = O_2 and O_3 absorption cross sections (Ackerman 1971).

σ_R = Rayleigh scattering cross section.

C_1, C_2 = Column of O_2 and O_3 above z.

M= Column of air above z.

z= Altitude level of volume element.

$F(\theta) = 1/\cos\theta$, $\theta \leq 75^\circ$.

$F(\theta)$=Chapman function for $\theta > 75^\circ$.

θ = Zenith angle.

The total atmospheric path length will increase as the zenith angle increases. This results in a secant functional dependence on the amount of absorption one observes as a function of time of day. When the zenith angle is getting large and the pathlength becomes quite long, the Chapman function more accurately describes the functional behavior than a pure zenith angle secant which is becoming infinite.

The multiple order scattering was done according to a simplified method (Isaksen et al. 1976) which assumes that one half of the scattered beam proceeds in the direction of the beam and that the other half goes in the opposite direction. It compares very well with more accurate and expensive methods used to solve the equation of radiative transfer. A consideration of multiple ccattering is important since it is a wavelength dependent quantity that increases rapidly with

decreasing wavelength until it reaches a region in the stratophere where O_2 and O_3 strongly absorb the incoming radiarion. Scattering, therefore, has its maximum effect of photon fluxes between 330-400 nm depending on the optical depth. The largest increase in fluxes will be found in the upper stratophere at large zenith angles and long path lengths where it may exceed 50 %.

The effect of the earth's albedo or surface reflection is most pronounced in the troposphere and is not a major factor in the NO_2 calculation. The treatment of the different wavelength regions that was done in this calculation is summarized in Table 2. A discussion of the method is given in the appendix of Johnston and Podolske (1978), except that the method of concentric rings was not used.

C. NO_2 CONCENTRATIONS

The data reported by Noxon is the first truly global-scale measurement of stratopheric NO_2 (Noxon et al. 1979; Noxon 1979). Ground based NO_2 measurements were made at noon to obtain a background and at various times before and after sunset to sample different thicknesses of the atmosphere. The atmospheric path length changes by as much as 50 times from noon to twilight, with the most drastic change occuring in the last half hour before sunset. From this Noxon extracted the overhead column concentration of NO_2 and obtained some estimate for its center of mass in altitude. The method hinges on the fact that Rayleigh scattering will scatter sunlight into the ground based spectrometer. Tropospheric pollution containing NO_2 does not interfere significantly because the pathlength is small.

TABLE 2

SUMMARY OF SOLAR INTENSITY SOURCES AND ATMOSPHERIC PROPAGATION TREATMENTS USED IN THE CALCULATION

REGION	I	II	III	IV
λ region (nm)	178-205	205-280	280-400	400-750
λ bin size (nm)	variable according to Hudson and Mahle, (1972).	1	1	5
Solar intensities.	Brueckner et al. (1976)	←---------- Ackerman (1971)----------→		
Absorption losses	O_2 & O_3	O_2 & O_3	none	none
Scattering losses	←----- Rayleigh scattering ------→		5 orders of Rayleigh scattering and surface reflection. Isaksen et al. (1976).	

The vertical column was measured at various locations at various times of year across the globe, although the equator and poles were rather scantily represented. A summary of the data is shown for the northern hemisphere-fall, southern hemisphere-spring in figure 5 and for the northern hemisphere-summer southern hemisphere-winter case in figure 6. The circles came from the latitude dependence studies, the squares from the day to day study, the triangles from the year to year study and the diamonds from the stratospheric temperature dependence study which are all separately shown and discussed by Noxon (1979). For the few measurements available in the southern hemisphere, Noxon noticed a rough hemispherical symmetry between 40°N and 40°S for the same season. All the data points were reflected to the other hemisphere with a six month seasonal phase shift so that for example, the spring NH - fall SH case also describes the fall NH - spring SH case.

Several other measurements of atmospheric NO_2 were made using balloons which can travel within the atmosphere and obtain vertical NO_2 concentration profiles. Concentration profiles as a function of altitude at various global locations were reported by Ackerman et al. (1974), Drummond and Jarnot (1979), Fontanella et al. (1974), Evans et al. (1976), Goldman et al. (1978), Harries et al. as quoted by Sundaraman (1976), Kerr et al. (1978), Murcray et al. (1974), and Ogawa (1979). Typically the experimental range was 20 - 35 km although the Goldman and Drummond profiles were measured to 40 km and the Drummond profile was extrapolated to 50 km by the authors.

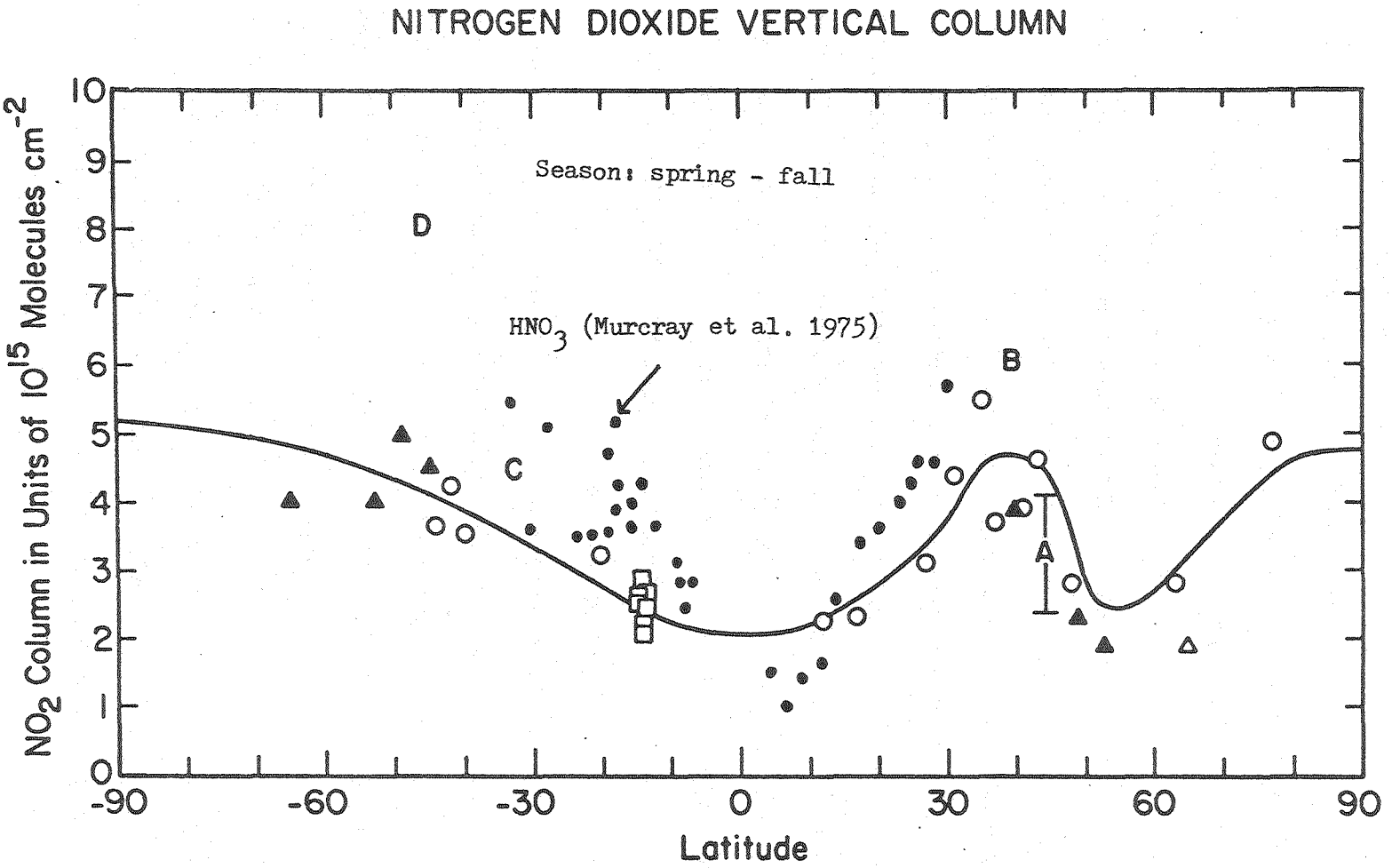
NITROGEN DIOXIDE VERTICAL COLUMN
Season: spring - fall
D
HNO3 (Murcray et al. 1975)
B
C
A
NO2 Column in Units of 10^15 Molecules cm^-2
Latitude
10
9
8
7
6
5
4
3
2
1
0
-90
-60
-30
0
30
60
90

FIGURE 5

FIGURE 6

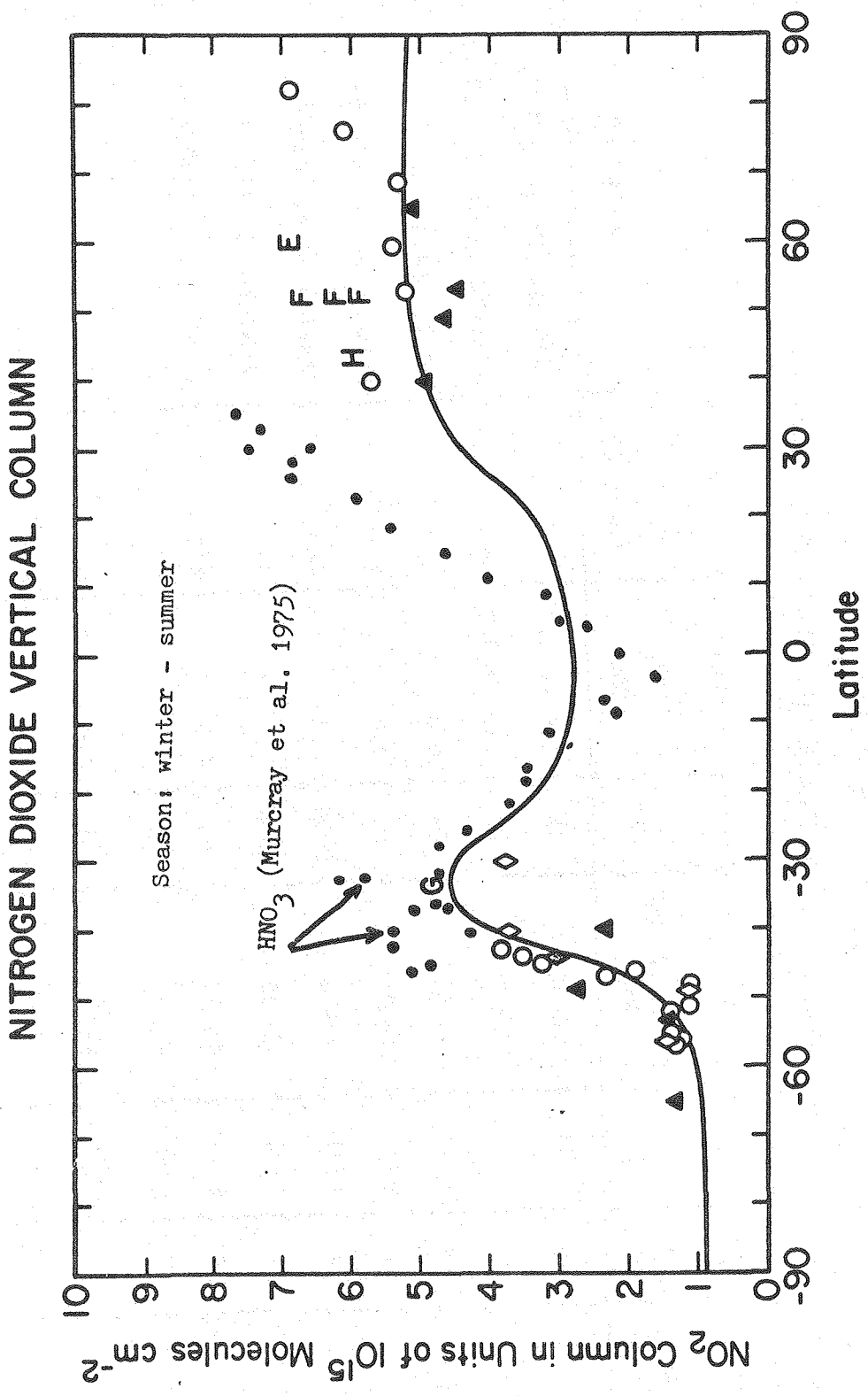
NITROGEN DIOXIDE VERTICAL COLUMN
Season: winter - summer
HNO_3 (Murcray et al. 1975)
NO_2 Column in Units of 10^{15} Molecules cm^{-2}
Latitude
-90
-60
-30
0
30
60
90
0
1
2
3
4
5
6
7
8
9
10
E
F
F
F
H
G

TABLE III

SUMMARY OF NO_2 BALLOON MEASUREMENTS CONVERTED TO COLUMNS

Item in Figs. 5, 6	Lat. °N	Mo/Yr	Range of OBS km	Time	C_{NO_2} OBS	C_{NO_2}, PM 15-50 km	Reference
A	44	5/74	20-36	PM	2.0 to 3.2		ACKERMAN et al. (1975)
			15-20	PM	0.4 to 0.8	2.4 to 4.1	FONTENELLA et al. (1974)
B	40	5/78	20-35	PM	4.8	5.9	OGAWA (1979)
C	32	9/73	18-28	PM	2.3	4.4	MURCRAY et al. (1975)
D	44	9/74	24-35	NOON	4.7	8.4	HARRIES et al. (1976)
E	59	7/74	15-35	NOON	5.4	7	EVANS et al. (1977)
F	52	8/76	15-35	PM	6.3	6.6	EVANS et al. (1978)
		8/76	15-35	PM	5.6	5.9	
		8/76	15-31	PM	5.0	6.1	
G	32	2/77	20-42	PM	4.6	4.9	GOLDMAN et al. (1978)
H	44	6/75	20-50	AM	2.8	6.0	DRUMMOND and JARNOT (1979)

In order to compare these independent balloon measurements with Noxon's columns, all the balloon profiles were extrapolated to cover the altitude range between 15 and 50 km, Morning and mid-day measurements were normalized so that everyprofile corresponded to evening conditions. Since most of the concentration lies in the altitude region where the NO_2 was measured, the extrapolation to regions beyond was a refinement without great consequences. The profile concentrations were then summed over the altitudes to give and overhead column. The resulting columns are listed in Table 3. Each entry is identified by a letter which is plotted in the appropriate figure 5 or 6. The line drawn in figures 5 and 6 is the interpolation between all the available data points and was used as the source of the NO_2 columns used in this calculation.

As well as obtaining the column or vertical profile, some of these experimenters obtained some indication of the concentration of NO_2 just after sunrise and just before sunset. One would expect the NO_2 to rapidly photolyze and stabilize at some low value immediately after sunrise and then to build up slowly during the day as the more slowly photolyzed species such as N_2O_5, HNO_3, $ClONO_2$, and $HOONO_2$ break apart. Noxon reported this diurnal PM/AM ratio as equal to two. Kerr and McElroy (1978) studied the PM/AM ratio as a function of altitude during the four separate profile measurements. Their PM/AM ratio was about two above 20 km and decreased to about 1.5 at altitudes below 20 km. Ridley et al. (1978) also studied the altitude dependence of the PM/AM ratio and obtained essentially the same results. The

PM/AM ratio has been used in this calculation to check on the proper behaviour and consistency of the computer model results.

III. CALCULATIONS WITH THE 1-D MODEL

A. INTRODUCTION

Noxon's measurements cover the latitude grid quite will and also cover the longitudinal or seasonal grid adequately, however they do not cover the altitude grid at all since the data are presented in terms of the total overhead column of NO_2 and not its vertical profile. In order to extract the vertical profile a one-dimensional vertical transport photochemical model was used. This model solves the time dependent chemical rate equations and the one dimensional transport numerically.

One can express the vertical flux of a chemical species as a sum of molecular diffusion with diffusion coefficient D and turbulent diffusion parameterized by K_z, the vertical eddy diffusion coefficient.

$$F = - D\left(\frac{\partial n}{\partial z} + \frac{n}{H} + \frac{n}{T}\frac{\partial T}{\partial z}\right) - K_z\left(\frac{\partial n}{\partial z} + \frac{n}{H_a} + \frac{n}{T}\frac{\partial T}{\partial z}\right) \qquad (8)$$

Here n is the number density of a component chemical species, H is the scale height of the component and H_a is the scale height of air. The scale height is defined as an increment in height where a component's pressure is reduced to a value 1/e of its initial value. In general, the contribution of the molecular diffusion term to the flux is 100 -1000 times less than the turbulent diffusion term all throughout the stratosphere. The temperature change with height is usually a constant over a small altitude range.

The continuity equation for the time evolution of a chemical species in a atmosphere where chemistry is occuring is given by,

$$\frac{\partial n}{\partial t} = P - L \cdot n - \frac{\partial F}{\partial z} \qquad (9)$$

This equation is more often expressed in terms of the mixing ratio or mole fraction, μ ,

$$\frac{\partial \mu}{\partial t} = \frac{P}{N} - L \cdot \mu - K_z \frac{\partial^2 \mu}{\partial z^2} + \frac{1}{N} \frac{\partial K_z \cdot N}{\partial z} \frac{\partial \mu}{\partial z} \qquad (10)$$

P and L are the chemical production and loss terms and N is the total number density of air at altitude z. Note that the constant concentration in the loss term is treated explicitly in order to make the numerical integration of the equation easier. It is this equation that is solved for each chemical species in the numerical model.

Chemical kinetics differential equations are notoriously difficult to solve because the rate of change of a species operates on vastly different time scales depending on the rate constants and concentrations of reactants and products. An example for the rate of ozone change from only the mechanisms in Table 1 follows;

$$\frac{d[O_3]}{dt} = k_1[O][O_2][M] - j[O_3] - k_2[O_3][O] - k_3[HO][O_3] - k_5[NO][O_3] - k_7[Cl][O_3]. \qquad (11)$$

The rate determining step in each reaction mechanism occurs on a much slower time scale than the other reactions so that any solution of the previous differential equation that is done on a time scale commensurate with the rate determining steps in the sum may gloss over the effects contributed by the faster reactions. On the other hand, if the time steps are chosen to be suitable for the fast-varying species the problem cannot be run to completion or steady state in a reasonable

amount of computer time.

One solution for handling such problems, called stiff problems, involves the use of a modified Newton's method using chords developed by Gear (1971) (Hindmarsch 1972). The Gear method uses variable time steps determined by a predictor-corrector iteration and a backwards differentiation formula. A system of kinetic differntial equations is generally only locally stiff, that is, only certain species are stiff for short periods of time in the calculation. For species and times when stiffness is not evident, most routines which use the Gear method switch into modified Adams methods. Such a combination of techniques make it possible to begin a simulation of a chemical system with initial values far from equilibrium and end up with an internally consistent steady state solution within a reasonable amount of computer time. It also makes it possible to continually introduce perturbations, such as is done in diurnal calculations where the sun's inclination angle varies and the sun sets every 12 hours, and still come to steady state rather quickly.

B. CALCULATIONS

The time dependent 1-D transport and photochemical model used was obtained from the Atmopheric Kinetics group at Lawrence Livermore Laboratory (Chang 1974; Chang et al. 1974). It was modified to include a total of twenty chemical species; O_3, O, OH, HO_2, H_2O_2, H_2O, N_2O, NO, NO_2, NO_3, N_2O_5, CH_4, CO, Cl, ClO, $ClONO_2$, CF_2Cl_2, $CFCl_3$, HCl, and HNO_3. The quickly reacting species $O(^1D)$, N, and H were calculated by steady state approximations. These approximations were tested

and found to be verified in regions of the stratosphere of interest in this calculation. Chemical reactions that occur among these twenty three species are listed in Table 4. The vertical transport was handled using the eddy diffusion coefficients of Stewart and Hoffert (1975). For a one-dimensional treatment such as this one to be valid, latitudinal and longitudinal transport components must be fast compared to the vertical transport. In a gross approximation, the mid-latitudes meet this criterion better than do the equator and poles, therfore the results from a 1-D model can be best compared with experimental data from the mid-latitudes.

The photochemical model was started with initial conditions for the concentration profiles that were typical for the unperturbed stratosphere. A natural background of 2 ppbv of total chlorine is prescribed. One approach to change the value of the NO_2 column was to multiply the NO_2 concentrations in the vertical profile by a constant. It was found, however, that after the photochemical model was allowed to come to steady state, the change in the total column was not very great since chemistry transformed most of the excess NO_2 to HNO_3. More satisfactory results were obtained by modifying the boundary values to a sufficiently high value so that after the model achieved steady state the overhead column gave the desired value. These values were made to span the range which Noxon saw in one particular season. In this way it was possible to construct vertical profile distributions that correspond to the various columns measured by Noxon throughout the globe. This was done separately for the three

TABLE 4

REACTION RATES

Rate constants from HAMPSON & GARVIN (1977) except as noted

$O(^3P) + O_2 + M \rightarrow O_3 + M$	$1.07*10^{-34}\exp(510/T)$	
$O_3 + O(^3P) \rightarrow 2\ O_2$	$1.9*10^{-11}\exp(-2300/T)$	
$O_3 + NO \rightarrow NO_2 + O_2$	$2.1*10^{-12}\exp(-1450/T)$	
$O(^3P) + NO_2 \rightarrow NO + O_2$	$9.1*10^{-12}$	
$N_2O + O(^1D) \rightarrow N_2 + O_2$	$5.5*10^{-11}$	
$N_2O + O(^1D) \rightarrow 2\ NO$	$5.5*10^{-11}$	
$N + O_2 \rightarrow NO + O(^3P)$	$5.5*10^{-12}\exp(-3220/T)$	
$N + NO \rightarrow N_2 + O(^3P)$	$8.2*10^{-11}\exp(-410/T)$	
$N + NO_2 \rightarrow 2\ NO$	$6.0*10^{-12}$	
$H_2O + O(^1D) \rightarrow 2\ OH$	$2.3*10^{-10}$	
$CH_4 + O(^1D) \rightarrow OH + 2\ HO_2 + CO$	$1.3*10^{-10}$	
$OH + O_3 \rightarrow O_2 + HO_2$	$1.5*10^{-12}\exp(-1000/T)$	
$O(^3P) + OH \rightarrow H + O_2$	$1.0*10^{-10}\exp(-250/T)$	
$HO_2 + O_3 \rightarrow OH + O_2$	$1.4*10^{-14}\exp(-590/T)$	A
$O(^3P) + HO_2 \rightarrow OH + O_2$	$1.0*10^{-10}\exp(-250/T)$	
$H + O_2 + M \rightarrow HO_2 + M$	$2.08*10^{-32}\exp(290/T)$	
$H + O_3 \rightarrow OH + O_2$	$1.42*10^{-10}\exp(-478/T)$	
$HO_2 + HO_2 \rightarrow H_2O_2 + O_2$	$3.9*10^{-14}\exp(1245/T)$	B
$OH + HO_2 \rightarrow H_2O + O_2$	$5.0*10^{-11}$	
$OH + NO_2 + M \rightarrow HNO_3 + M$	$4.0*10^{-12}*M/(1.12*10^{18}+M)$	
$OH + HNO_3 \rightarrow H_2O + NO_3$	$8.0*10^{-14}$	
$OH + H_2O_2 \rightarrow HO_2 + H_2O$	$1.0*10^{-11}\exp(-750/T)$	
$NO + NO_3 \rightarrow NO_2 + NO_2$	$1.87*10^{-11}$	

TABLE 4
contd.

$N_2 + O(^1D) + M \rightarrow N_2O + M$	$3.5*10^{-37}$	
$N + NO_2 \rightarrow N_2O + O\ (^3P)$	$2.0*10^{-11}\exp(-800/T)$	
$O(^3P) + NO + M \rightarrow NO_2 + M$	$1.55*10^{-32}\exp(584/T)$	
$NO + HO_2 \rightarrow OH + NO_2$	$3.3*10^{-12}\exp(254/T)$	A
$H_2 + O(^1D) \rightarrow OH + H$	$2.7*10^{-10}$	
$OH + OH \rightarrow H_2O + O(^3P)$	$1.0*10^{-11}\exp(-550/T)$	
$N + O_3 \rightarrow NO + O_2$	$5.5*10^{-12}\exp(-650/T)$	
$NO_2 + O_3 \rightarrow NO_3 + O_2$	$1.23*10^{-13}\exp(-2470/T)$	
$CH_4 + OH \rightarrow H_2O + CO + 2\ HO_2$	$2.36*10^{-12}\exp(-1710/T)$	
$OH + OH + M \rightarrow H_2O_2 + M$	$1.2510^{-32}\exp(900/T)$	
$O(^3P) + H_2O_2 \rightarrow OH + HO_2$	$2.75*10^{-12}\exp(-2125/T)$	
$Cl + O_3 \rightarrow O_2 + ClO$	$2.7*10^{-11}\exp(-257/T)$	
$O(^3P) + ClO \rightarrow Cl + O_2$	$7.7*10^{-11}\exp(-130/T)$	
$ClO + NO \rightarrow Cl + NO_2$	$2.2*10^{-11}$	
$Cl + CH_4 \rightarrow CO + HCl + 2\ HO_2$	$7.3*10^{-12}\exp(-1260/T)$	
$Cl + H_2 \rightarrow HCl + H$	$4.9*10^{-11}\exp(-2340/T)$	
$Cl + HO_2 \rightarrow HCl + O_2$	$3.0*10^{-11}$	
$HCl + OH \rightarrow Cl + H_2O$	$3.0*10^{-12}\exp(-425/T)$	
$HCl + O(^3P) \rightarrow Cl + OH$	$1.14*10^{-11}\exp(-3370/T)$	
$ClONO_2 + O(^3P) \rightarrow NO_3 + ClO$	$4.5*10^{-12}\exp(-840/T)$	
$CF_2Cl_2 + O(^1D) \rightarrow Cl + ClO$	$2.0*10^{-10}$	
$CFCl_3 + O(^1D) \rightarrow 2\ Cl + ClO$	$2.0*10^{-10}$	
$NO_2 + NO_3 + M \rightarrow N_2O_5 + M$		C
$N_2O_5 \rightarrow NO_2 + NO_3$		C

TABLE 4

contd.

$NO_2 + NO_3 \rightarrow NO + NO_2 + O_2$	$2.5*10^{-14}exp(-1127/T)$	
$NO_3 + O \rightarrow NO_2 + O_2$	$1.0*10^{-11}$	
$NO_3 + NO_3 \rightarrow 2\ NO_2 + O_2$	$8.5*10^{-13}exp(-2450/T)$	
$CO + OH \rightarrow CO_2 + H$	$1.4*10^{-13}+7.33*10^{-33}*M$	D
$Cl + HNO_3 \rightarrow HCL + NO_3$	$1.0*10^{-11}exp(-2170/T)$	
$ClO + NO_2 + M \rightarrow ClONO_2 + M$	$3.3*10^{-23}*T^{-3.34}$ $/(1+8.7*10^{-9}*T^{-.6}*M^{.5})$	

PHOTOLYSIS REACTIONS

$O_2 + hv \rightarrow 2\ O(^3P)$	E	$HCl + hv \rightarrow Cl + H$	
$O_3 + hv \rightarrow O(^3P) + O_2$		$ClONO_2 + hv \rightarrow ClO + NO_2$	
$O_3 + hv \rightarrow O(^1D) + O_2$		$CF_2Cl_2 + hv \rightarrow 2\ Cl$	
$NO_2 + hv \rightarrow NO + O(^3P)$		$CFCl_3 + hv \rightarrow 3\ Cl$	
$N_2O + hv \rightarrow N_2 + O(^3P)$		$N_2O_5 + hv \rightarrow 2\ NO_2 + O(^3P)$	F
$NO + hv \rightarrow N + O(^3P)$		$NO_3 + hv \rightarrow NO_2 + O(^3P)$	F
$HNO_3 + hv \rightarrow OH + NO_2$		$NO_3 + hv \rightarrow NO + O_2$	F
$H_2O_2 + hv \rightarrow 2\ OH$			

Alternate rate constant sources:

A HOWARD (1978)
B COX (1978)
C CONNEL and JOHNSTON (1979)
D CHAN et. al. (1977)
E HUDSON and MAHLE (1977)
F GRAHAM and JOHNSTON (1978)

regions: the poles, the midlatitudes, and the tropics.

For the mid-latitude case the model was brought to steady state using a constant sun at half intensity for a thirty year total integration period. Four different sets of boundary values for NO and NO_2 were used to span Noxon's observed column values. This was followed by three days of diurnal calculations with a maximum time step of 200 seconds. The photolysis rates varied continuously according to the computed radiation flux which depends on the solar angle that was varying throughout the day. The result was four sets of stratospheric NO_2 vertical distributions as a function of time of day, whose concentration was consistent with the local concentration of ozone and other chemical species. The NO_2 overhead columns values calculated by the model from the derived profiles roughly bracketed the range found by Noxon at mid-latitudes. It was found that the concentration of NO_2 at any given altitude was proportional to the total stratospheric NO_2 column so linear interpolation factors could be derived. This made it possible to calculate the NO_2 profile for any NO_2 column starting from a given PM vertical profile. Such calculations were done for each time of day to give a complete set of interpolated diurnal profiles based on a model calculation.

For the tropical and polar regions a thirty year run of the model would not lead to a meaningful steady state, because a 1-D model cannot adequately simulate atmospheric transport for such a long time in those regions. The problem was approached by calculation with a half intensity sun until a quasi-steady state was established,

which generally took about seven days. The calculation was started with observed values for slowly varying species such as ozone, air density, temperature, water vapor and nitric acid for the appropriate global region. Various boundary values of NO_2 spanning Noxon's observed ones in the tropics and the poles were again introduced. A quasi-steady state was established among the fast atmospheric species, i.e. O, HO, HOO, H_2O_2, NO, NO_2, NO_3, N_2O_5, Cl, ClO and $ClONO_2$. This was followed by three days of diurnal calculations as in the mid-latutude case, Again it was possible to derive the linear interpolation factors that allowed the calculation of a profile corresponding to any desired NO_2 column.

The polar case was handled just like the midlatitude case when the earth's orientation was that of spring or fall equinox. This is reasonable since the maximum in the solar intensity on the earth occurs on the equator and decreases toward both poles as geometry dictates. The whole globe was assumed to be in daylight for 12 hours and in darkness for 12 hours. When the earth is at solstice, one pole receives illumination continually whereas the other pole is in complete darkness. The maximum solar intensity in this case is at 23° latitude, due to the earth's insolation. In order to adequately model this case it was nesessary to calculate the number of hours each latitude band was in daylight. It was also necessary to determine the solar intensity in each of these latitude bands .

Although on a global scale the surface area of the polar regions is quite small, it is possible that this region may have profound

effects on the global NO_2. The continuous source of light during the polar summer may continue to photolyze species such as HNO_3 which can then build up the concentration of NO_2 to quite high values. Once the solar intensity and the duration of the day were calculated, the model calculations were done in the same way as the equinox case.

C. CHECKS OF THE MODEL RESULTS

To check for the internal chemical consistency of such an approach to generate NO_2 profiles, the computed ozone concentration at the end of the diurnal calculation was compared with the input profiles from Dütsch's data. Not much change was observed. NO_x is in rapid photochemical equilibrium above about 35 km and the partioning between NO and NO_2 depends on the ozone concentration. Therefore the stability of the ozone concentration serves as a rough check verifying that no gross errors exist and that the chemistry used in the model is consistent with the in-situ chemistry.

One can further verify the high altitude behavior of the chemistry involving NO_2 by examining a study of the solar proton event of 1972 (Solomon and Crutzen 1980). The study confirmed that the chemistry of the mid and upper strtosphere is sufficiently well understood to adequately describe the ozone losses observed after a massive in-situ injection of NO_x. Since the same chemistry is used to generate the vertical profiles, this result adds confidence to the model results.

Another separate verification of the model approach can be obtained by studying the sensitivity of the profile to various concentrations of HNO_3. The concentration of HNO_3 is believed to reflect

long term global transport, and since HNO_3 is slowly photolyzed to NO_x, the NO_2 profiles may show a transport effect also (Wofsy 1978). A nitric acid concentration is reported by both Lazrus and Gandrud (1974), who used a filter collection technique, and by Murcray et al. (1975), who reported columns above 18 km based on infrared emission. Murcray found columns of HNO_3 that varied from 0.9 - 5.4 x 10^{15} molec/cm^2 in the latitude interval between 20°N and 20°S. Lazrus and Gandrud report tropical mixing ratios at 18 km between 0.2 and 0.75 ppbm.

The nitric acid study in the model was simulated by choosing two nitric acid profiles that bracketed the experimental observations which was followed by a model calculation to quasi-steady state as is appropriate for tropical regions. The results listed below for 5:30 PM show that the two extreme input cases for nitric acid result in a difference of about 5 % on the total column rate of the NO_2 + O reaction. In the lower stratosphere i.e. at 18 km where HNO_3 acts as the main chemical resevoir for NO_x, the effect on the NO_2 + O reaction is small. Overall it appears that the uncertainty in the shape of the HNO_3 profile does not introduce much uncertainty into the instantaneous rates calculation.

	Case 1	Case 2
Column of HNO_3 x 10^{15} molecules cm^{-2}	1.2	5.6
HNO_3 at 18 km, ppbm	0.36	2.2
Column rate of $NO_2 + O \longrightarrow NO_2 + O_2$ x 10^{12} $cm^{-2}s^{-1}$	3.8	4.0

The results of the synthesized NO_2 profiles around the globe are summarized in the contour plot in figure 4 on page 72. NO_2 is averaged

over the daytime only since at night much of the free NO_2 becomes bound as N_2O_5. From the contour plot one can see the behavior observed by Noxon; the high NO_2 columns at both poles and at mid-latitudes at 30°, the low tropical values, the winter cliff above $50^\circ N$ and the trough in spring. The maximum in the NO_2 concentration occurs at about 30 km. This value is slightly higher than that observed by most balloon measurements where it occurs at 24 - 27 km. The model profile however, tracks Drummond's profile quite closely, especially between 30 - 45 km and does reasonably well near the altitude of maximum concentration. See figure 7. Curve A is the NO_2 profile observed by Drummond and Jarnot (1979) which has an integrated vertical column of 2.8×10^{15} molec/cm^2, B and C are profiles generated by the model with integrated columns of 2.4 and 1.0×10^{15} molec/cm^2 respectively. Noxon's altitude of maximum concentration varies between 20 and 28 km. The major discrepancy between the model calculation of NO_2 and the observation of Noxon and others is the variability of the observed altitude of maximum NO_2 not reproduced by the model. Since the maximum occurs in the lower stratosphere where the concentration of O atoms is small, it will not affect the results of the instantaneous rates calculation for $NO_2 + O \longrightarrow NO + O_2$. This discrepancy may be evidence for either a horizontal transport mechanism which is introducing NO_2 or a chemical resevoir species that produces NO_2 upon reaction or photolysis. It is also possible that the greater uncertainty that Noxon places on his determination of the altitude of maximum concentration may explain the discrepancy. The altitude

FIGURE 7

OBSERVED AND CALCULATED NO_2 PROFILES ONE HOUR AFTER SUNRISE

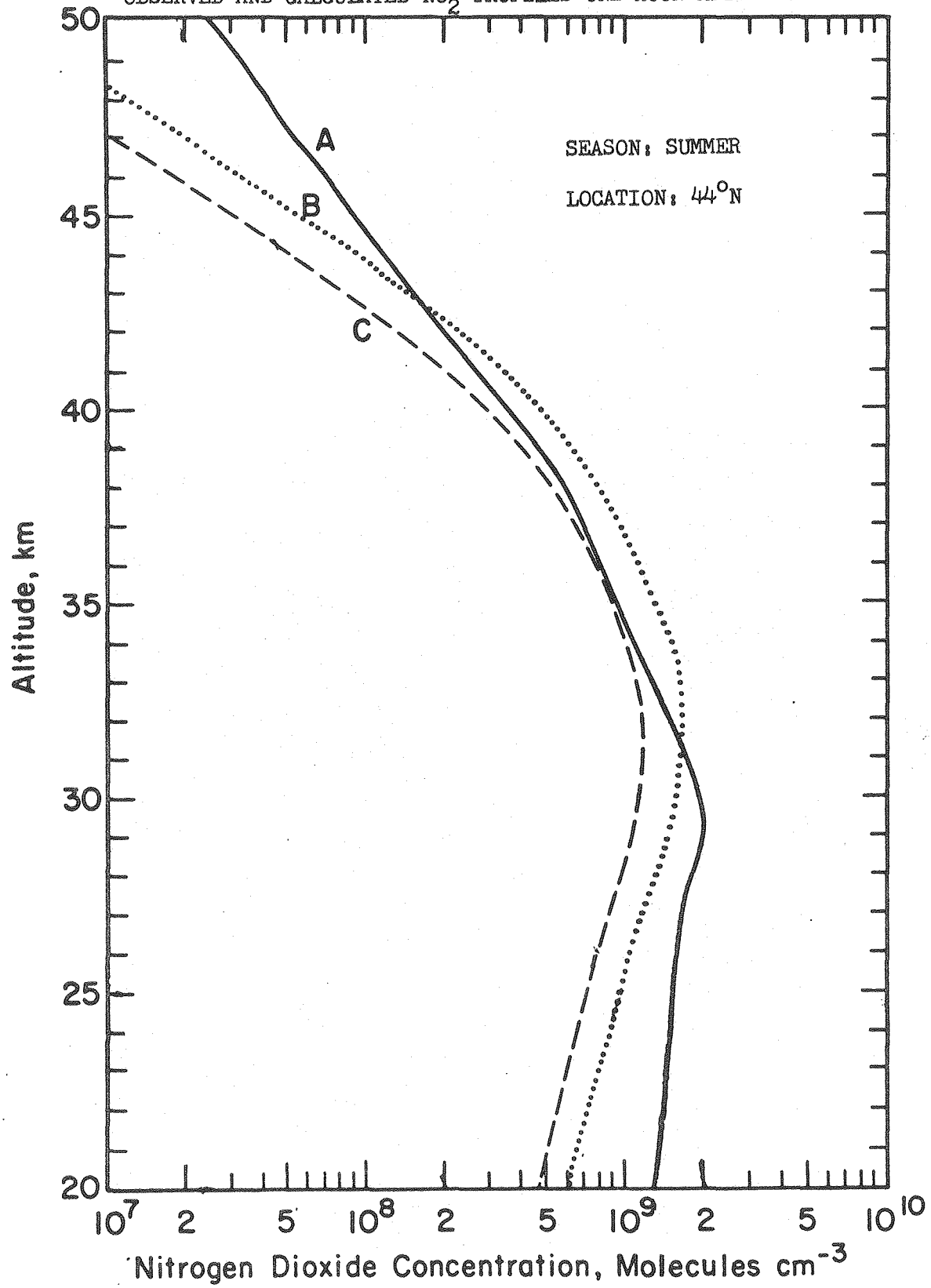

of maximum concentration is a derived rather than a directly observed quantity.

IV. INSTANTANEOUS RATES CALCULATIONS

A. RESULTS

Instantaneous rates calculations were done as a function of height (50 one km altitudes), longitude or time of day (24 fifteen degree intervals), and latitude (10 ten degree intervals) for the two spring-fall equinox cases and the two winter and summer solstice cases. Only one plot each of the equinox and solstice cases is provided in the contour plots, since the differences between the two hemispheres was small. The contour plots for the reaction rates are presented as 24 hour average rates whereas the plots for the concentration of chemical species are presented as 12 hour daytime averages for the equinox case and averages over the sunlit portion of the day for the solstice case.

In each grid point concentrations of O_3 and NO_2 were input as primary data. The concentrations of NO_2 and O as well as the solar intensity were calculated or extrapolated as stated previously. The instantaneous rates calculations were done for ozone production from O_2 photolysis, $P(O_3) = 2j[O_2]$, ozone destruction by oxygen species, $L(O_x) = 2k[O][O_3]$, and ozone destruction by nitrogen species, $L(NO_x) = 2k[O][NO_2]$. Another ozone destruction mechanism $NO_2 + O_3 \rightarrow NO + 2O_2$ was also investigated.

The 24 hour zonal average of ozone production is shown in figure 8. It shows a broad maximum in the upper stratosphere and a large value over the polar summer. The rate of ozone destruction by oxygen species is shown in figure 9 and the ratio of the two rates $L(O_x)/P(O_3)$ is shown in figure 10. From the ratio one can see that

FIGURE 8

RATE OF OZONE PRODUCTION FROM O_2 PHOTOLYSIS, MOLECULES CM^{-3} S^{-1}

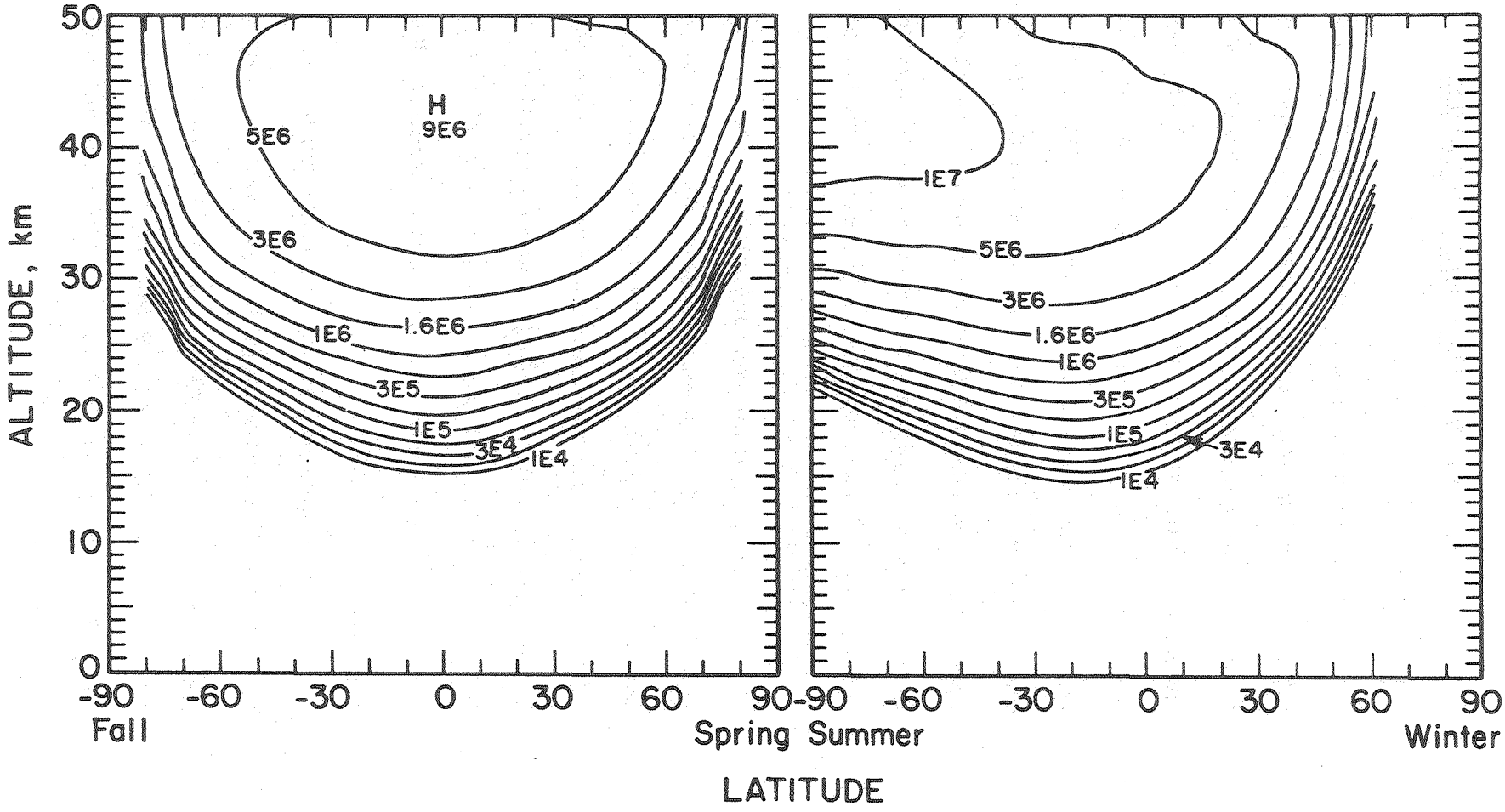

FIGURE 9

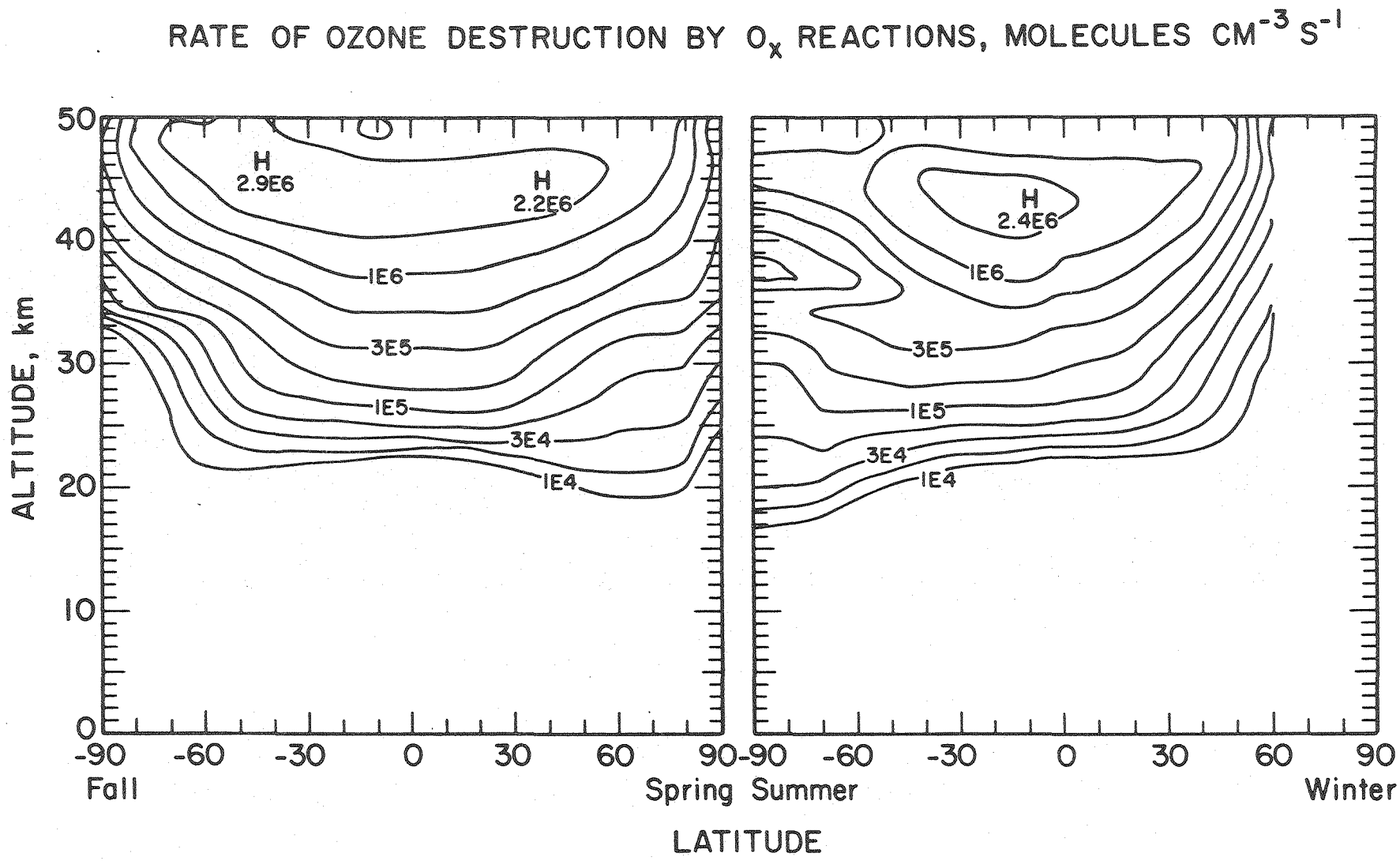
RATE OF OZONE DESTRUCTION BY O_x REACTIONS, MOLECULES CM^{-3} S^{-1}
ALTITUDE, km
50
40
30
20
10
0
H
2.9E6
H
2.2E6
H
2.4E6
1E6
3E5
1E5
3E4
1E4
-90
-60
-30
0
30
60
90
Fall
Spring
Summer
Winter
LATITUDE

FIGURE 10

RATIO OF RATE OF OZONE DESTRUCTION BY O_x TO RATE OF OZONE FORMATION BY O_2 PHOTOLYSIS

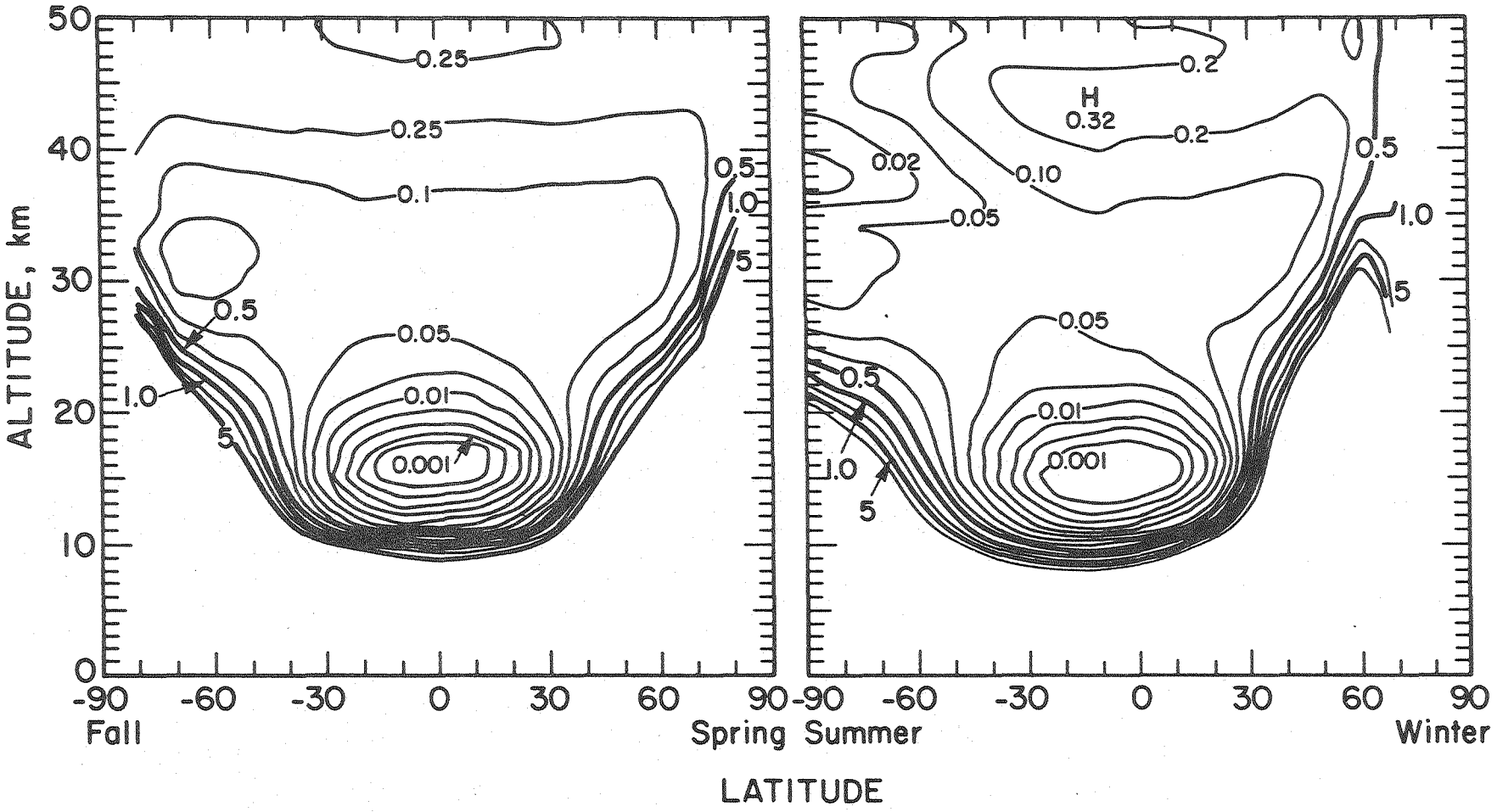

at about 40 km the loss due to O_x is about 25 % of the total rate of ozone production. This percentage rapidly decreases at lower altitudes till it reaches a region below the ozone maximum where oxone is produced 1000 times faster than it is destroyed by O_x. The heavy lines in figure 10 outline a region where O_x reactions destroy ozone at a rate comparable to ($L/P = 0.5$) to a rate much faster than ($L/P = 5.0$) the rate that ozone is produced by solar radiation. This high ozone destruction occurs in a region where the photochemical production of ozone is very slow. Ozone production from O_2 occurs only from solar radiation at wavelengths less than 242 nm, which is strongly filtered by oxygen and ozone , whereas the ozone destruction is brought about by oxygen atoms generated by ozone and NO_2 photolysis, which is driven by visible as well as ultraviolet radiation. Thus, ozone, brought to a region by transport, undergoes slow photochemical destruction where the rate of ozone formation from O_2 photolysis is essentially zero.

The 24 hour zonal average rate of ozone destruction by NO_x is shown in figure 11 . The maximum rate of ozone destruction by NO_x occurs at midlatitudes between 30 and 40 km. Ozone is rapidly destroyed by the $NO_2 + O$ reaction at a rate of 10^6 molecules/second in a band 15 km wide stretching from pole to pole at the equinox. During the solstice this band is 20 km wide over the summer pole and rapidly falls to zero as one approaches the winter pole.

The ratio of ozone destruction by NO_x to its production by photolysis $L(NO_x)/P(O_x)$, is shown in figure 12. The heavy lines in this figure enclose the region where ozone destruction by NO_x exceeds

FIGURE 11

RATE OF OZONE DESTRUCTION BY NO_x REACTIONS, MOLECULES CM^{-3} S^{-1}

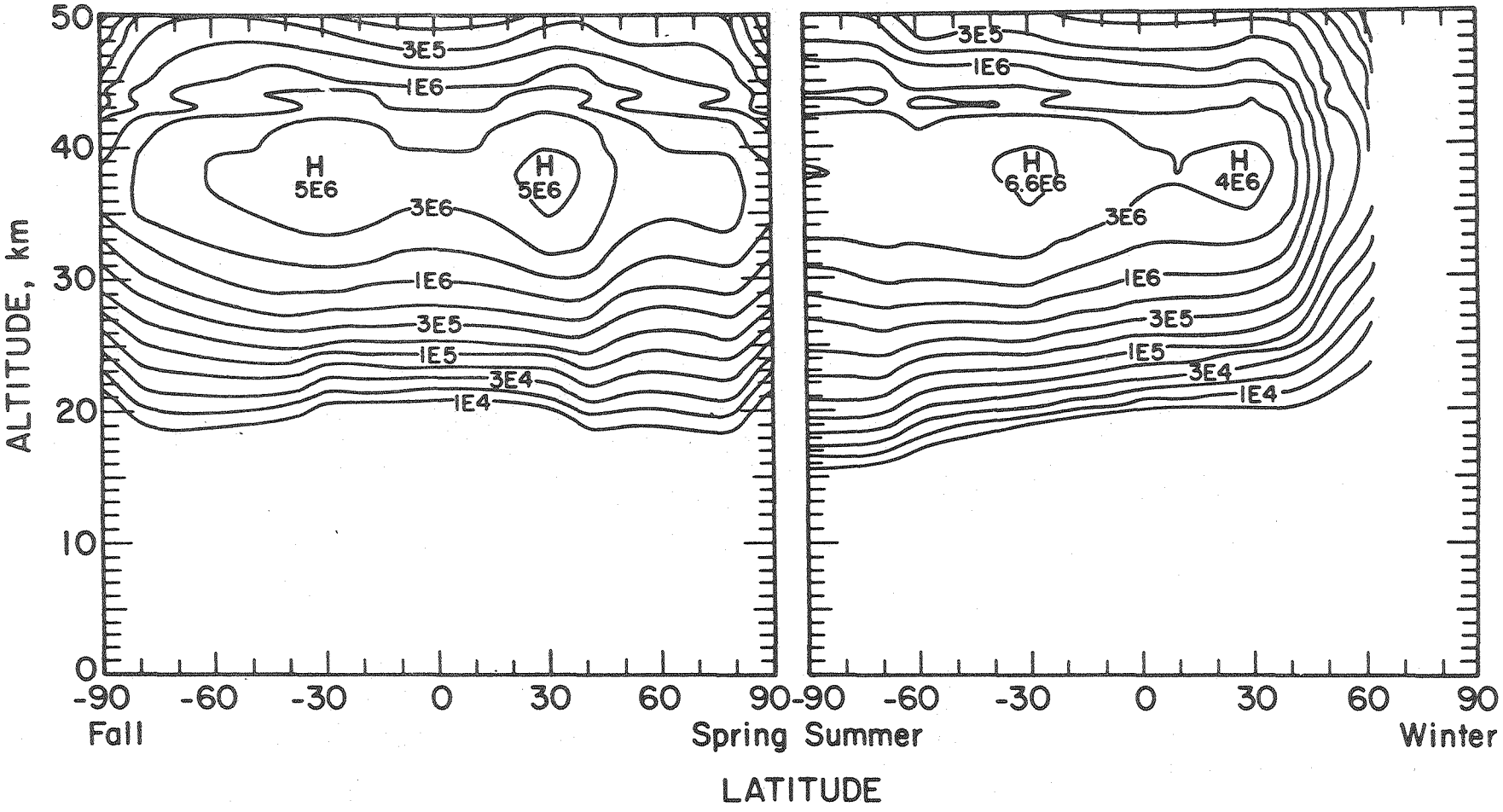

FIGURE 12

RATIO OF RATE OF OZONE DESTRUCTION BY NO_x TO RATE OF OZONE FORMATION BY O_2 PHOTOLYSIS

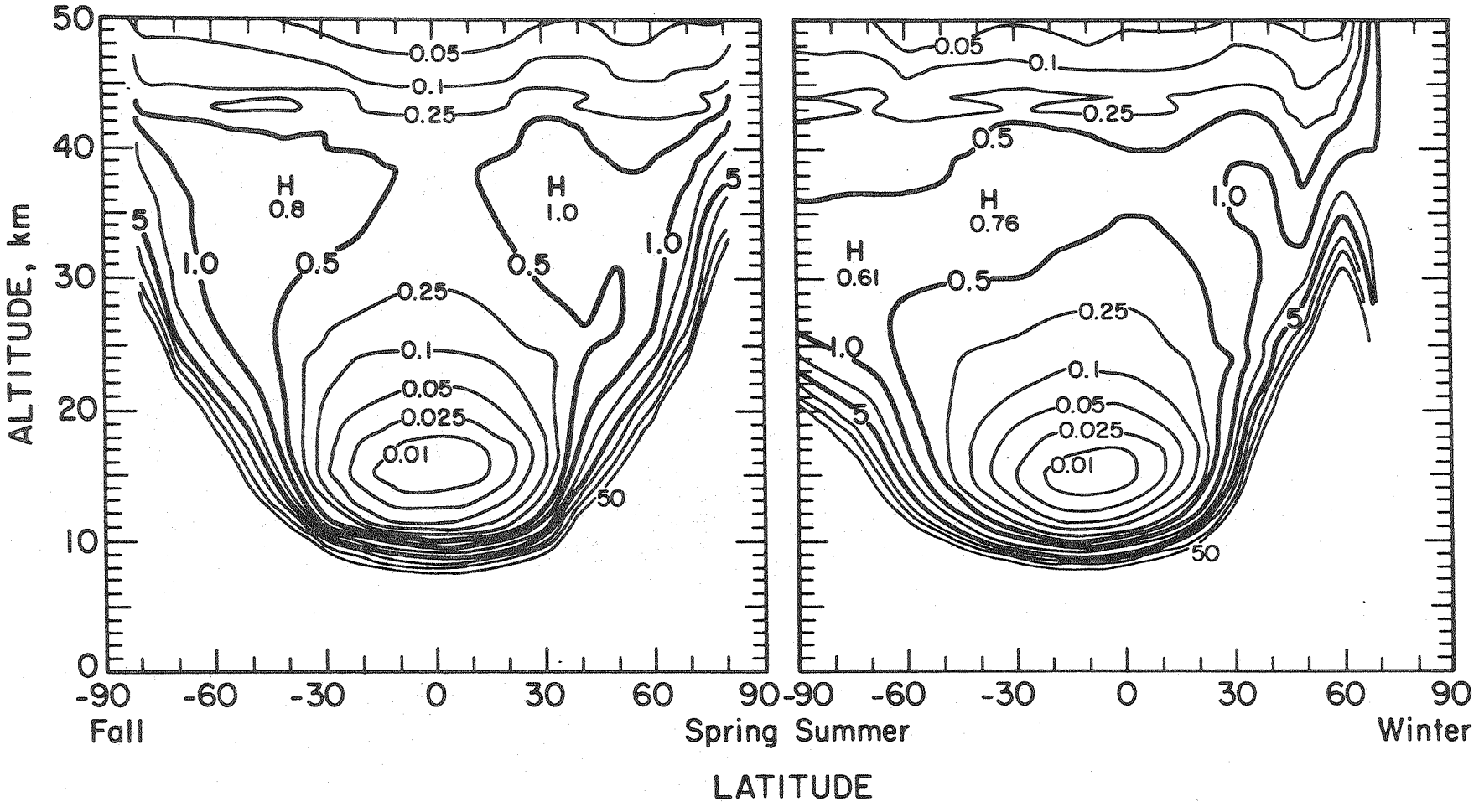

50 % of the local production to where it is less than five times the local production rate by O_2 photolysis. This implies that NO_x is destroying ozone which is brought to that region from a net ozone production region by atmospheric transport. In the solstice case the ozone destruction by NO_x lies in a band 10 km wide from the summer pole to 60°N. In the equinox case the zone of maximum ozone destruction by NO_x occurs in two large areas over the mid-latitudes.

The extent of loss of ozone from a less important NO_x cycle was also investigated.

$$NO + O_3 \longrightarrow NO_2 + O_2 \qquad (12)$$

$$NO_2 + O_3 \rightarrow NO_3 + O_2 \qquad (13)$$

$$NO_3 + h\nu \rightarrow NO + O_2 \text{ (or } NO_2 + O) \qquad (14)$$

net: $2\ O_3 \longrightarrow 3\ O_2$

The rate of ozone destruction may be expressed as $2k[NO_2][O_3]Q$, where Q is the ratio for the two branching paths for NO_3 photolysis. Using the quantum yields determined by Graham and Johnston (1978), the contribution to the global ozone desruction by this cycle is only 0.03 % of the ozone production. The contribution is even less if one uses the more recent quantum yield determination by Magnotta and Johnston (1980). This is mainly due to the slow rate for the $NO_2 + O_3$ reaction, especially since the altitudes of maximum concentrations of NO_2 and ozone coincide. At lower altitudes such as between 1 - 10 km the global integrated rate of this reaction is sufficiently high to be important in the troposphere where the lifetimes of NO_2 and ozone are longer. At these altitudes this reaction is sufficient-

ly effective to be on the order of a few percent of the magnitude of the rate of ozone production by methane smog reactions (Chameides and Walker 1976).

Some more ozone can be lost through a minor pathway in the oxygen family, $L(O_x)$, when the reaction $O_3 + O(^1D) \rightarrow 2\ O_2$ operates. The concentration of $O(^1D)$ in the stratosphere is low enough so that this reaction is not a factor in the ozone balance.

Another perturbation on the instantaneous rates calculation is an ozone source term from methane smog oxidation (Fishman et al. 1979). This effect is negligible in the 30 - 40 km altitude region where the NO_2 + O reaction predominates. The methane smog oxidation reaction sequence is an important local source of ozone below 20 km, so it would need to be considered if one were studying an ozone balance in the tropsphere.

FIGURE 13

OZONE PHOTOCHEMICAL REPLACEMENT TIME

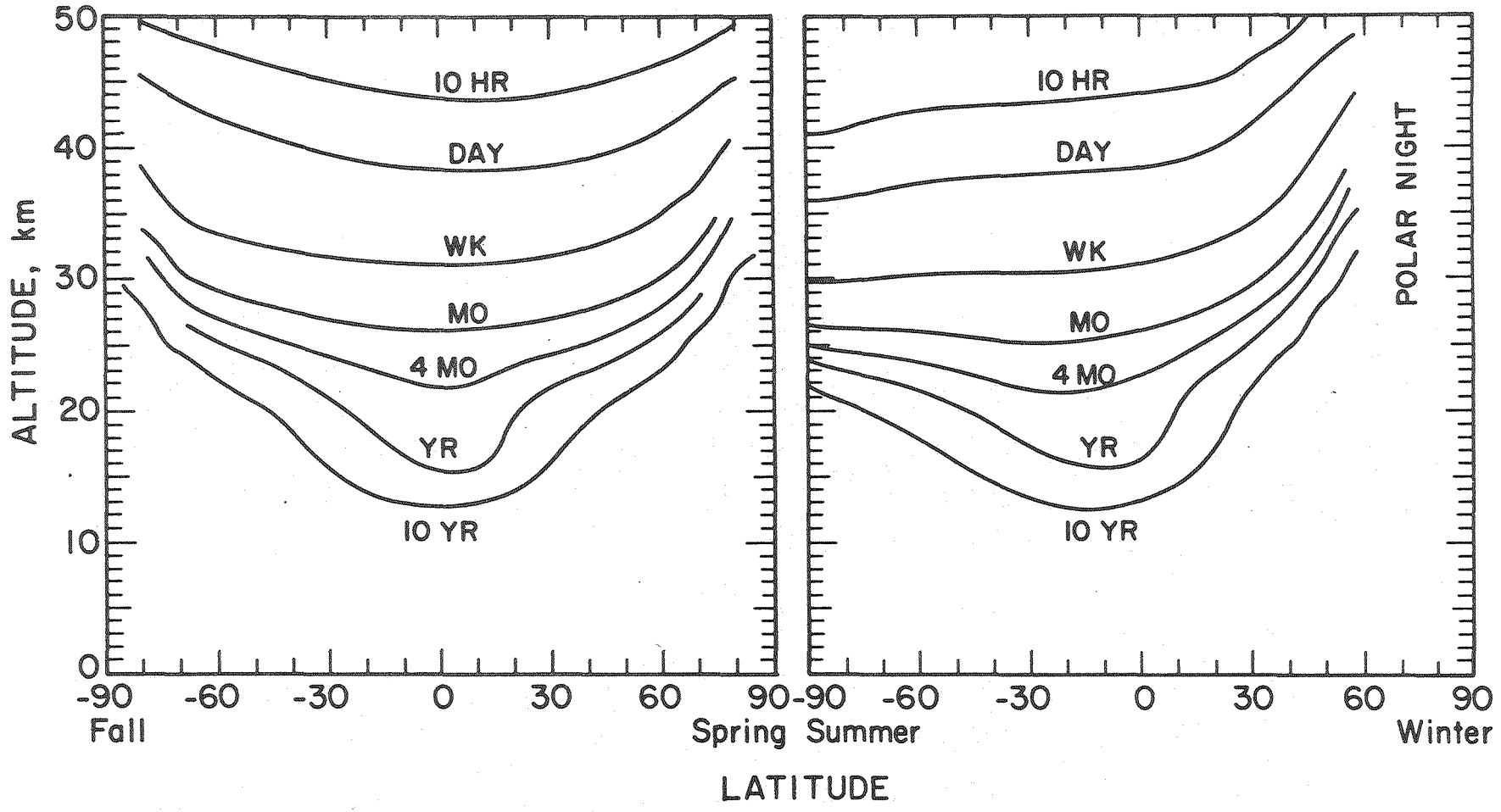

B. EFFECTS OF TRANSPORT ON THE INSTANTANEOUS RATES

The ratio of the measured local ozone concentration and the local ozone production rate gives an indication of the photochemical replacement time for ozone. Figure 13, plotted as a daytime average, shows that above 30 km the photochemical lifetime is on the order of one week, and between 25 - 30 km it increases to about one month. Since it increases dramatically to one or more years in the lower stratosphere and troposphere, it is necessary to see how the photochemical lifetime compares to the residence time of a parcel of air in a particular grid point of the calculation (Brewer and Wilson 1968). In the general case in regions where transport is slower than photochemistry one can make conclusions about the ozone balance and infer from the results of an instantaneous rates calculation where on the globe transport is taking place. In general this is true above where the photochemical replacement time is between 1 - 4 months. Most of the ozone production and destruction by O_x and NO_x occurs above this region. If one is in a grid point where the photochemical lifetime is greater than about four months then vertical and horizontal transport will be the major source of ozone inputs and deficits assuming no other chemical source for ozone (Fishman et al. 1979).

For the specific reaction considered here, i.e. $NO_2 + O \rightarrow NO + O_2$ the requirements are not so stringent. NO_2 is a directly measured quantity and the oxygen atom has a very short photochemical lifetime. It is continuously being produced by ozone which is directly measured. The method of instantaneous rates can be directly applied in this case.

It is necessary to examine each chemical system separately before instantaneous rates can be applied. For example, if the oxygen atom had another major chemical source term besides ozone that was not measured , the previous arguments about photochemical stady state would need to be satisfied.

Vigorous stratospheric poleward transport due to the general circulation of the atmosphere results in a large maximum at the winter pole which lasts until about April (Gebhart et al. 1970). This is true even though photolysis is not producing or destroying any local ozone. One can see from table 6 that the instantaneous rates calculation preserves this feature which was introduced through Dütsch's data. A slight asymmetry in the hemispheres with the northern hemisphere having more ozone was also preserved.

As was mentioned before, horizontal transport may have a profound effect on the global distribution of NO_2. In the winter especially at high altitudes, i.e. above 60°N, the NO_2 virtually disappears. This may be due to slow conversion to HNO_3 during the winter months when the lifetime of HNO_3 can become quite long (on the order of 10^7 seconds). The slow conversion could not be reversed until spring when the photolysis rate for HNO_3 increased. Possible mechanisms for this conversion with a timescale of a few months are (Wofsy 1978):

1) $NO_2 + OH + M \rightarrow HNO_3 + M$ if photolysis of HNO_3 is ineffective in the long wavelength tail ($\lambda > 315$ nm).

2) The slow reaction of $N_2O_5 + H_2O \rightarrow 2\ HNO_3$.

3) A changed temperature coefficient for N_2O_5.

It is possible that poleward transport of NO_2 is occuring, but this effect is difficult to sort out due to the short photochemical lifetime of NO_2 and the uncertainty of mechanisms for the gain and loss of NO_2. One can approach this problem by observing global distributions of other NO_2 reservoir species such as HNO_3. Murcray et al.'s (1975) integrated HNO_3 column data for April 1974 is shown in figure 5 and data for January 1974 is shown in figure 6 by the solid points. The units Murcray used for his HNO_3 columns were converted using STP conversions from the US Standard Atmosphere, 1976. One can see that the behavior of NO_2 and HNO_3 is similar where data exists, however the lack of data near both poles makes it difficult to make any quantitative conclusions about HNO_3 as a transport reservoir. If one expects HNO_3 to mimic NO_2 closely due to a similar response to solar flux only, perhaps Noxon's NO_2 columns would have shown a sharper dip in the equator if more data were available. The range of NO_2 columns considered in the sensitivity study is sufficient to include this uncertainty. Again it is clear that the data for chemical species must be obtained near the equator because its large spherical area contributes significantly to the global averages and near the poles for species that can act as chemical reservoirs to enable one to make more definitive conclusions about chemical transport.

TABLE 5

SUMMARY OF INSTANTANEOUS RATES CALCULATIONS

Alt. Band km	Lat.	Prod. O_3 $2\ j[O_2]$	Loss of O_3		Ratio L/P		
			O_x $2\ k[O][O_3]$	NO_x $2\ k[O][NO_2]$	O_x	NO_x	Both
	-80	14	2	28	0.13	1.95	2.08
	-70	33	3	20	0.09	0.61	0.70
	-60	51	5	21	0.11	0.40	0.51
	-50	67	9	26	0.14	0.39	0.53
	-40	81	13	49	0.16	0.60	0.76
	-30	94	14	64	0.15	0.68	0.83
	-20	106	16	47	0.15	0.44	0.59
	-10	112	17	36	0.15	0.32	0.47
	0	119	16	35	0.13	0.29	0.42
	10	117	16	37	0.13	0.31	0.44
	20	110	14	45	0.13	0.41	0.54
	30	100	13	53	0.13	0.53	0.66
	40	83	12	44	0.15	0.53	0.68
	50	67	9	39	0.13	0.58	0.71
	60	48	5	32	0.11	0.66	0.77
	70	28	3	26	0.11	0.93	1.04
	80	9	2	20	0.19	2.18	2.37
45-50		140.2	32.4	9.2	0.23	0.07	0.30
40-45		171.2	42.4	45.2	0.25	0.26	0.51
35-40		155.4	19.0	89.2	0.12	0.57	0.69
30-35		104.0	7.2	57.4	0.07	0.55	0.62
25-30		43.4	2.6	15.4	0.06	0.35	0.41
20-25		8.8	0.52	1.8	0.06	0.30	0.36
15-20		0.9	0.04	0.12	0.04	0.13	0.17
15-45		484	72	209	0.15	0.43	0.58

V. CONCLUSIONS

The 24 hour average rates for the spring-fall case were summed over 15 - 45 km to give average column rates. These are summarized in the first section of table 5. For each latitude, the average column rates of $P(O_3)$, $L(O_x)$, $L(NO_x)$ as well as the ratios $L(O_x)/P(O_3)$, $L(NO_x)/P(O_3)$ and $[L(O_x) + L(NO_x)]/P(O_3)$ are shown.

Near both poles one sees that both production and loss rate are about one tenth the equatorial value. The loss of ozone due to NO_x is enhanced somewhat by the large solar zenith angle, since the photolysis of NO_2 is not as effective near the poles as it is near the equator. The atmosphere is optically thin in the NO_2 absorption wavelengths, therefore the enhancement would be small. One would expect a similar effect for oxygen atom production due to the photolysis of ozone in the visible. Again since the atmosphere is optically thin in this region, the enhancement of oxygen atoms would be small. In any case those enhancements would be overpowered by the decreased concentration of oxygen atoms one finds at the poles. The polar $L(NO_x)$ rates are about half the equatorial ones. If one looks at the ratio of both loss mechanisms to production one sees that the ozone is destroyed about twice as fast as it is formed. Again this is evidence of horizontal and vertical transport. In the mid-latitudes where the concentration of NO_2 is highest, the ratio of loss to production by O_x is 15 % and by NO_x is 40 - 70 %. The equator has the same rate for O_x , but for NO_x the ratio is about 30 %.

One can clearly see the effects of global asymmetry of O_3 and

FIGURE 14

OZONE MIXING RATIOS (PPMV) AND REGION OF HEAVY OZONE DESTRUCTION BY NITROGEN OXIDES

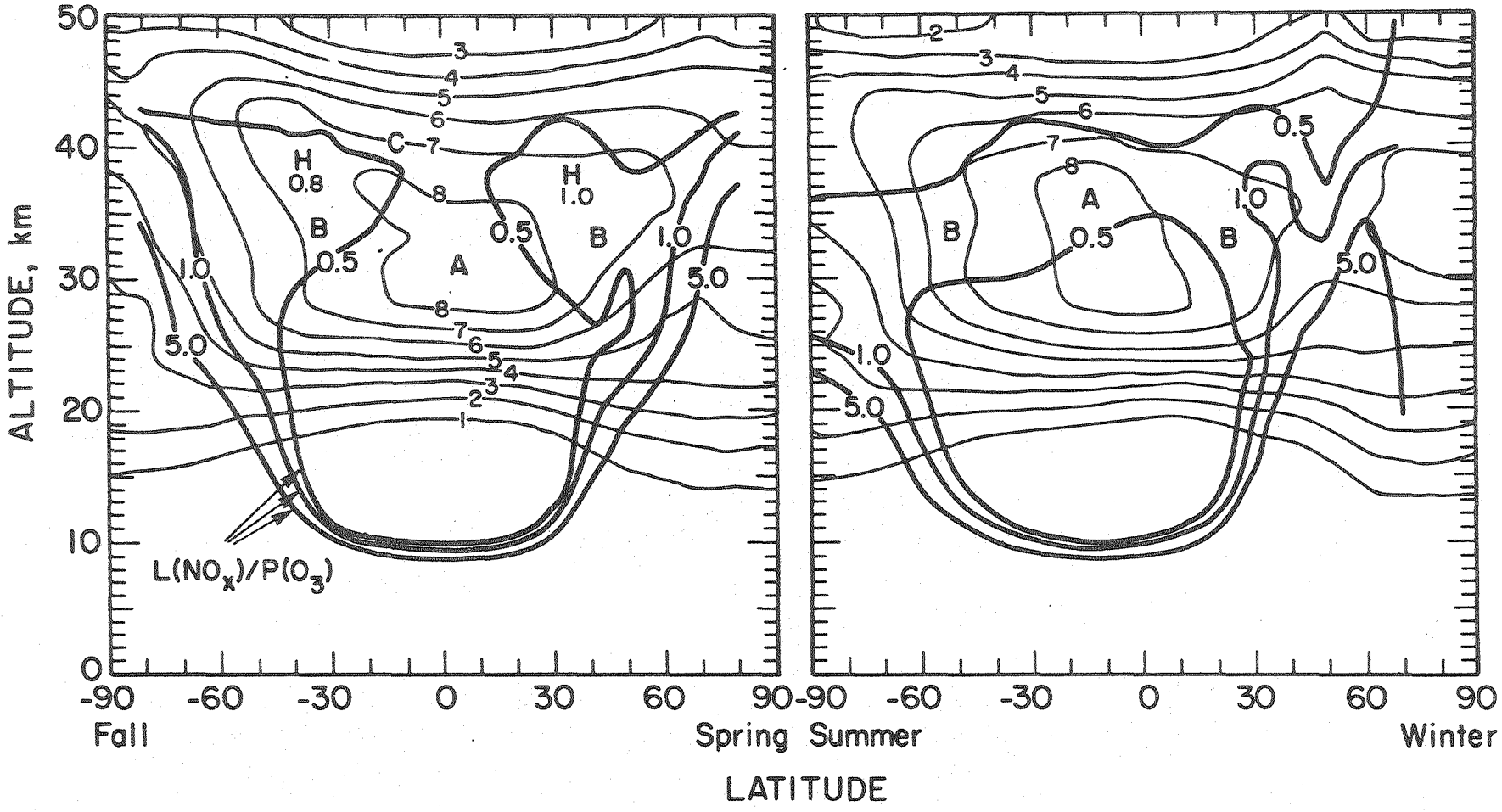

NO_2 concentrations by comparing the northern and southern hemispheres in table 6. The northern hemisphere which has more ozone also has more ozone production. The loss of ozone by O_x appears to be almost uniform in both hemispheres but may have slightly less loss in the northern hemisphere where the increased O_3 may shield the lower altitudes from O_3 photolysis. The loss of O_3 by NO_x follows Noxon's columns. The total loss by NO_x in the northern hemisphere is slightly higher than in the southern hemisphere, but the peak loss rate is highest in the southern hemisphere.

The ratio $L(NO_x)/P(O_3)$ has been superimposed on the contour map of ozone mixing ratio to produce figure 14. Region B defines the area where NO_x destroys ozone at least 50 % as fast as it is formed. Region A defines the maximum mixing ratios for ozone and region C shows the point where the oxygen photolysis is maximum. Region B lies across the region of maximum mixing ratio for ozone in the summer NH-winter SH season and it forms two large areas on each side of the ozone maximum mixing ratio for the spring NH- fall SH season. It is possible to gain some insight from the photochemical source region in the tropical middle stratosphere to the photochemically inert lower polar stratosphere by observing on the spring-fall map a region from point A to a point 18 km above the north pole. As one follows along this line from the equator to about 40° N, the rate of ozone production from O_2 photolysis is much faster than destruction by NO_x or O_x. When the line crosses into region B, which is the region where a large ozone destruction by NO_x is occuring, the absolute rate of ozone forma-

TABLE 6

The loss and production rates are averaged over 24 hours. The units are 10^{29} seconds^{-1}. The total daytime NO_2 (TD NO_2) is summed over the sunlit hemisphere. The units are 10^{32} molecules. All are summed over 15 - 45 km.

Season	$P(O_3)$	TD NO_2	$L(NO_x)$	L/P
spring	484	146	209	0.43
summer	449	119	222	0.50
fall	480	135	187	0.39
winter	527	134	228	0.43

TABLE 7

Sensitivity test where the NO_2 columns of figures 5 and 6 were scaled by 2/3 and 4/3. When the season is summer in the northern hemisphere $P(O_3) = 449 \times 10^{29}$ sec^{-1} and $L(O_x) = 75 \times 10^{29}$ sec^{-1}. When the season is fall in the northern hemisphere $P(O_3) = 480 \times 10^{29}$ sec^{-1} and $L(O_x) = 77 \times 10^{29}$ sec^{-1}.

NH season	REL. NO_2	TD NO_2	$L(NO_x)$	L/P
summer	2/3	81.5	145	0.32
summer	1	119	222	0.50
summer	4/3	155	297	0.66
fall	2/3	100	127	0.26
fall	1	135	187	0.39
fall	4/3	195	295	0.61

tion and destruction by O_x is low.

The 24 hour average rates from the instantaneous rates calculation were summed over the latitudes and over various altitude bands. Table 5 presents the results over five km altitude bands and over the entire altitude range between 15-45 km. The role of $L(NO_x)$ in balancing ozone between 45-50 km is quite small; it accounts for 7 % of the total production in the altitude band. $L(O_x)$ destroys a about 23 % in the same region. Between 40 - 45 km NO_x and O_x are equally important in destroying ozone, each accounting for 25 %. In the altitude region between 30 and 40 km NO_x destroys about 57 % of the ozone produced whereas O_x only destroys 10 %. In the lower stratosphere between 25 and 30 km, ozone destruction for both mechanisms becomes less important, $L(O_x)$ is 6 % of $P(O_3)$ and $L(NO_x)$ is 35 %. Below 25 km both mechanisms become extremely slow and care must be taken to correctly account for the transport before a balance can be discussed. Over the entire range 15 - 45 km the O_x reactions destroy 15 % of the photochemically produced ozone and NO_x reactions destroy 43 %.

A sensitivity test was carried out in which the sunset NO_2 columns of figures 5 and 6 were scaled by factors of 2/3 and 4/3 which were chosen to be more conservative than the $\pm$ 20 % Noxon estimated for the accuracy of the NO_2 columns. This error factor, $\pm$ 33 % , also incorporates most of the balloon soundings. The results are summarized in Table 7. The global average over the complete altitude range 15 - 45 km for $L(NO_x)$ was 29 % for the lower

limit NO_2 and 63 % for the upper limit. Thus the global rate of ozone destruction by NO_x is reported as 45 15 %. The global rate of ozone destruction by O_x is 15 % of the production rate.

The three quantities $P(O_3)$, $L(O_x)$, and $L(NO_x)$ are independent and were derived from different sets of atmospheric measurements. If measurements of species that enter other catalytic cycles such as those of HO_x and Cl_x families were available, instantaneous rates calculations could be made for them also. The total global ozone balance based on experimental observations could then be a check to verify the completeness and accuracy of stratospheric photochemical mechanisms. This would be possible for reactions directly involving ozone as well as other reactions because of the highly coupled nature of the stratospheric photochemical reactions. It is clear that the key to the puzzle is a reliable set of in-situ measurements for the unstable intermediates, the radicals, and for the stable species, the photochemical sinks.

VI. POSTSCRIPT

A correction has been tended by Noxon which raises some of the NO_2 columns by a factor of 1.6 and the rest by a factor of 1.25 (Noxon 1980). This will also tend to raise the concentrations of NO_2 used in the instantaneous rates calculation. The overall trends observed in the calculation will not be changed, but all the values need to reflect the fact that the mean global level of daytime NO_2 has risen by 25 %. This factor falls within the range chosen for our sensitivity study, $\pm$ 33 %, therefore an examination of table 7 should show the effects that these new NO_2 columns have on the calculated instantaneous rates for the loss of ozone due to NO_x.

Noxon, J.F., J. Geophys. Res. 85, 4560 (1980)

VII. FIGURE CAPTIONS.

Figure 1. Temperature in the troposphere and stratosphere. The south pole is - 90° and the north pole is 90° in all the contour plots. The first panel is the equinox average of Dütsch's (1978) values for March, April and May; the second panel is the solstice average for December, January and February.

Figure 2. Ozone concentration in units of 10^{12} molecules cm^{-3}. Data is from Dütsch (1978).

Figure 3. Atomic oxygen concentration, 12 hour, daytime average, calculated as described in the text.

Figure 4. Daytime average of nitrogen dioxide concentration in units of 10^{9} molecules cm^{-3}.

Figure 5. Observed PM vertical columns of stratospheric nitrogen dioxide, fall-spring: ○ NOXON (1979), Figure 1; □ NOXON, Figure 2; ▲ NOXON, Figure 3; A ACKERMAN et al. (1974); B OGAWA (1979); C MURCRAY et al. (1974); D HARRIES et al. (1976). The line is an interpolation used as the primary data for this study. Sensitivity studies were made with NO_2 columns 2/3 and 4/3 of this line. Included for comparison, ● HNO_3 columns from MURCRAY et al. (1975) for April 1975, same units as NO_2.

Figure 6. Observed PM vertical columns of stratospheric nitogen dioxide, winter-summer: ○ NOXON (1979), Figure 1; △ NOXON, Figure 3; ◇ NOXON, Figure 6; E EVANS et al. (1977); F EVANS et al. (1978); G GOLDMAN et al. (1978); H DRUMMOND and JARNOT (1979). The line is as described in the previous figure. The HNO_3 columns are for January 1974.

Figure 7. Nitrogen dioxide profile between 20 and 50 km as observed by DRUMMOND and JARNOT (1979), line A; the integrated vertical column is 2.8×10^{15} molecules cm^{-2}; 44°N, June 1975, one hour after sunrise. Lines B and C represent model NO_2 profiles respectively from 2.4 and 1.0×10^{15} molecules cm^{-2} between 20 and 50 km, one hour after sunrise.

Figure 8. Rate of ozone production from O_2 photolysis, $P(O_3) = 2\ j[O_2]$, 24 hour average, in units of molecules $cm^{-3}\ s^{-1}$.

Figure 9. Rate of ozone destruction by the Chapman reactions, $L(O_x) = 2\ k[O][O_3]$, 24 hour average, in units of molecules $cm^{-3}\ s^{-1}$.

Figure 10. The ratio of the rate of ozone destruction by O_x to the rate of ozone formation by O_2 photolysis. $L(O_x)/P(O_3) = \frac{2k[O][O_3]}{2j[O_2]}$.

Figure 11. The rate of ozone destruction by NO_x, $L(NO_x) = 2k[O][NO_2]$, in units of molecules $cm^{-3}\ s^{-1}$.

Figure 12. Ratio of ozone destruction by NO_x to production by photolysis of oxygen, $R = \frac{L(NO_x)}{P(O_3)} = \frac{2k[O][NO_2]}{2j[O_2]}$.

Figure 13. Ozone photochemical replacement time, ratio of ozone concentration to ozone production rate, $P(O_3)$.

Figure 14. The ratio $L(NO_x)$ / $P(O_3)$, Figure 12, superimposed on ozone mixing ratios. Region A is characterized by a maximum O_3 ratio, region B by fast ozone desruction by NO_x and region C by the maximum rate of O_3 production from oxygen photolysis.

VIII. REFERENCES

ACKERMAN, M. (1971), Ultraviolet solar radiation related to mesospheric processes, in Mesospheric Models and Related Experiments, edited by G. Fiocco, D. Reidel, Hingham, Mass., pp. 149-159.

ACKERMAN, M., FONTANELLA, J. C., FRIMOUT, D., GIRARD, A., LOUISHARA, N., and MULLER, C. (1975), Simultaneous Measurements of NO and NO_2 in the Stratosphere, Planet. Space Sci. 23, 651-650.

BREWER, A. W. and WILSON, A. W. (1968), The Regions of Formation of Atmospheric Ozone, Ouart. J. Roy. Meteorol. Soc. 94, 249-265.

BREUCKNER, G. E., BARTOE, D. F., MOE, O. K. and VAN HOOSIER, M. E. (1976), Absolute Solar Intensities and their Variations with Solar Activity. 1. The Wavelength Region 1750-2100 Å, Astrophy. J. 209, 935-944.

CHAMEIDES, W. C. and WALKER, J. G. (1976), A Time Dependent Photochemical Model for Ozone Near the Ground, J. Geophys. Res. 81, 413-420.

CHAN, J. S., USELMAN, W. M., CALVERT, J. G. and SHAW, J. A. (1977), The Pressure Dependence of the Rate Constant for the Reaction HO + CO → H + CO_2, Chem. Phys. Lett. 45, 240-243.

CHANG, J. S. (1974), Similations, Perturbations and Interpretations, Proceedings of the Third Conference on CIAP, U. S. Department of Transportation, DOT-TSC-OST-74-15, 330-371.

CHANG, J. S., HINDMARSCH, A. C., and MADSEN, N. K. (1974), Simulations of Chemical Kinetics and Transport in the Stratosphere, in Stiff Differential Systems, (R. A. Willoughby, ed., Plenum, New York)pp. 51-65.

COX, R. A. (1978), Kinetics of the HO_2 Radical Reactions of Atmospheric Interest, Symposium on the Geophysical Aspects and Conseouences of Changes in the Composition of the Stratosphere, Toronto, World Meteorological Organization, Publication No. 511.

CONNELL, P. and JOHNSTON, H. S. (1979), The Thermal Dissociation of N_2O_5 in N_2, Geophys. Res. Lett. 6, 553-556.

DRUMMOND, J. R. and JARNOT, R. F. (1979), Infra-red Measurements of Stratospheric Composition. II. Simultaneous NO and NO_2 Measurements, Atmospheric Physics Memorandum No. 78.1, Clarendon Laboratory, University of Oxford.

DUTSCH, H. U., 1969, Atmospheric Ozone and Ultraviolet Radiation, World Survey of Climatology, (Vol. 4, D. F. Rex, ed., Elsevier Publishing Company, Amsterdam, London, New York), pp. 383-432.

DUTSCH, H. U. (1978), Vertical Ozone Distribution on a Global Scale, Pure Appl. Geophys. 116, 511-529.

EVANS, W. F. J., KERR, J. B., McELROY, C. T., O'BRIEN, R.S., RIDLEY, B. A., and WHARDLE, D. I. (1977), The Odd Nitrogen Mixing Ratio in the Stratosphere, Geophys. Res. Lett. 4, 235-238.

EVANS, W. F. J., FAST, H., KERR, J. B., McELROY, C. T., O'BRIEN, R. S., and WHARDLE, D. I. (1978), Stratospheric Constituent Measurements from Project Stratoprobe, Symposium on the Geophysical Aspects and Conseouences of Changes in the Composition of the Stratosphere, To Toronto, World Meteorological Organization, Publication No. 511.

FISHMAN, F., SOLOMON, S., and CRUTZEN, P. J. (1979), Observational and Theoretical Evidence in Support of a Significant In-situ Photochemical Source of Tropospheric Ozone, Tellus 31, 432-446.

FONTANELLA, J. C., GRAMONT, L., and LOUISNARD, N. (1974), Vertical Distribution of NO, NO_2 and HNO_3 as Derived from Stratospheric Absorption Spectra, Proceedings of the Third Conference on CIAP, U. S. Department of Transpotation, DOT-TSC-OST-74-15, 454-457, and also in Appl. Opt. 14, 825-828.

GEAR, C. W., Stiff Equations, in Numerical Initial Value Problems in Ordinary Differential Equations (Prentice Hall Inc., Englewood Cliffs, New Jersey, 1971), pp. 209-223.

GOLDMAN, A., FERWALD, F. G., WILLIAMS, W. S., and MURCRAY D. G. (1978), Vertical Distribution of NO_2 in the Stratosphere as Determined from Balloon Measurements of Solar Spectra in the 4500 Å Region, Geophys. Res. Lett. 5, 320-325.

GRAHAM, R. A., and JOHNSTON, H. S. (1978), The Photochemistry of NO_3 and the Kinetics of the $N_2O_5 - O_3$ System, J. Phys. Chem. 82, 254-268.

HAMPSON, R. F. and GARVIN, D. (1977), Reaction Rate and Photochemical Data for Atmospheric Chemistry, NBS Special Publication 513.

HARRIES, J. E., MOSS, D. G., SWANN, N. R. W., NEILL, G. F., and GILDWANG, P. (1976), Simultaneous Measurements of H_2O, NO_2 and HNO_3 in the Daytime Stratosphere from 15 to 35 km, Nature 259, 300-302.

HINDMARSCH, A. C. (1972), GEAR: Ordinary Differential Equation System Solver, Lawrence Livermore Laboratory Report UCID-30001, Rev. 1.

HOWARD, C. J. (1978), Recent Developments in Atmospheric HO_2 Chemistry, Symposium on the Geophysical Aspects and Consequences of Changes in the Composition of the Stratophere, Toronto, World Meteorological Organization, Publication No. 511.

HUDSON, R. D., and MAHLE, S. H. (1972), Photochemical Rates of Molecualar Oxygen in the Mesosphere and Lower Thermosphere, J. Geophys. Res. 77, 2902-2914.

ISAKSEN, I. S. A., MIDTBO, K., DUNDE, J., and CRUTZEN, P. J. (1976), A Simplified Method to Include Molecular Scattering and Reflection in Calculations of Photon Fluxes and Photodissociation Rates, Institute for Geophysics, University of Oslo, Oslo, Norway, Reort 20, pp. 1-21.

JOHNSTON, H. S. and WHITTEN, G. (1973), Instantaneous Photochemical Rates in the Global Stratosphere, Pure Appl. Geophys. 106-108, 1468-1489.

JOHNSTON, H. S. and WHITTEN, G. (1975), Chemical Reactions in the Stratosphere as Studied by the Method of Instantaneous Rates, Int. J. Chem. Kinet., Symposium No. 1, 1-26.

JOHNSTON, H. S. (1975), Global Ozone Balance in the Natural Stratosphere, Rev. Geophys. Space Phys. 13, 637-649.

JOHNSTON, H. S. and PODOLSKE, J. (1978), Interpretations of Stratospheric Photochemistry, Rev. Geophys. Space Phys. 16, 491-519.

KERR, J. B. (1977), private communication.

KERR, J. B. and McELROY (1978), private communication.

LAZRUS, A. L., and GANDRUD, B. W. (1974), Distribution of Stratospheric Nitric Acid Vapor, J. Atmos. Sci. 31, 1102-1108.

MAGNOTTA, F. and JOHNSTON, H. S. (1980), Photodissociation Quantum Yield for the NO_3 Free Radical, Geophys.Res. Lett. 7, 769-772.

MURCRAY, D. G., GOLDMAN, A., WILLIAMS, W. J. MURCRAY, F. H., BROOKS, J. N., VAN ALLEN, J., STOCKEN, R. N., KOSTERS, J. J., BARKER, D. B., and SNIDER, D. E. (1974), Recent Results of Stratospheric Trace-gas Measurements from Balloon-Borne Spectrometers, Proceedings of the Third Conference on CIAP, U. S. Department of Transportation, DOT-TSC-OST-74-15, pp. 184-192.

MURCRAY, D. G., BARKER, D. B., BROOKS, J. N., GOLDMAN, A., and WILLIAMS, W. J. (1975), Seasonal and Latitudinal Variation of the Stratospheric Concentration of HNO_3, Geophys. Res. Lett. 2, 223-225.

NOXON, J. F. (1978), Stratospheric NO_2 in the Antarctic Winter, Geophys. Res. Lett. 5, 1021-1022.

NOXON, J. F., WHIPPLE, E. C. JR., and HYDE, R. S. (1979), Stratospheric NO_2. I. Observational Method and Behavior at Mid-latitudes, J. Geophys. Res. 84, 5047-5065.

NOXON, J. F. (1979), Stratospheric NO_2. II. Global Behavior, J. Geophys. Res. 84, 5067-5076.

NOXON, J. F., (1980), Erratum, J. Geophys. Res. 85, 4560-4561.

OGAWA, T. (1979), private communication.

RIDLEY, B. A., SCHIFF, H. I., SHAW, A., and MEGIL, L. R. (1975), In-situ Measurements of Stratospheric Nitric Oxide Using a Balloon-Borne Chemiluminescent Instrument, J. Geophys. Res. 80, 1925-1929.

SOLOMON, S. and CRUTZEN, P. J. (1980), in preparation.

STEWART, R. W. and HOFFERT, M. I. (1975), A Chemical Model of the Troposphere and Stratosphere, J. Atmos. Sci. 32, 195-210.

WOFSY, S. C. (1978), Temporal and Latitudinal Variations of Stratospheric Trace Gases: A Critical Comparison Between Theory and Experiment, J. Geophys. Res. 83, 364-378.